UNIVERSIDAD DE CHILE
FACULTAD DE CIENCIAS FÍSICAS Y MATEMÁTICAS
DEPARTAMENTO DE INGENIERÍA MECÁNICA

TECHNO-ECONOMIC ANALYSIS OF THE INTEGRATION OF LARGE-SCALE HYDROGEN PRODUCTION AND A HYBRID CSP+PV PLANT IN NORTHERN CHILE

TESIS PARA OPTAR AL GRADO DE
MAGÍSTER EN CIENCIAS DE LA INGENIERÍA, MENCIÓN MECÁNICA

FRANCISCO JAVIER MORAGA RAMÍREZ

PROFESOR GUÍA:
FRANK DINTER

MIEMBROS DE LA COMISIÓN:
MARÍA TERESA CERDA GUEVARA
RAMÓN FREDERICK GONZÁLEZ
WILLIAMS CALDERÓN MUÑOZ

Este trabajo ha sido parcialmente financiado por ANID / ANID Becas / Magíster Nacional 22200035

SANTIAGO DE CHILE
2022

RESUMEN DE LA TESIS PARA OPTAR AL GRADO DE MAGÍSTER EN CIENCIAS DE LA INGENIERÍA, MENCIÓN MECÁNICA
POR: FRANCISCO MORAGA RAMÍREZ
FECHA: 2022
PROF. GUÍA: FRANK DINTER

TECHNO-ECONOMIC ANALYSIS OF THE INTEGRATION OF LARGE-SCALE HYDROGEN PRODUCTION AND A HYBRID CSP+PV PLANT IN NORTHERN CHILE

El hidrógeno verde ha sido considerado como uno de los vectores energéticos del futuro, y Chile puede convertirse en líder en su producción debido a su gran potencial de energías renovables. La electricidad barata para producir hidrógeno verde es uno de los factores clave para que el hidrógeno solar sea un método de producción rentable. Sin embargo, sin almacenamiento de energía, la capacidad operativa de los electrolizadores es pequeña y, por tanto, la proporción de la inversión en el costo nivelado del hidrógeno ($LCOH_2$) aumenta debido a la baja utilización de los electrolizadores. En esta tesis se propuso realizar un análisis técnico-económico de la integración de la producción de hidrógeno verde a gran escala y una planta híbrida CSP + PV de 100 MW_e en el norte de Chile, uno de los puntos solares más importantes del mundo. Una planta solar híbrida aprovecha el bajo costo de la tecnología PV y la capacidad de despacho de la CSP con almacenamiento, lo que aumenta las horas de producción renovable, creando condiciones ideales para el desarrollo de la industria del hidrógeno verde. Para comprender mejor la utilidad de dicha integración, se comparó el rendimiento de la planta solar híbrida con el rendimiento ofrecido por cada tecnología solar independiente y con una conexión a la red mediante un contrato PPA. El análisis se llevó a cabo utilizando un código desarrollado con PySAM, una librería de código abierto basada en Python, que no sólo proporciona acceso a todas las capacidades del software System Advisor Model (SAM), sino que también ayuda a implementar escenarios personalizados de nuevas tecnologías. Este estudio ha constatado que la producción de hidrógeno a partir de energía solar no es económicamente competitiva con el hidrógeno de origen fósil en 2021. Sin embargo, también ha demostrado que para la próxima década el acoplamiento fotovoltaico-electrolítico será capaz de alcanzar valores rentables y el mínimo $LCOH_2$ de las vías consideradas. Aunque las plantas híbridas no alcanzarían valores tan bajos como la PV en 2030, esta integración ofrece costos más bajos que la producción de hidrógeno basada solo en CSP. Además, en condiciones favorables, las plantas híbridas también podrían alcanzar el rango de valores del hidrógeno basado en combustibles fósiles (menos de 2 USD/kg_{H2}) y beneficios adicionales si se analiza cada configuración de forma holística. De hecho, una planta híbrida consigue la mayor producción anual de hidrógeno, el menor costo específico de almacenamiento y el mayor potencial de reducción de emisiones de CO_2 equivalentes de todos los escenarios estudiados. Los resultados de esta tesis proporcionan una buena referencia para futuros estudios y serán de interés para los responsables de la toma de decisiones y de políticas de transición energética. El código desarrollado está disponible en código abierto para que más investigadores puedan investigar otros escenarios de producción de hidrógeno solar.

Abstract

Green hydrogen has been considered as one of the energy carriers of the future, and Chile can become a leader in its production due to its great renewable energy potential. Cheap electricity is one of the key drivers for making green hydrogen a cost-effective production method. However, without energy storage, only a small operational capacity of electrolyzers can be achieved, and therefore, the share of the investment in the levelized cost of hydrogen ($LCOH_2$) increases because of the low utilization of the electrolyzers. This thesis set out to conduct a techno-economic analysis of the integration of large-scale green hydrogen production and a hybrid CSP + PV plant of 100 MW_e in northern Chile, one of the world's solar hotspots. A hybrid solar plant takes advantage of the low cost of PV technology and the dispatchability of CSP with storage, which increases the hours of renewable production, creating ideal conditions for the development of the green hydrogen industry. For a better understanding of the usefulness of such integration, the performance of the hybrid solar plant was compared with the performance offered by each independent solar technology and with a grid-connection via a PPA mechanism. The analysis was carried out using an in-house code developed with PySAM, an open-source library based on Python that not only provides access to all capabilities of the System Advisor Model (SAM) software, but also helps to implement and integrate custom scenarios of novel technologies. This study has found that solar-based hydrogen production is not economically competitive with fossil fuel hydrogen in 2021. However, this study has also shown that for the next decade PV-electrolysis coupling will be able to achieve cost-effective values and the minimum $LCOH_2$ of the considered pathways. Although hybrid solar plants do not reach values as low as stand-alone PV in 2030, this integration offers lower costs of production than hydrogen production based on stand-alone CSP. Furthermore, under favorable conditions, hybrid solar plants could also achieve the value range of fossil fuel-based hydrogen (i.e., below $2 per kg of hydrogen) and additional benefits if each tested configuration is analyzed holistically. In fact, a hybrid solar plant achieves the highest annual hydrogen production, the lowest specific cost of storage and the highest CO_2 equivalent emission reduction potential of all the scenarios under study. The results of this thesis provide a good benchmark for future studies and will be of interest to decision and policy makers in energy transition. Equally important, the developed code is available in open source so that more researchers can further investigate other solar hydrogen production scenarios.

Keywords: hybrid CSP+PV plant, Photovoltaic energy (PV), Concentrated Solar Power (CSP), green hydrogen, electrolyzers, PySAM, Levelized Cost of Hydrogen ($LCOH_2$).

A mis padres Juan y Gilda,

por creer en mí,

incluso cuando ni yo mismo lo hacía.

Agradecimientos

Sin el apoyo de muchas personas, la realización de este trabajo nunca se habría llevado a cabo. Deseo expresar mi más sincero reconocimiento y agradecimiento a las siguientes personas:

Al Dr. Frank Dinter, mi profesor guía, por permitirme realizar este trabajo bajo su dirección y brindarme su ayuda, conocimientos y apoyo. Gracias por confiar en mí y abrirme las puertas del Centro de Tecnologías para Energía Solar de Fraunhofer Chile Research (FCR-CSET).

A María Teresa Cerda, mi profesora co-guía, porque a pesar de tener una agenda muy atareada, siempre se dio tiempo de atender mis dudas y colaborar con mi tesis. Muchas gracias por su apoyo técnico y especialmente por su calidad humana.

Al Dr. Williams Calderón y al Profesor Ramón Frederick, miembros de la Comisión Evaluadora, por sus valorables comentarios y sugerencias para que este trabajo saliera adelante de la mejor manera posible.

No puedo pasar por alto el importante y desinteresado apoyo que me bridó Aloïs Salmon, quien me instó a adoptar y aprender nuevas plataformas y herramientas de programación para llevar a cabo esta tesis. A Catalina Sandoval, del Centro de Escritura Académica - Armadillo Lab, gracias por sus consejos para lograr una mejor escritura en inglés y por las conversas que hicieron más agradable cada tutoría.

Por último, el agradecimiento más profundo y sentido va para mi familia. Gracias a mis padres y hermanos, por su apoyo, cariño y comprensión.

A mis tíos Glezis Ramírez y Verónica Díaz, por abrirme las puertas de su hogar y por brindarme su compañía y apoyo durante mi estadía en Santiago. Gracias de nuevo por su amable hospitalidad. Finalmente, a mi primo y amigo Glezis Ramírez, gracias por las risas y los buenos momentos compartidos que distendieron las arduas jornadas de estudio.

A todos ustedes, muchas gracias de corazón.

Contents

List of Tables

List of Figures

Abbreviations and acronyms

ALK	Alkaline
CAPEX	Capital expenditure
CO_2	Carbon dioxide
CSP	Concentrated Solar Power
GH_2	Gaseous hydrogen
H_2	Hydrogen
HTF	Heat Transfer Fluid
IEA	International Energy Agency
IRENA	International Renewable Energy Agency
kW	kilo Watt
kWh	kilo Watt hour
LCOE	Levelized Cost of Energy ($/kWh)
$LCOH_2$	Levelized Cost of Hydrogen
LFR	Linear Fresnel Reflector
LH_2	Liquid hydrogen
LHV	Lower heating value
MW	Mega Watt
OPEX	Operating expenditure
PEM	Proton Exchange Membrane / Polymer Electrolyte Membrane
PTC	Parabolic-Trough Collector
PPA	Power Purchase Agreement
PV	Photovoltaics
SM	Solar Multiple
SMR	Steam Methane Reforming
SOEC	Solid Oxide Electrolysis Cells
SPD	Solar Parabolic Dish
SPT	Solar Power Tower
TES	Thermal Energy Storage
USD	United States dollar

1. Introduction

1.1. Motivation

In the face of climate change and on the basis of the Paris Agreement, in June 2019, the Chilean government announced that Chile was committed to achieve carbon neutrality by 2050, i.e., that the country reaches a state of balance between emissions and absorptions of greenhouse gases, mainly carbon dioxide (CO_2). To achieve this ambitious goal, one of the great allies that has gained strength recently is green hydrogen, i.e., hydrogen generated by renewable energy sources without producing polluting emissions [1]. Although there are several renewable energy-based solutions for producing hydrogen, currently the most established option for producing green hydrogen is the electrolysis of water powered by renewable electricity [2]. Nowadays, both the public and private sectors agree on the fundamental role that this energy vector can play in the decarbonization strategy. For this reason, on November 3rd, 2020, the Government of Chile launched the National Green Hydrogen Strategy, which has three main objectives: to have 5 GW of electrolysis capacity under development by 2025, to produce the cheapest green hydrogen by 2030 and to be among the top 3 exporters by 2040 [3].

While green hydrogen has begun to gain prominence, one of the main barriers that limits its use on a large-scale is the cost of the energy required for its production. According to the Ministry of Energy, between 50 and 80% of the cost of hydrogen corresponds to the electricity supply. As a consequence of the latter, Chile has been identified as one of the most competitive countries for the development and production of green hydrogen due to the enormous potential for generating electricity from renewable resources, particularly solar energy. To take advantage of this solar resource, there are two main types of solar energy technologies: photovoltaics (PV) and concentrating solar-thermal power (CSP). On the one hand, PV systems are the most economical and widespread solar electric technology in the world. This type of technology uses solar cells and converts sunlight directly into electricity without the need for moving parts. However, electrical storage in PV is currently not feasible, so its production is intermittent and limited by daily and seasonal fluctuations. The latter makes it difficult to guarantee a year-round baseload production that can be used for large-scale green hydrogen production. On the other hand, CSP technology integrated with Thermal Energy Storage system (TES) represents a suitable option to improve the dispatch capacity and the capacity factor; however, it has a much higher cost mainly due to the cost of storage and solar field necessary to ensure a continuous and reliable generation of electricity. To solve the limitations of each technology, the concept of hybrid CSP + PV plant has been studied by different authors in recent years [4]–[12] and seeks to exploit the main advantage of each of the solar technologies in an optimal manner and in a single application.

Previous studies in the area have focused on the study of hybrid solar plants for electricity generation in particular or integrated to the production of fresh water [13], cooling or process heat [14]. However, very little is currently known about hybrid CSP + PV plants dedicated to green hydrogen production in the world, and to date there are no Chile-based studies on the subject. Moreover, the few green hydrogen studies carried out in Chile have focused on studying the production of green hydrogen with wind energy in Patagonia [15], [16] or with solar energy in the Atacama Desert [17], but using the renewable generation sources separately, and not from a comprehensive point of view. Only one paper refers to the combination of wind and photovoltaic energy [18], leaving a clear and interesting research niche to combine CSP + PV hybridization with hydrogen production in northern Chile, where in addition to having a large solar resource, the most important mining projects are concentrated, with critical infrastructure already available (gas pipelines, ports, highways, power lines).

In order to contribute to filling this gap, this thesis seeks to perform a techno-economic feasibility analysis of hybrid solar energy supply for hydrogen production based on low temperature electrolysis, considering its production and its subsequent conditioning to be stored. As input, it will use electrical energy produced by a combined PV and CSP plant of central tower in northern Chile, particularly in the vicinity of Antofagasta, considering two-time scenarios (current: 2021 and midterm: 2030). For comparison, the performance of the hybrid solar plant will be contrasted with that achieved by the stand-alone plants and that of a grid-connected electrolysis plant, using a Python-based code developed specifically for this purpose. Therefore, the originality and novelty lie both in the object of study and in the simulation tool used. Finally, it is worth highlighting that the vast majority of the data sources used in this thesis cover the years 2018-2021, which provides an updated perspective on the economics of green hydrogen production in northern Chile.

In summary, combining solar technologies in a hybrid plant could be a promising way to stabilize the hydrogen supply and achieve a higher number of hours of electrolyzer operation, ensuring a higher volume of hydrogen produced to guarantee a constant supply for current demand (e.g., industrial and refining uses) or for emerging applications (e.g., hydrogen injection into gas grids (blending) or fuel cell electric vehicles). This research will contribute to a deeper understanding of the relationship between hybrid solar plants and hydrogen production, as well as to generate fresh insight into the knowledge of this promising alternative for a successful decarbonization of the Chilean energy sector and the resulting mitigation of climate change effects.

1.2. Objectives

1.2.1. General Objective

The main objective of this thesis is to evaluate the technical and economic feasibility of a **power-to-hydrogen** project in a strategic location in northern Chile. The project consists of a large-scale green hydrogen production system integrated with a hybrid solar power plant, which optimally combines a photovoltaic (PV) and central receiver concentrating solar power (CSP) system with thermal energy storage (TES).

1.2.2. Specific Objectives

- Create a code to model and simulate a hybrid plant with a CSP system that dispatches power in response to the output of the PV system.

- Select the most suitable technology for the production and storage of hydrogen and model its performance.

- Perform a parametric analysis for different uncertain components of the hybrid solar plant, identifying the main tradeoffs and selecting the best configuration that minimizes the cost of hydrogen production.

- Determine the levelized cost of energy (LCOE), the green hydrogen production rate, the CO_2 emissions avoided, the levelized cost of hydrogen ($LCOH_2$) and its projections in order to show the current and future scenarios.

- Analyze the results obtained by the hybrid solar plant and contrast them with the performance achieved by each stand-alone solar plant, as well as the performance achieved by an indirect on-grid connection via a Power Purchase Agreement (PPA) mechanism.

1.3. Scope and Delimitations

This research is descriptive and explanatory in nature with respect to the production of green hydrogen from hybrid solar plants, and focused on the first four stages of the hydrogen value chain: energy source, production, conditioning and storage. However, it is beyond the scope of this thesis to consider its transport and distribution to its final consumers ("off-takers"). Future works may consider end-consumers, which could be local (such as Minera Escondida, located 90 km from the project location) or international, exporting it from the port of Mejillones (located 100 km from the project). Additionally, this study was limited to the production of pure green hydrogen, in liquid and gaseous state, but not another types of compounds such as ammonia, methane, methanol or other synthetic fuels. Finally, the reader should bear in mind that this thesis did not make a specific study of the origin of the water for hydrogen production, so the costs and other technical characteristics were assumed based on the literature available so far. A full discussion of freshwater access and water stress in northern Chile is beyond the scope of this study.

1.4. Thesis Structure

The thesis has been organized in the following way:

Introduction to the topic, objectives and scope of the work are contained in chapter 1. Chapter 2 is devoted to review the state of the art and the theory behind the electrolysis process and solar energy basics. Chapter 3 is concerned with the methodology used for this study, with the sequential activities necessary for the completion of this work. Chapter 4 presents the results and discussion of this thesis, focusing on technical and economic aspects. Chapter 5 and 6 deals with the conclusions and outlook for future work respectively. The bibliography used for this work can be found in chapter 7. Finally, the Python codes developed for this thesis are included in annexes.

2. Theoretical Framework

2.1. Green Hydrogen

Amid the climate change crisis and its devastating consequences, there is an urgent need to move away from conventional forms of energy production towards an energy model based on renewable sources and net-zero global carbon emissions. According to the Report on the Global State of the Climate 2020 presented by the World Meteorological Organization (WMO), to limit the increase in world temperature to 1.5ºC, global emissions must be reduced by 45% by 2030, reaching almost zero by 2050; otherwise, climate change will become a phenomenon of no return, with serious toll on people's lives and health [19].

One of the solutions being developed to meet such emissions reduction targets in some countries, including Chile, is green hydrogen, i.e., hydrogen generated through the electrolysis of water using renewable electricity. Until the moment of writing this thesis, 17 governments have released hydrogen strategies, more than 20 governments have publicly announced they are working to develop strategies, and numerous companies are seeking to tap into hydrogen business opportunities [2]. The evidence seems to suggest that green hydrogen could play a crucial role as an energy vector in the energy transition to net zero emissions, decarbonizing sectors where direct electrification is more challenging ("hard-to-abate" sectors of the economy), such as long-haul transport or industry (chemical, steel and oil refinery industries).

This close integration between the main energy consuming sectors (such as the heating, transport and industrial sectors) and energy producing sectors is known as "sector coupling", and green hydrogen plays a pivotal role in achieving this. The coupling of sectors through hydrogen is reflected in Figure 1, where it is possible to observe the interlinking of the energy supply and end-use sectors with one another, increasing the level of flexibility while facilitating the integration of variable renewable energy into the power system. In summary, green hydrogen presents the opportunity to accelerate the energy transition as well as the possibility to work towards a greenhouse gas free future and economy for the decarbonization of the energy matrix and its transition to carbon neutrality.

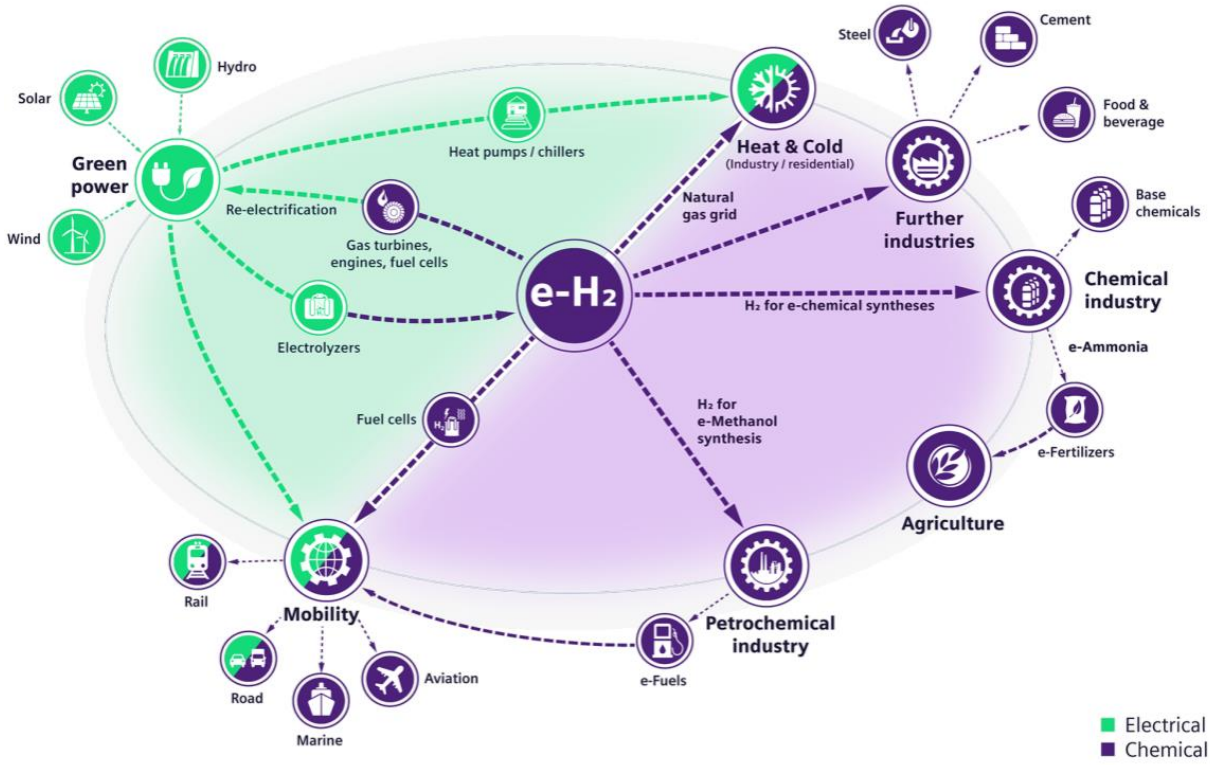

Figure 1: Sector Coupling [20]

Although it may seem so, the use of hydrogen as a fuel is not new, but until recently it was not considered as a 100% sustainable alternative to generate large amounts of energy. In fact, hydrogen in Chile was only considered as a feedstock or raw material for the chemical industry, but not as a fuel. However, on 13 February 2021, Law No. 21.305 on Energy Efficiency was published in the Official Gazette of the Republic of Chile, where hydrogen is expressly declared as a fuel and empowers the Ministry of Energy to regulate it and treat it as an energy resource. An adequate regulatory framework is essential to develop the green hydrogen industry. In this regard, in May 2021, the Chilean Ministry of Energy and the Superintendency of Electricity and Fuels (SEC) published the first support guide for the authorization of special hydrogen projects [21], in order to provide guidance to individuals and companies interested in implementing projects in this promising area, which is attracting the interest of national and international stakeholders.

The rise of hydrogen is due to multiple factors. On the one hand, in technical terms, hydrogen has great potential and versatility as an energy carrier, that is, it can be used in direct combustion processes, transformed into synthetic fuels or reconverted into electrical energy, where it releases only heat and water vapor instead of toxic gases. On the other hand, the green hydrogen industry in Chile could not only help to make energy development more sustainable, but could also be beneficial for the economy, as it could generate more than 22,000 direct and indirect jobs by 2030 and 91,000 by 2050 [22].

2.2. Hydrogen Properties

Hydrogen is a colorless, odorless and tasteless gas with unique characteristics that make it very interesting, and some of them are summarized in Table 1:

Table 1: Physical properties of hydrogen [23]

Property	Hydrogen	Comparison
Density (gaseous)	0.089 kg/m^3 (0°C, 1 bar)	1/10 of natural gas
Density (liquid)	70.79 kg/m^3 (-253°C, 1 bar)	1/6 of natural gas
Boiling point	-252.76°C (1 bar)	90°C below LNG
Energy per unit of mass (LHV)	120.1 MJ/kg	3x that of gasoline
Energy density (LHV)	0.01 MJ/L	1/3 of natural gas
Specific energy (liquefied, LHV)	8.5 MJ/L	1/3 of LNG
Flame velocity	346 cm/s	8x methane
Ignition range	4–77% in air by volume	6x wider than methane
Autoignition temperature	585°C	220°C for gasoline
Ignition energy	0.02 MJ	1/10 of methane

One of the characteristics that makes it more attractive to decarbonize many sectors of the economy is its gravimetric energy density. Figure 2 presents a comparison of specific energy (energy per mass or gravimetric density) and energy density (energy per volume or volumetric density) for several fuels based on lower heating values.

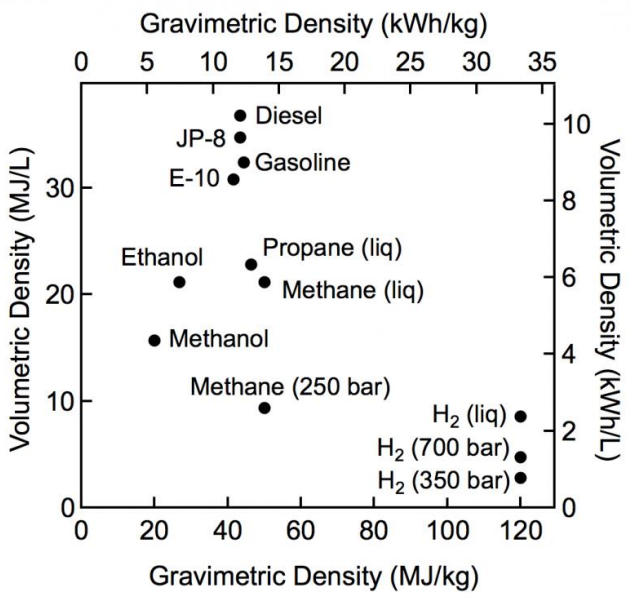

Figure 2: Gravimetric and volumetric density of hydrogen and other fuels [24]

From Figure 2 it is clear that on a mass basis, hydrogen has the highest energy per mass of the different energy carrier options, with nearly three times the energy content of gasoline. In contrast to the high gravimetric energy density, the corresponding volumetric density of hydrogen is low: liquid hydrogen has a density of 8 MJ/L, whereas gasoline has a density of 32 MJ/L. In other words, hydrogen has a high amount of energy per unit mass (gravimetric density), but low energy density per unit volume, which means that larger volumes of hydrogen must be moved to meet identical energy demands compared to other fuels.

2.3. Hydrogen Production

Despite being one of the most abundant elements on Earth and the most abundant element in the universe, hydrogen is not found as an independent molecule (in isolation). Therefore, it must be extracted from other hydrogenated compounds (such as coal, oil, natural gas, biomass, water among other compounds in which hydrogen is one of the constituents) through a very wide variety of technologies (reforming, gasification, electrolysis, pyrolysis, water splitting and many others). It should be noted that because pure hydrogen requires other energy sources to be produced, it is not considered a primary energy source, but a secondary energy source or as an energy carrier, i.e., a substance that stores energy and releases it in a controlled manner when required.

Virtually all hydrogen today is produced from natural gas and coal because of its favorable economy, but with very significant CO_2 emissions. For instance, of the ~90 Mt H_2 used in 2020, about 80% was produced from fossil fuels, mostly unabated [25]. On the other hand, electrolysis – the electrochemical process that uses electricity to split water (H_2O) into hydrogen (H_2) and oxygen (O_2) – only played a minor role: less than 0.1% of the world's dedicated hydrogen production came from water electrolysis, mainly used in where high purity hydrogen was needed.

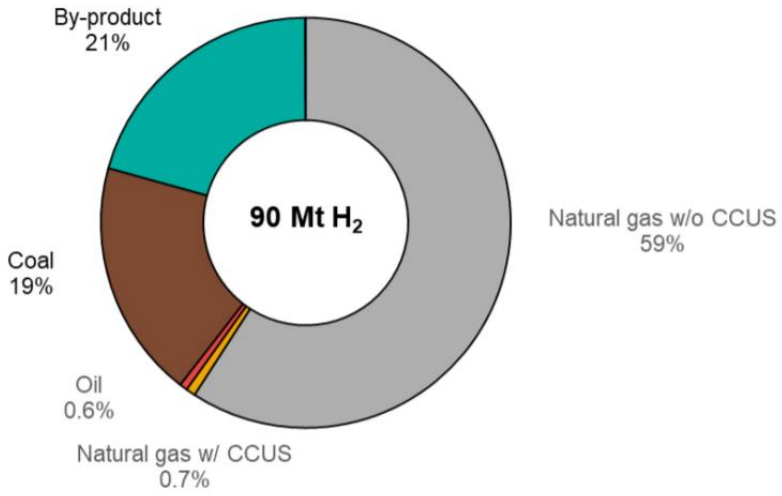

Figure 3: Sources of hydrogen production, 2020 [25]

As can be seen in Figure 3, Global hydrogen demand of ~90 Mt in 2020 was met almost entirely by fossil fuel-based hydrogen, with 72 Mt H_2 (79%) coming from dedicated hydrogen production plants, mainly for oil refining and chemical production. The remainder (21%) was by-product hydrogen produced in facilities designed primarily for other products, mainly refineries in which the reformation of naphtha into gasoline results in hydrogen.

2.3.1. Solar Energy-Based Hydrogen Production

There are numerous sources of hydrogen and possible alternative routes leading to its production; however, no hydrogen production technique will guarantee sustainability unless it is produced from renewable sources. Due to the latter, the present section discusses possible alternatives of solar hydrogen production. Hydrogen production using solar energy or solar-aided hydrogen production technologies can offer potential solutions to both ensuring sustainability in energy generation systems and designing environment-friendly systems. These systems can be classified mainly into four types: concentrated solar thermal energy, photovoltaic, photo-electrolysis, and bio-photolysis, as shown in Figure 4.

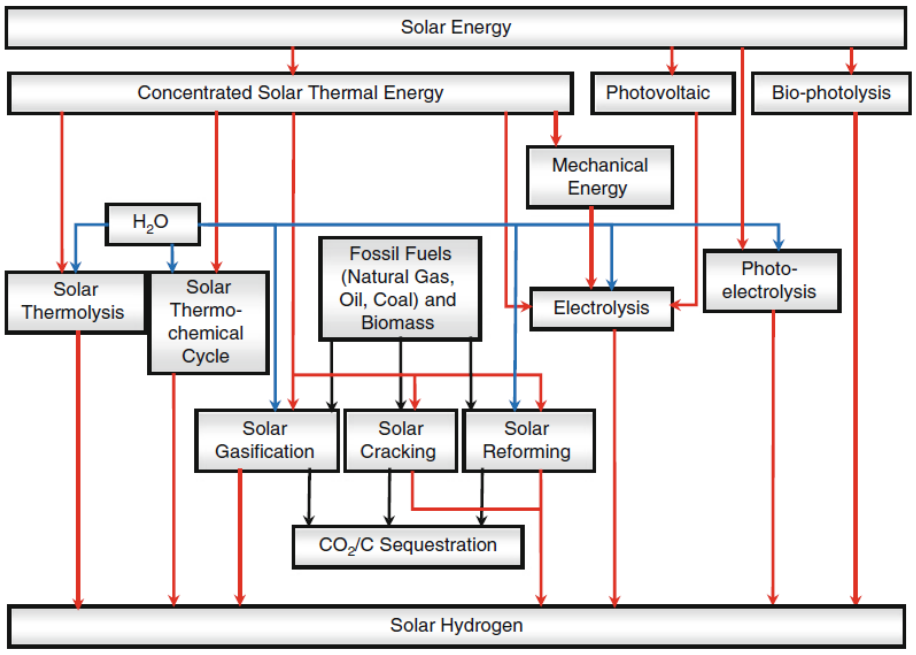

Figure 4: Sustainable pathways for hydrogen generation from solar energy [26]

Photovoltaic, photo-electrolysis, and bio-photolysis are considered low-temperature applications, whereas solar thermolysis, solar thermochemical cycles, solar gasification, solar reforming, and solar cracking are high-temperature applications of concentrated solar thermal energy [26].

This research focuses on large scale production of solar hydrogen via electrolysis of water, powered by a mix of solar energy technologies (PV + CSP). In the case of CSP, the thermal energy collected can be employed to the steam power cycles for power production. The significant amount of power produced is fed to the electrolyzer for hydrogen production after meeting the system requirements. On the other hand, PV technology allows the direct transformation of solar radiation into electricity, which can be connected directly to the electrolyzer, because unlike CSP technology, it does not need an inverter, reducing current conversion losses (AC/DC). Further details of these solar technologies will be provided in the following sections.

2.3.2. Electrolyzers

The device that produces hydrogen in Power-to-Gas (P2G) projects is called an electrolyzer. There are three main technologies of electrolyzers: alkaline; proton-exchange or polymer-electrolyte membrane (PEM) and solid oxide electrolysis cells (SOECs). Their main technical and economic characteristics are summarized in Table 2:

Table 2: Techno-economic characteristics of different electrolyzer technologies [23]

	Alkaline electrolyzer			PEM electrolyzer			SOEC electrolyzer		
	Today	2030	Long term	Today	2030	Long Term	Today	2030	Long Term
Electrical efficiency (%, LHV)	63–70	65–71	70–80	56–60	63–68	67–74	74–81	77–84	77–90
Operating Pressure (bar)	1–30			30–80			1		
Operating temperature (°C)	60–80			50–80			650 – 1000		
Stack lifetime (Operating hours)	60000 – 90000	90000 – 100000	100000 – 150000	30000 – 90000	60000 – 90000	100000 – 150000	10000 – 30000	40000 – 60000	75000 – 10000
Load range (%, relative to nominal load)	10–110			0–160			20–100		
Plant footprint (m^2/kW_e)	0.095			0.048					
CAPEX (USD/kW_e)	500 – 1400	400 – 850	200 – 700	1100 – 1800	650 – 1500	200 – 900	2800 – 5600	800 – 2800	500 – 1000

According to data reported by the IEA, by 2020 alkaline electrolyzers dominate global installed capacity with 61%, while PEMs have a 31% share. The remaining 8% of installed capacity is unspecified electrolyzer technology and SOECs [25]. From a technological point of view, SOECs electrolyzers are not a mature technology to operate on a large scale, which means that they are only available in demo or laboratory versions. Because of the latter, this study focused only on PEM and alkaline electrolyzers.

2.3.2.1. Alkaline Electrolyzer

Alkaline electrolyzers are the most developed and commercially available technology for producing hydrogen at significant rates today. Their principle of operation is based on the immersion of the two electrodes in an alkaline liquid electrolyte (pH > 7) of KOH (caustic) which is circulated through the electrolytic cells. The operating range of alkaline electrolyzers covers a minimum load of 10% to full design capacity, and as they do not require precious materials, capital costs are relatively low compared with other electrolyzer technologies.

2.3.2.2. Polymer Electrolyte Membrane Electrolyzer (PEM)

A proton-exchange membrane or polymer-electrolyte membrane (PEM) technology differs from alkaline electrolysis because it does not require any electrolytic liquid. In this case, a thin splitting polymer membrane is used, allowing a close proximity of the electrodes [27]. The area requirements of PEM electrolyzer systems are relatively small, making them potentially more attractive than alkaline electrolyzers in dense urban or industrial areas. However, current materials for electrode catalysts (platinum, iridium), bipolar plates (titanium) and membrane materials are expensive, so overall costs for PEMs are higher than for alkaline electrolyzers.

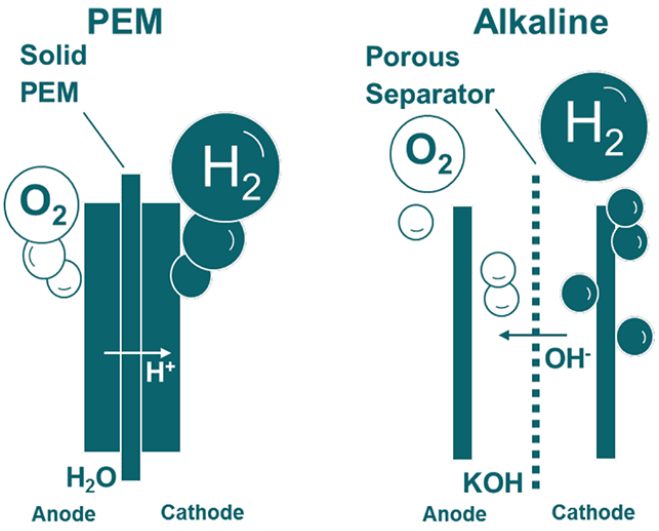

Anode	$H_2O \rightarrow \frac{1}{2}O_2 + 2H^+ + 2e^-$	$2H_2O + 2e^- \rightarrow 2OH^- + H_2$	Anode
Cathode	$2H^+ + 2e^- \rightarrow H_2$	$2OH^- \rightarrow \frac{1}{2}O_2 + H_2O + 2e^-$	Cathode
Total reaction	$H_2O \rightarrow \frac{1}{2}O_2 + H_2$	$H_2O \rightarrow \frac{1}{2}O_2 + H_2$	Total reaction

Figure 5: Schematic of PEM and alkaline electrolyzers [20]

2.4. Hydrogen Storage

In order to be used for energy purposes, hydrogen must first be obtained and then stored. The main hydrogen storage methods that have been tested and evaluated include storage in physical form (as either a gas or a liquid), in solids (hydrogen may be adsorbed onto or into a material) and in other compounds (metal hydrides, organic carriers, adsorbent materials, among others). The currently most commercially feasible options for hydrogen storage are compression at high pressure and liquefaction at cryogenic temperature (i.e., gaseous and liquid storage, respectively); therefore, they were the storage methods considered by this study.

2.4.1. Compressed Gaseous Hydrogen (GH_2)

The most common method to increase the volumetric energy density of gaseous hydrogen is to compress it to very high pressures (between 350 and 900 bar) for storage, using a series of compressors and stepwise compression until the desired pressure is reached. Therefore, tanks storing hydrogen under these conditions must be made of carbon fiber lined with aluminum, steel, or specific polymers to withstand high stresses, as well as a large number of fatigue cycles due to tank loading and unloading. The main components of a pressurized hydrogen storage tank are shown in Figure 6.

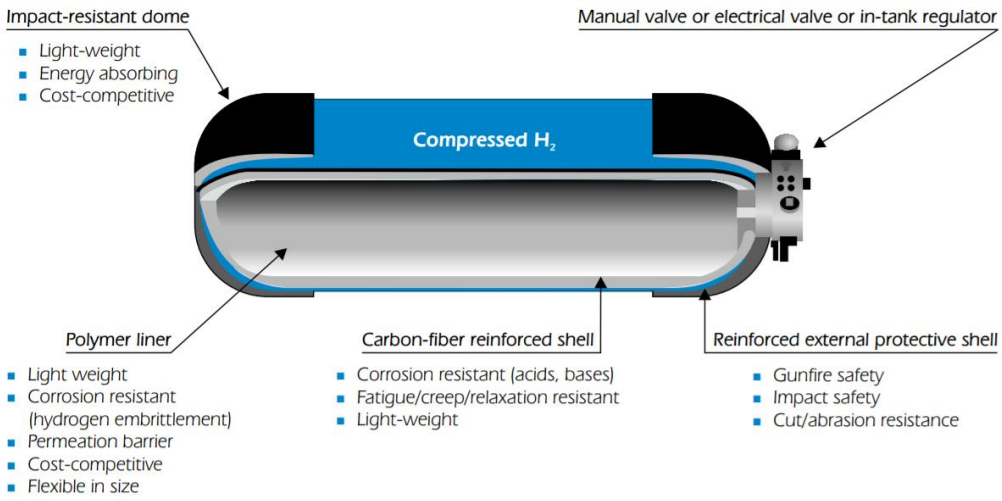

Figure 6: Schematic of a typical compressed H_2 gas composite tank [28]

2.4.2. Liquid Hydrogen (LH_2)

Hydrogen can also be stored as a liquid at very low temperatures (-253°C). Liquefaction reduces the volume to approximately 1/800 of the gaseous state (and therefore less space is required), making mass transport far more efficient, but technically challenging to store due to cryogenic temperatures. In this state, it is under near atmospheric pressure, so storage tanks do not require pressure strength, but must be heavily insulated, to retain the sub-zero temperature and to minimize the evaporation losses caused by thermal leakage (boil-off). The main components of a liquid hydrogen storage tank are shown in Figure 7.

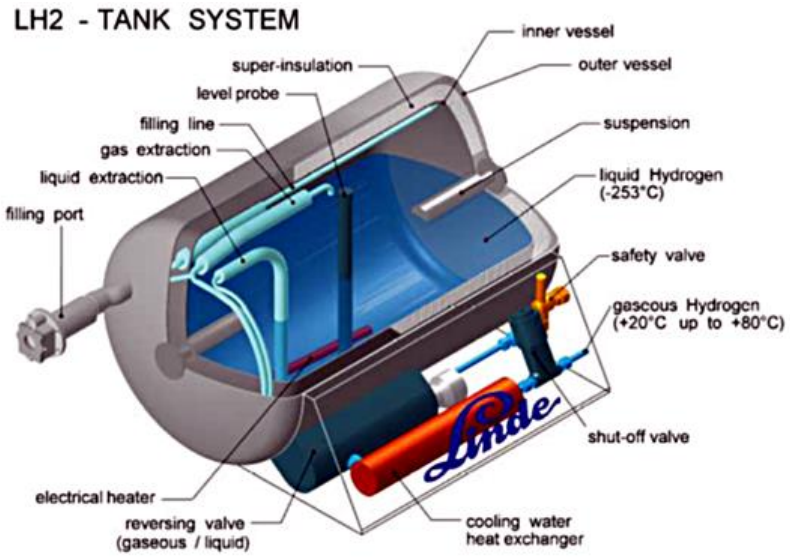

Figure 7: Schematic of a typical liquid hydrogen storage tank [29]

2.5. Hydrogen Economy

As previously stated, hydrogen can be produced from different energy sources and technologies, however, global hydrogen production is currently dominated by the use of fossil fuels, the lowest cost option. To compare different production methods from an economic point of view, the most commonly used metric is the levelized cost of hydrogen ($LCOH_2$). This metric is an economic measure used to compare the lifetime costs of a hydrogen production plant with the total amount of hydrogen expected to be produced during the lifetime of the plant, expressed as cost per kg of hydrogen produced (USD/kg_{H2}). The formula used to calculate the $LCOH_2$ and further details on this metric are provided in the Methodology section.

Figure 8 shows the current and projected levelized cost of hydrogen from different technologies. It is clear that today, renewable energy production is significantly more expensive than hydrogen from fossil fuels. In particular, steam reforming of natural gas (the reference production method for hydrogen) is in the range of USD 0.50 - 1.70 / kg_{H2}, while the use of renewable energy is between USD 3.00 - 8.00 / kg_{H2}.

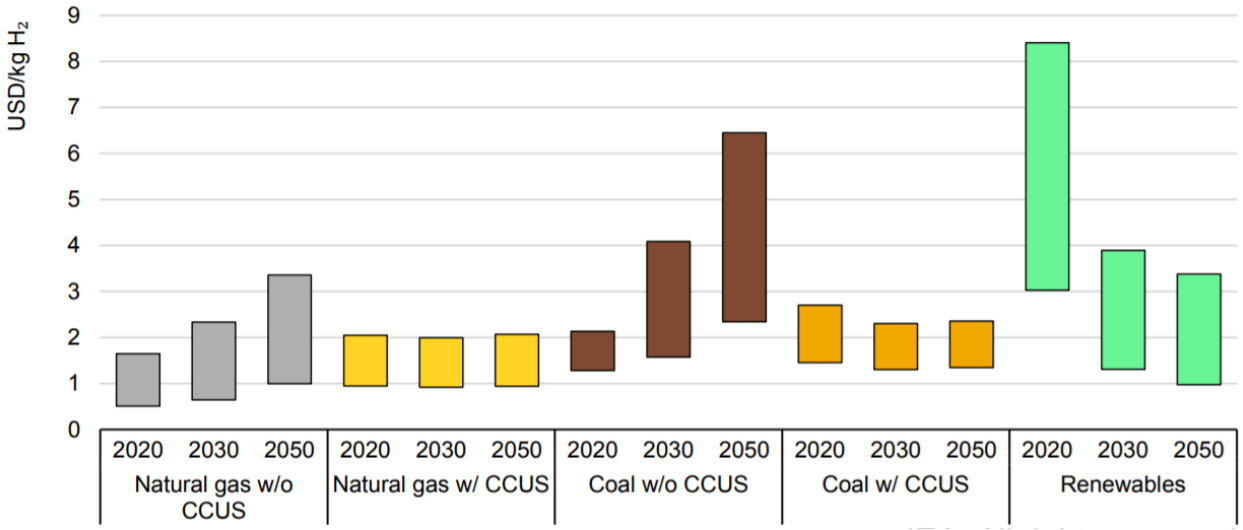

Figure 8: Levelized cost of hydrogen production by technology in 2020, 2030 and 2050 [25]

Although the production of hydrogen from renewable energies is currently not the most economical method, the use of natural gas and coal means that hydrogen production generates significant CO_2 emissions. Because of this, the deployment of electrolysis from renewable energies as a source of electricity is the way forward to produce zero-emission or green hydrogen. Figure 9 shows the levelized cost of hydrogen production from solar PV and wind (offshore and onshore) for 2020 and 2050.

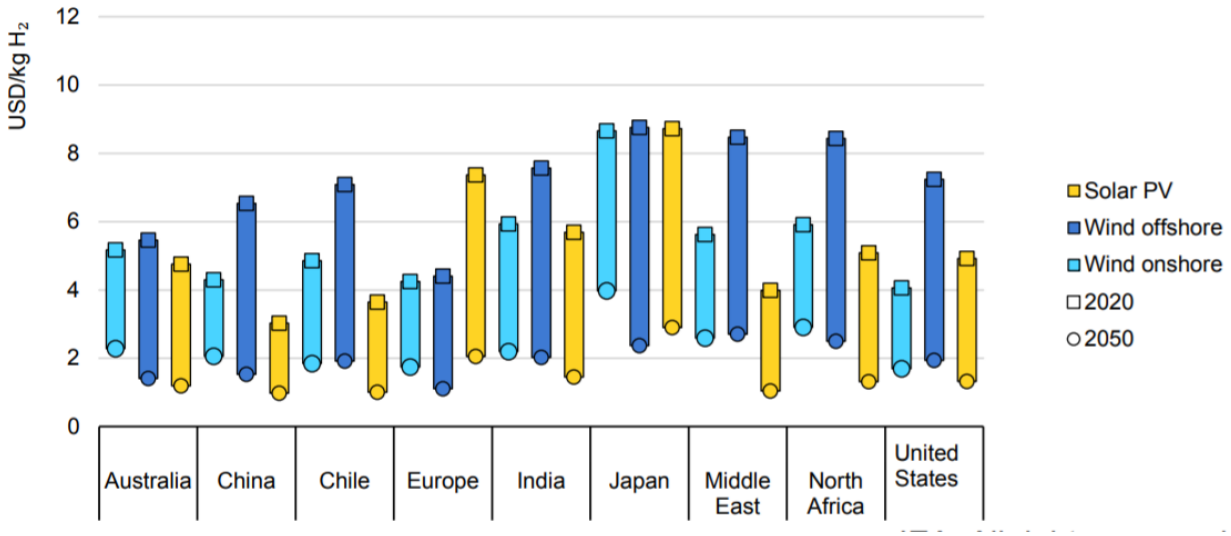

Figure 9: Levelized cost of hydrogen production from renewables by technology and region, 2020 and 2050 [25]

Within the technical and economic factors that determine the cost of producing hydrogen from water electrolysis, the most pertinent are electricity costs, electrolyzer capital expenditure (CAPEX), conversion efficiency and annual operating hours. For a better understanding of how some of the parameters influence the cost of hydrogen from electrolysis, the IEA generated the graph in Figure 10 [30]:

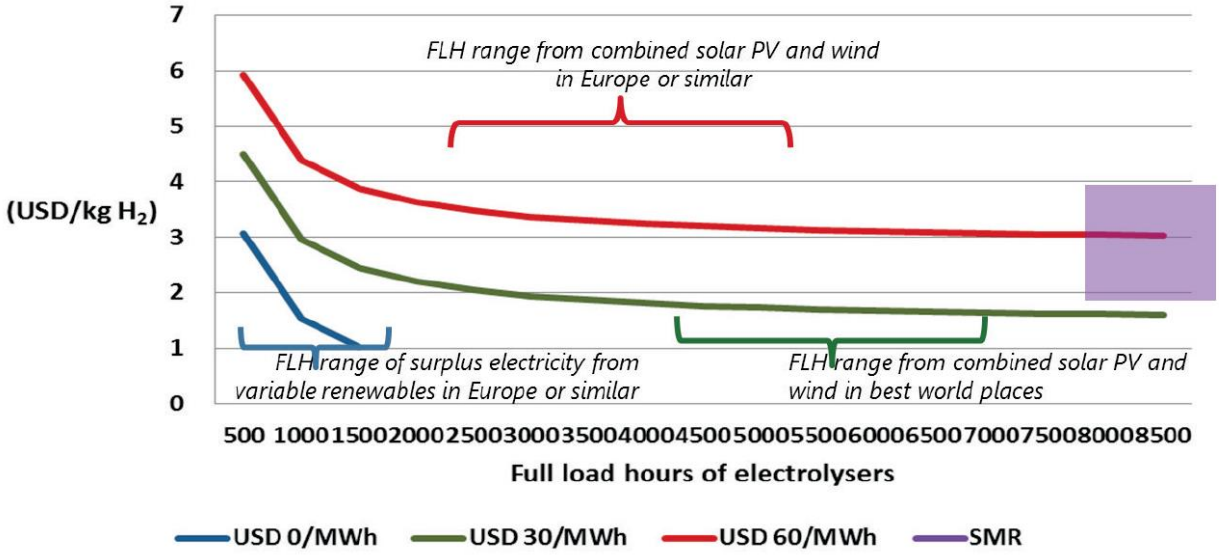

Figure 10: Cost of hydrogen from electrolysis for different electricity costs and load factors [30]

As can be seen in Figure 10, the higher the load factor of the electrolyzer, the cheaper the cost of a unit of hydrogen, because the fixed investments are diluted in a higher amount of hydrogen production. Additionally, if the cost of electricity is sufficiently low, it is possible to produce green hydrogen more cost-effectively than from fossil sources (purple rectangle). The blue line symbolizes the "surplus" electricity supply from variable renewable energies, which is assumed to have no economic value as it represents a curtailment and is therefore available only occasionally. The red line represents the cost of hydrogen from wind power or utility-scale PV plants in areas with good but not exceptional resources, and the green line represents the possible cost of hydrogen from solar and wind power in the world's best resource areas, as in the case of northern Chile.

In its report "The Future of Hydrogen" [23], the IEA also studies the relationship between the cost of electricity, load factor and cost of hydrogen production, but this time it incorporates the effect that the CAPEX of the electrolyzer has on the cost of producing hydrogen, as shown in Figure 11. The analysis shows that with low operating hours, the investment cost dominates, as it is spread over a smaller amount of hydrogen. This could happen when using only curtailed electricity, or coupling with PV without any storage or backup. The electricity cost becomes dominant as the number of operating hours increases; therefore, a combination of low electricity costs and high load factors would allow renewables-based hydrogen generation to compete with Steam Methane Reforming (SMR), its closest competitor.

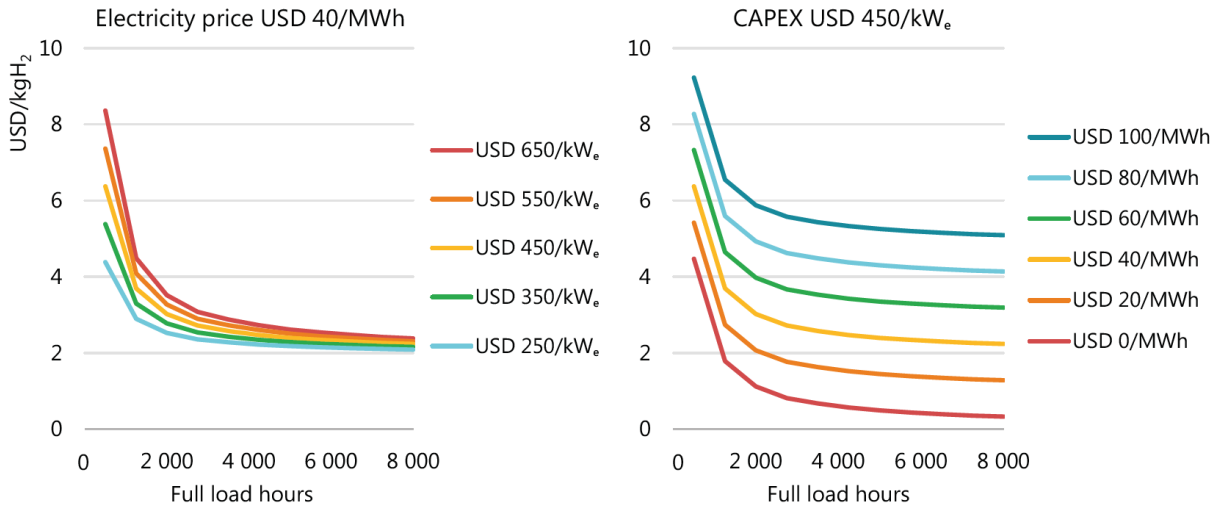

Figure 11: Future levelized cost of hydrogen production by operating hour for different electrolyzer investment costs (left) and electricity costs (right) [23]

In conclusion, it is clear that reducing CAPEX is crucial when there are less than 3000 operating hours per year, i.e., a low load factor. However, if the load factor increases, it is not the capital cost of electrolyzers that dominates, but the cost of electricity to compete against fossil-fuel-derived hydrogen, which represents a great opportunity for high-potential countries for low-cost renewable electricity generation, such as Chile.

2.6. Chile's National Green Hydrogen Strategy

In order to reach national and international climate targets and to reduce the dependency on fossil fuels, Chile has set out to promote the hydrogen industry. On 3rd November 2020, the Government of Chile launched the National Green Hydrogen Strategy, which has three main objectives:

- Have 5 GW of electrolysis capacity under development by 2025
- Produce the cheapest green hydrogen on the planet by 2030
- Be among the top 3 exporters by 2040

Based on these three objectives, it is clear that Chile has ambitious goals to be a reference for Green Hydrogen in international markets. Nevertheless, Chile competes with other countries, such as Australia, South Africa, Morocco and the Middle East, which are geographically closer to the main consumers (Japan, Korea, China and Europe). However, Chile has the potential to be one of the most efficient and competitive producers of green hydrogen in the world, due to its enormous wealth of renewable energies.

2.7. Green Hydrogen Projects in Chile

Although at the time of writing this thesis several initiatives are already in portfolio or in progress within the framework of the National Green Hydrogen Strategy promoted by the Government of Chile, the main ones are presented below:

- **HyEx Project**

It is a project of the ENGIE company that contemplates both the use of solar energy and energy from the grid to produce green hydrogen in the Antofagasta region, which will be used in the Haber-Bosch process to produce ammonia destined for Enaex's Prillex plant for the production of explosives for the mining industry.

- **AES Gener**

The AES project contemplates the use of desalinated water for the production of hydrogen in northern Chile, which will be used for the production of ammonia. The power source to use has not yet been specified.

- **Cerro Pabellón Geothermal Power Plant**

It is a project of the company Enel Green Power in conjunction with ENAP, which is located in the workers' camp of the geothermal plant "Cerro Pabellón" at 4,500 meters above sea level in the commune of Ollagüe, Antofagasta Region. The project consists of a hybrid renewable plant, based on a 50 kW PEM electrolyzer together with lithium batteries and photovoltaic modules, to supply electricity to remote microgrids operating in island mode 24/7. This project covers the energy needed for the water treatment plant and the central building of the Cerro Pabellón workers' camp of more than 600 technicians working at the plant, reducing diesel fuel consumption by more than 90%.

- **HYDRA Project**

This project is led by the Australian-based applied research center CSIRO Chile, ENGIE and Mining3, and it consists of designing and manufacturing a new powertrain that allows mining vehicles to operate 100% on green hydrogen to replace the use of diesel. This will allow conventional vehicles to be replaced by these new vehicles composed of state-of-the-art batteries and hydrogen fuel cells.

- **Haru Oni Hydrogen Project**

The Haru Oni project (HIF pilot project) is part of Siemens Energy, together with several international companies, seeking to develop and implement the world's first large-scale integrated and commercial plant for the production of environmentally-friendly and climate-neutral fuel. The project uses wind energy from the strong, steady winds of Magallanes, Chile's southernmost region, to split water through a process of electrolysis, producing oxygen and hydrogen. The hydrogen is combined with captured carbon dioxide to produce synthetic methanol. Finally, some of the methanol is converted into synthetic gasoline, coined by the developer as e-gasoline.

- **HNH Project**

This project is owned by the Austrian companies AustriaEnergy and Ökowind, together with Trammo, a commodities trader based in the United States. The project contemplates the use of wind energy and desalinated water for the production of hydrogen in the Magallanes region, which will be used for the production of ammonia, the basis to produce fuels, fertilizers, textiles, sanitizers, steel, explosives, refrigerants, food preservatives, chemicals, electricity, among others.

2.8. Potential for Solar Hydrogen Production in Chile

One of the largest individual cost components for green hydrogen production is the cost of the renewable electricity needed to feed the electrolyzer. Due to the latter, a low cost of electricity is a very important condition to reduce the cost of hydrogen production. This creates an opportunity to produce hydrogen at locations around the world that have optimal renewable resources, such as the Atacama Desert in northern Chile. In this sense, according to the IEA [23], Chile is among the most promising countries to produce green hydrogen at low cost, through photovoltaic and wind energy, due to the great solar potential of the Atacama Desert and the strong winds from Patagonia in Magallanes, as shown in Figure 12.

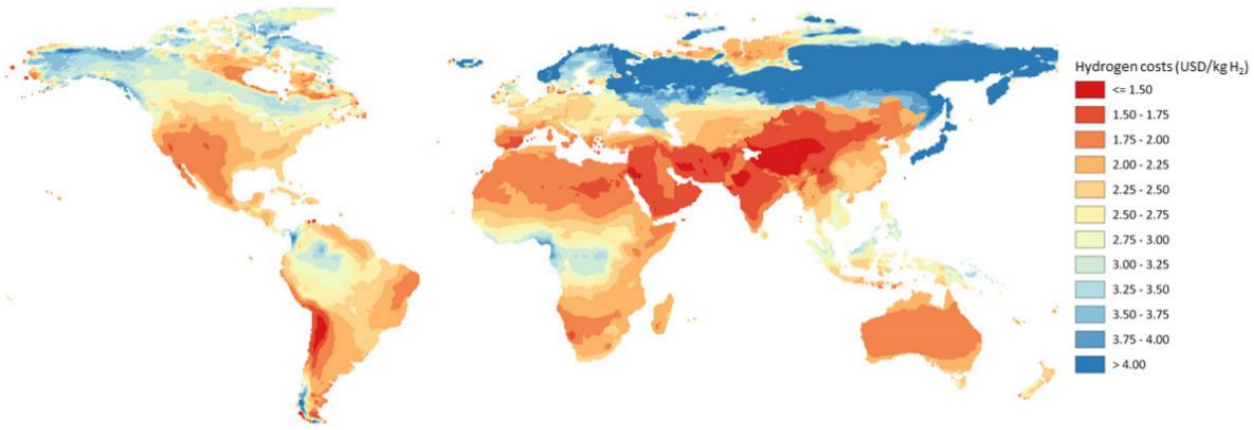

Figure 12: Hydrogen production cost from hybrid solar PV and wind systems in 2030 [25]

In recent years, there has been an increasing amount of literature claiming that Chile's Atacama Desert has the highest levels of solar irradiance in the world. In this sense, Chile has a great opportunity to collect part of that energy and use it to produce heat and electricity in most of its territory, considering the Global Horizontal Irradiance (GHI), the Direct Normal Irradiance (DNI), the availability of vast land and a growing energy demand [31]. On the one hand, GHI is the sum of direct and diffuse radiation received on a horizontal plane and is a reference for PV applications. On the other hand, DNI is the only component that can be reflected and concentrated; therefore, it is one of the most crucial aspects when assessing and optimizing a CSP plant. The potential of these components of solar radiation in the Chilean territory is clearly reflected in Figure 13:

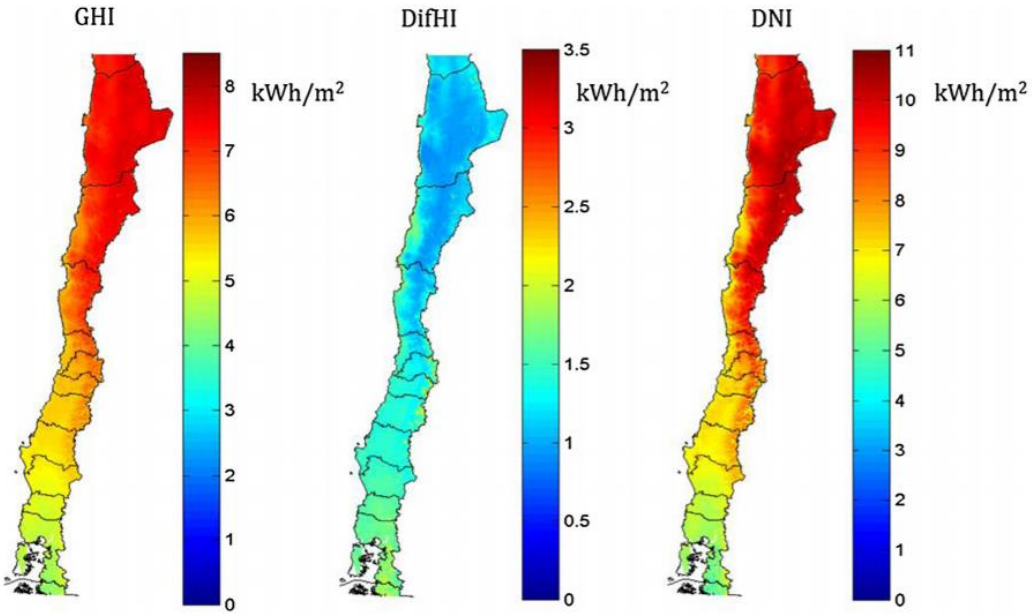

Figure 13: Daily totals of radiation in yearly average [31]

As shown in Figure 13, thanks to its geography, the Atacama Desert has one of the highest levels of solar radiation in the world. Higher levels of solar radiation led to higher energy production and therefore a lower LCOE (Levelized Cost of Energy), i.e., the average cost per unit electricity (usually expressed in USD/MWh). The formula used to calculate the LCOE and further details on this metric are provided in the Methodology section.

2.9. Power Purchase Agreements (PPA)

A PPA (Power Purchase Agreement) is an agreement or contract for the sale of energy between a generator and an "off-taker", generally for a fixed period of time and at an agreed price that is profitable for both parties, as illustrated in Figure 14. On the one hand, power generators seek to achieve these PPAs because they secure a stable selling price over a long period of time and revenues with which to finance their projects. On the other hand, buyers secure a stable and predictable cost of energy without being exposed to fuel price volatility.

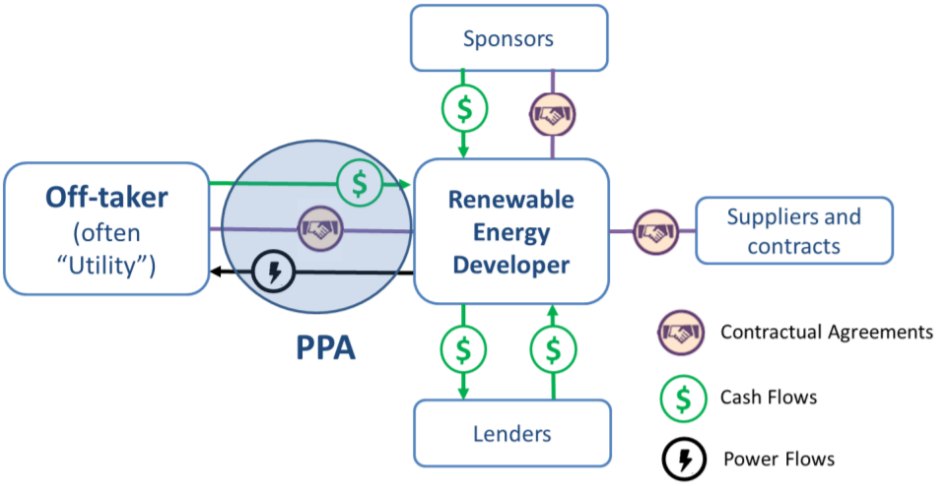

Figure 14: PPA Model [32]

In general, there are two main types of PPAs: off-site and on-site. Off-site green PPAs are those where the energy production does not take place on the customer's premises. The advantage of off-site schemes is that they allow for the development of larger capacity plants with better locations for electricity production. However, as there is no direct physical delivery of power, the electricity is transmitted through the grid and mixed with power production from other power plants, so there is no certainty of the green origin of each MWh contracted under the PPA mechanism. In contrast, a green on-site PPA is one where the renewable energy production is located at the customer's site, thus ensuring that all energy produced at the facility is 100% renewable.

2.10. Solar Energy Technologies

In general, there are two ways to transform solar energy to electricity: concentrated solar power (CSP) and photovoltaic (PV). The following sections provide background on these two technologies and the hybridization of them.

2.10.1. Solar Photovoltaic (PV)

Photovoltaic solar energy (PV) is obtained by converting sunlight into electricity using a technology based on the photoelectric or photovoltaic effect. When the sun's radiation falls on one of the faces of a cell (or an array of solar cells, called modules), a difference in electrical potential is produced between the two faces that causes electrons to jump from one place to another, thus generating electrical current.

Currently PV systems are the most widely deployed solar technology in Chile, with an installed solar PV generation capacity of 4,341.74 [MW] (until November 2021) [33]. Although the installed capacity has grown considerably in recent years, its true potential is still under development. According to GIZ, Chile has a solar PV potential of 1,237,903 MW (fixed array) and 1,640,128 MW (tracked array).

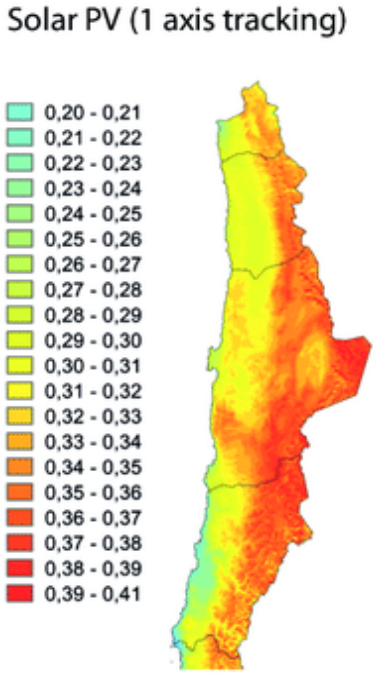

Figure 15: Potential capacity factors for solar PV in the North of Chile [34]

An important metric to evaluate the output of a PV plant is the plant factor, i.e., the ratio between the real energy generated by a power plant and the energy generated if it had worked at 100% (rated capacity). In other words, the plant factor is a measure of the capacity utilization of the plant over time. Figure 15 shows the annual plant factor distribution of PV configuration with tracking in northern Chile. From this figure it can be seen that the north of Chile is a zone that concentrates areas with annual PV plant factors of more than 30%, which is quite high for this type of technology, compared to other areas with less solar resources, which reach average values of only 20%.

Photovoltaic systems have long been integrated for multiple purposes. Due to the nature of this research, one application that arouses the most interest is using photovoltaic energy for the production of green hydrogen. The most common method of solar-based hydrogen production utilizes photovoltaic (PV) cells in combination with water electrolysis. In the system illustrated in Figure 16, PV cells are used to create electrical energy to feed the electrolyzer, which passes this electric current through water, causing the water molecules to separate into hydrogen and oxygen gases.

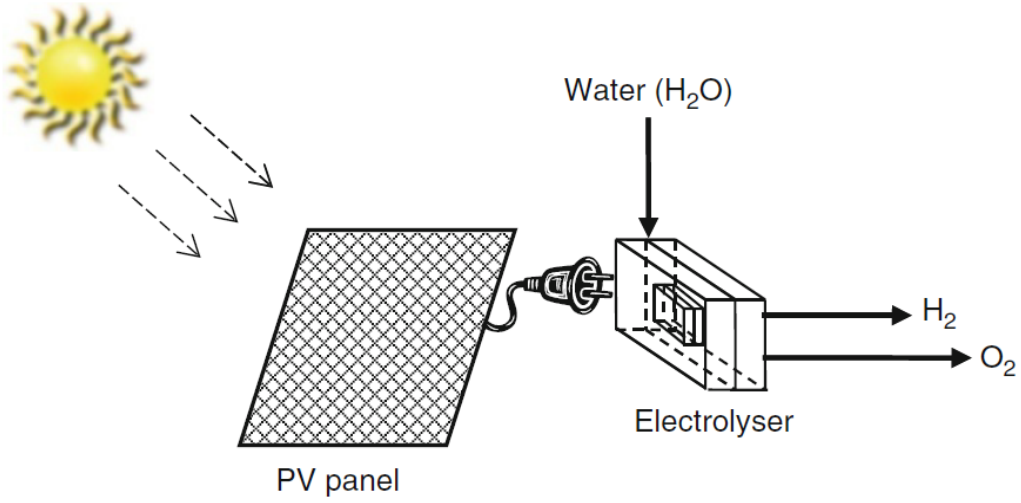

Figure 16: Schematic diagram of photovoltaic hydrogen production system [26]

2.10.2. Concentrated Solar Power (CSP)

Another method of converting solar energy to electricity is with concentrated solar power (CSP) technology. Unlike PV technology which is a direct conversion, CSP first generates thermal energy through high-temperature heat from mirrors that concentrate the sun's energy onto a receiver to create steam, which can be used directly, or to drive turbines and generators in a conventional steam Rankine cycle. At present, CSP technologies exist in four optical types:

a) Line-Focusing Systems:

- **Parabolic Trough Collectors (PTC)**

A parabolic trough is a type of solar thermal collector that tracks the diurnal position of the sun with the complete parabolic mirror structure on a fixed horizontal axis. A PTC uses a mirror in the shape of a parabolic cylinder to reflect and concentrate the sun's rays on a focal line (absorber tubes). The receiver absorbs the incoming radiation and transforms it into thermal energy which is collected by a heat transfer fluid (HTF) circulating within the receiver tube. This method can be used to generate thermal energy for industrial processes or to produce electrical energy.

- **Linear Fresnel Reflector (LFR)**

A linear Fresnel reflector is a linear focus system that uses a series of long rows of slightly curved mirrors to concentrate the sun's rays onto a tube (absorber) that is mounted above the mirrors. These mirrors generally have an independent tracking system of an axis fixed to a steel structure on the ground, to follow the movement of the sun.

b) Point-Focusing Systems:

- **Solar Parabolic Dish (SPD)**

A parabolic dish is a point-focus concentrator which focus the sun's rays on the focal point of the dish. The thermal energy can then be either converted into electricity using an engine–generator coupled directly to the receiver or transported through pipes to a power conversion system.

- **Solar Power Tower (SPT)**

The solar power tower (also denominated central receiver system) is a type of power plant that uses a large number of individually tracking mirrors (called heliostats) to focus the sun's rays onto a fixed receiver located on the top of the tower. Solar tower systems have qualities that make them of special interest for power generation, such as a high concentration factor that can range from 500 to 1000, which means higher receiver temperatures and therefore higher efficiencies, as shown in Table 3.

Table 3: Comparative table of technical parameters of CSP technologies [12]

Items	PTC	LFR	SPT	SPD
Capacity, MWe	10–200	10–200	10–150	0.01–0.4
Operating temperature range, ◦C	150–400	150–400	300–1200	300–1500
Annual efficiency from solar to electricity, %	15	8–10	20–35	20–35
Required area, m^2/MWh	4–6	6–8	8–12	30–40
Maximum efficiency of the plant, %	14–20	~18	23–45	~30
Water requirement, m^3/MWh	3 (wet cooling) 0.3 (dry cooling) 0.4–1.7 (hybrid)	3 (wet cooling) 0.2 (dry cooling)	2–3 (wet cooling) 0.25 (dry cooling) 0.1–1 (hybrid)	0.05–1 (For cleaning mirrors)
Molten salt storage	Commercially Available	Possible but not proven	Commercially Available	Possible but not proven
Steam conditions, ◦C/bar	380 to 540/100	260/50	540/100 to 160	Does not apply

Graphically, the four main CSP design typologies are shown in Figure 17:

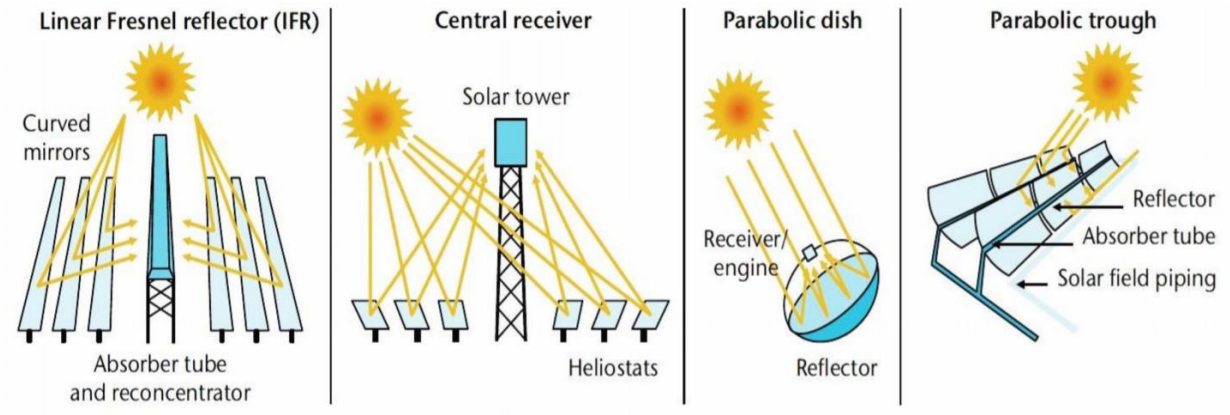

Figure 17: Main CSP technologies [35]

Like PV technology, CSP could also be integrated into an electrolyzer for water electrolysis. An alternative is to use concentrating solar power (CSP) to first generate electrical power, which can be later utilized to run an electrolysis plant, as shown in Figure 18.

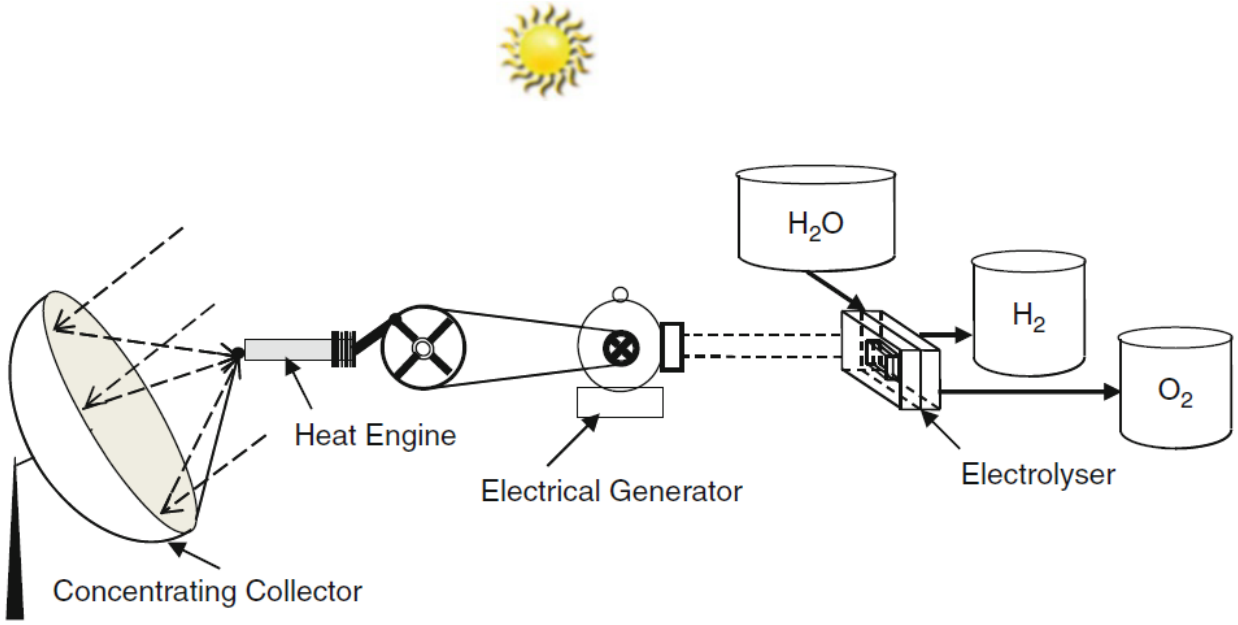

Figure 18: Schematic of a solar thermal hydrogen production system [26]

Although virtually any type of CSP technology could be integrated into hydrogen production, this study is limited to solar power tower systems because of the higher system efficiency compared to line-focus CSP systems and due to the exceptional conditions offered by some areas of Chilean territory for the large-scale development of this type of technology [36].

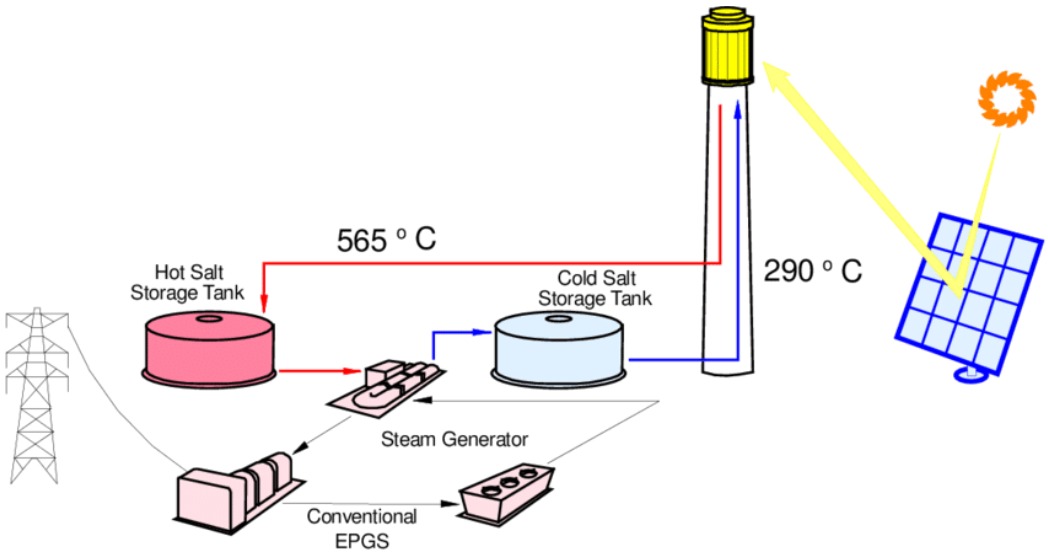

Figure 19: Molten salt power tower system configuration [37]

Figure 19 shows a flow diagram of a solar power tower or central receiver system, a solar thermal power generation technology currently under extensive development worldwide. Its principle of operation is based on the concentration of normal direct solar radiation (DNI) by means of a solar field of mirrors or heliostats, which reflects the radiation at the top of the tower. Subsequently, molten salt from the cold tank circulates around the receiver heating from 290°C to 565°C and then flows in pipes to the thermal storage. The salt will be used to generate steam inside a molten salt steam generator. The steam feeds a Rankine cycle turbine, where the energy of this steam is converted into rotating mechanical energy, which is eventually transformed into electricity. Finally, the cooled salt is returned to the cold thermal storage system to repeat the cycle. A recent study carried out by [38], reveals that Chile presents areas with great potential for the development of large-scale central receiver concentrated solar power plants, due to a low levelized cost of energy. Additionally, the same study concludes that the best zone is located among the Arica and Parinacota region and the northern part of the Coquimbo region, which shows an average cost of 89 USD/MWh, with a minimum of 76 USD/MWh near Copiapó, as shown in Figure 20.

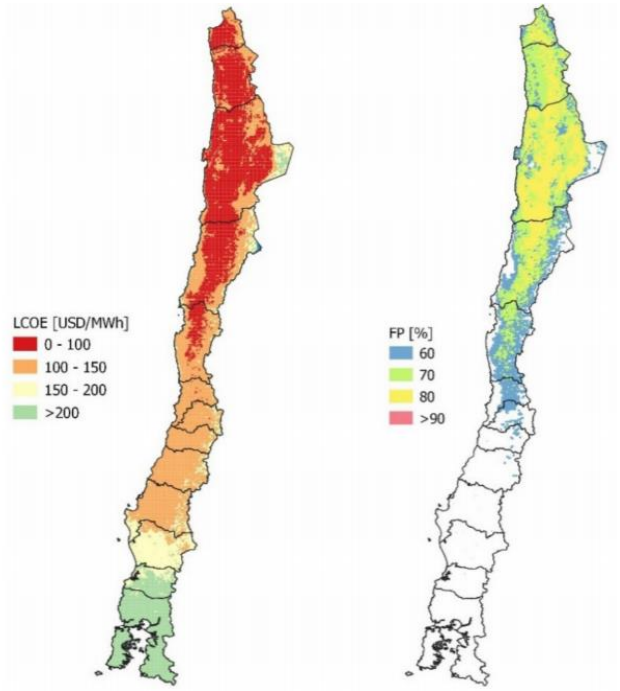

Figure 20: LCOE and Plant Factor Maps of CSP Towers in Chile [38]

A solar tower (or central receiver) system consists of the following main subsystems:

- **Tower:** concrete or steel tower that houses the receiver on top.

- **Heliostat field:** a large number of solar-tracking mirrors (called heliostats) to reflect the sun's rays onto a receiver at the top of the tower.

- **Receiver:** absorbs concentrated solar energy and transfers that heat to a flowing medium.

- **Storage:** heat storage system that allows the generation of electricity when there is insufficient solar energy available. For this thesis, a 2-tank molten salt (60% $NaNO_3$ 40% KNO_3) system is considered, which is directly connected to the tower. At design conditions, molten salt enters and exits the receiver at 290°C and 565°C, respectively.

- **Power block:** power cycle that converts thermal energy into electricity. Current utility-scale systems generate electricity primarily through a conventional steam Rankine cycle.

Two key parameters for the design of this type of CSP technology are the solar multiple and the TES hours, i.e., the thermal storage capacity of the plant.

- **Solar Multiple (SM)**

The solar multiple describes the relation between the thermal power produced by the solar field at the design point and the thermal power required by the power block at nominal conditions. For instance, a CSP plant with a solar multiple equal to 1 has a solar field large enough to provide the rated capacity of the turbine under nominal irradiation conditions (plants without storage). On the other hand, a CSP plant with a solar multiple greater than 1 means that there is more energy to collect than the engine can transform and therefore thermal energy storage (TES) is required; otherwise, the energy is lost, as shown in Figure 21:

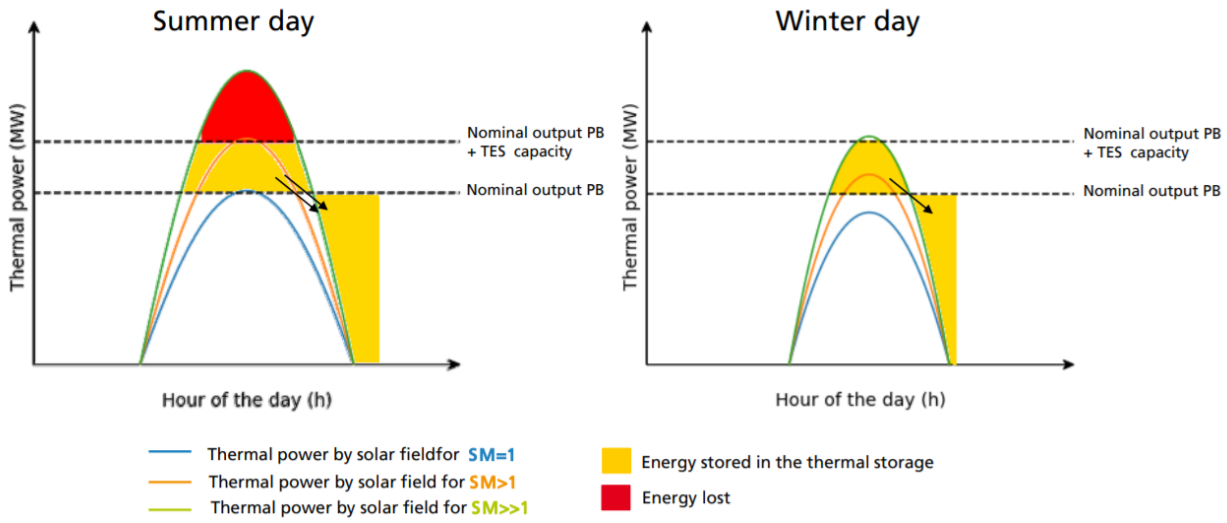

Figure 21: Daily thermal power production for different solar field multiples [39]

- **Full Load Hours of Storage**

This metric indicates the number of hours the CSP plant can operate at full load (rated capacity) with the storage system as the only energy source. Thermal energy storage not only makes the system more dispatchable, it also makes it more cost-effective and improve its performance by reducing the mismatch between supply and demand. With the use of TES, CSP tower plants decouple solar energy collection from electricity generation, allowing the technology to generate stable grid power through cloudy periods and throughout the night.

The metrics described above must be chosen carefully. If the solar multiple is too large, the solar heat collected without thermal storage would be wasted and unnecessarily high investment costs would result. On the other hand, as the storage hours and the thermal capacity of the storage system increase, the costs will also increase, so a cost-effective analysis is required for the overall system.

2.10.3. Concept of Hybrid CSP+PV Power Plants

A CSP+PV hybrid plant consists of the combination of photovoltaic (PV) and concentrating solar power (CSP) technologies to take advantage of the best qualities of each and minimize their weaknesses to generate electricity. Figure 22 shows a conceptual diagram of a hybrid solar plant:

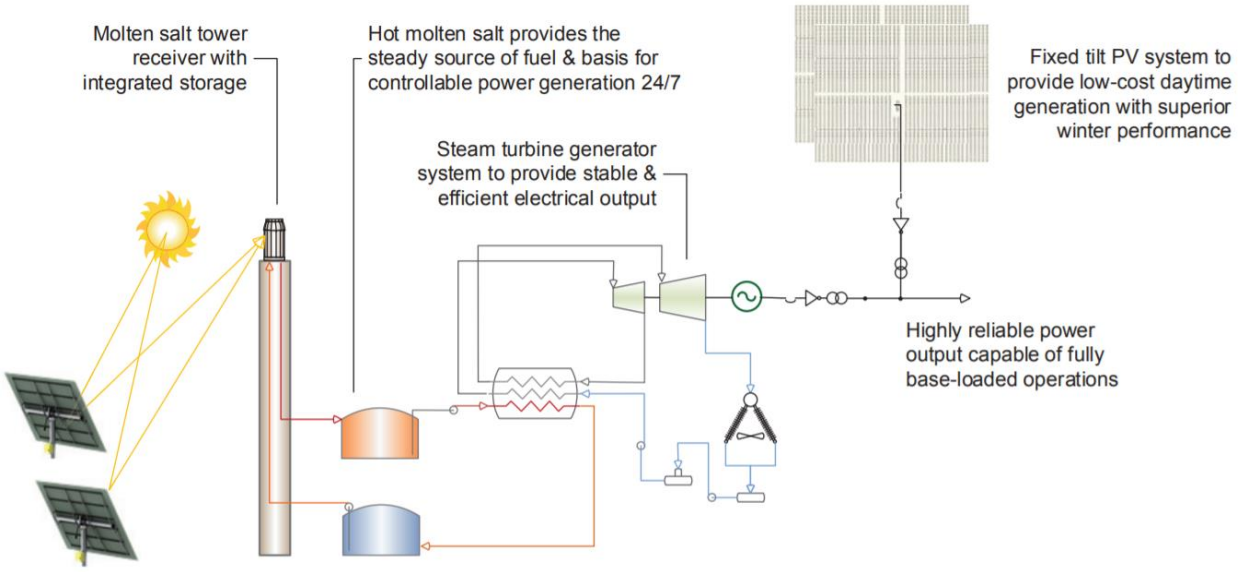

Figure 22: Schematic diagram of hybrid solar power plant [40]

A hybrid solar plant can achieve the following characteristics:

- This combination of technologies makes it possible to produce reliable, safe, efficient and clean energy that reduces, or even completely eliminates, the polluting emissions associated with the use of fossil fuels. In addition, it has higher overall efficiency in contrast to a stand-alone CSP plant.

- Reduce the levelized cost of energy (LCOE) compared to a stand-alone CSP plant. In particular, hybrid solar plants could achieve an intermediate (but not necessarily average) cost between PV and CSP. On the one hand, the PV plant has priority dispatch during solar hours, as it is a cheaper technology. On the other hand, the CSP plant responds to PV generation by trying to achieve a nominal power or base load during hours of low or no solar radiation, using the energy stored in the TES system.

- Achieve higher capacity factors than stand-alone plants, thus facilitating a more flexible and dispatchable operation. This improvement in the capacity factor is due to the fact that the PV energy is used during sunshine hours, while the CSP system stores the energy produced for use when there is no more solar radiation, mitigating the effects of the variability of solar production under intermittent conditions.

Hybrid solar plants are not just a theoretical concept, but a reality in Chile. In fact, on 8th June 2021, the Cerro Dominador project was officially inaugurated, which includes a 100 MW_e PV plant and a 110 MW_e molten salt tower, with a thermal storage capacity in molten salts of 17.5 hours.

Figure 23: CSP-PV hybrid power plant Cerro Dominador, Maria Elena/Chile [41]

This combination of solar technologies, which allows a less variable power supply to an electrolyzer, could lead to competitive hydrogen production costs. The latter is explained by the fact that two of the main parameters affecting the final cost of producing each kilogram of hydrogen are precisely the cost of electricity and the load factor of the electrolyzer, i.e., the hours of operation or use of this device, which is limited by the capacity factor of the renewable plant. Indeed, in November 2021, a couple of months after the start of this thesis, the Cerro Dominador project was awarded funds from the European Union's Directorate-General for International Partnerships and the Chilean Agency for International Development Cooperation (AGCID) for the development of green hydrogen projects [42]. In particular, they will carry out a study, together with the international consultant CEA-Liten (French Institute for Energy Transition), to assess the techno-economic feasibility of hydrogen production and green fuels, using 24/7 clean energy from the combination of photovoltaic and concentrating solar power, which is precisely the main objective previously set for this thesis.

2.10.4. State of the Art of Hybrid CSP+PV Power Plants

In recent years, there has been an increasing amount of literature on hybrid solar plants with particular emphasis on electricity production. However, currently very little is known about the use of hybrid solar plants for the production of green hydrogen.

In 2015, Green et al. [40] published a paper in which they described a tower CSP plant of 100 MW_e hybridized with a 60 MW_{ac} PV plant in Chile's Atacama Desert. The authors also analyzed the effect of the PV tilt angle, concluding that for a fixed-tilt PV system with a high tilt angle (in order to minimize seasonal differences) it is possible to achieve capacity factors up to about 90%, whereas stand-alone CSP technology only 80%. Also in 2015, Platzer [43] showed that by an appropriate combination of CSP and PV it is possible to achieve capacity factors higher than 70% and lower costs than a stand-alone CSP solar plant, which would have to increase the size of the solar and storage field for comparable power outputs.

In 2016, Petrollese, M., & Cocco, D [5] reported a hybrid solar power generation system based on a PV system with a battery bank and Fresnel-type collector with a direct two-tank TES system. The results indicated that the hybrid solar plant provides 30-40% less cost than a stand-alone Fresnel plant, depending on the location analyzed. In another major study, Cocco et al. [44] analyzed the advantages of hybrid solar systems in terms of dispatchability. The authors demonstrated that the combination of Parabolic Trough (PTC) and Concentrating Photovoltaic (CPV) leads to an efficient use of the dispatch capacities of the PTC plant thanks to the TES section, while the CPV plant is fully utilized, especially during hours of high solar radiation, to satisfy a constant power curve. This view is supported by Starke et al. [4] who found that competitive energy costs can be achieved while maintaining capacity factors higher than 80% for hybrid solar power plants.

In the same vein, Parrado et al. [6] analyzed the economic performance of CSP + PV systems in the Atacama Desert, Chile. This study calculated the LCOE up to 2050 for three solar plants: stand-alone PV, a stand-alone CSP with 15 hours of TES and a hybrid PV-CSP plant consisting of 20 MW_p of PV and 30 MW_e of CSP with 15 hours of TES. The authors concluded that the PV-CSP hybrid plant is a feasible option for electricity generation, as well as being effectively able to meet the electricity demand profile of the mining industry in the area, reducing the carbon footprint, with specific energy costs reaching values between 80 and 90 USD/MWh by 2050. Similarly, in a study conducted by Pan and Dinter [45], it was shown that a hybrid solar plant located in South Africa (100 MW_e of PV and 100 MW_e of CSP) could achieve higher annual energy yields than stand-alone plants and capacity factors of up to 90%. This combination of solar technologies achieves specific electricity costs between 0.133 and 0.157 USD/kWh for base load capacity that can replace the generating capacity of older coal-fired plants. Likewise, Zhai

et al. [7] holds the view that a hybrid solar plant in China could achieve energy costs 4.3% higher than a stand-alone PV plant, but 22.6% lower than a stand-alone CSP plant.

More recently (2021), Hernández, et al. [12] published a paper in which they demonstrated that hybrid solar plants, under a particular set of conditions, are shown to be more cost-effective than their closest competitor for the Chilean grid, gas-based generation. This study helps to understand why this line of research is of great interest in the field of solar energy, not only as a theoretical study, but also as a practical application.

So far, very little attention has been paid to the role of hybrid solar plants in the production of green hydrogen. A recent Advanced Review [14] summarized much of the research done so far on hybrid and polygeneration CSP plants (electricity, process heat, cooling and freshwater). Although this review identifies green hydrogen as one of the potential by-products of a CSP plant, it does not report studies on the integration of hybrid plants dedicated to green hydrogen production through electrolysis. In addition, a recent report by the German Concentrated Solar Power Association [41] highlighted that CSP plants in combination with other renewable energies can make a significant contribution to reducing hydrogen production costs. This would make green hydrogen competitive with hydrogen from fossil sources. Finally, a study conducted by Aprà, et al. [46], states that CSP with storage in combination with solar PV could provide the clean energy needed to create green hydrogen. The latter study only mentions hybrid solar plants for hydrogen production as an idea, but does not go into further details.

In conclusion, the evidence presented in this section confirms the need to assess and understand the benefits of integrating hybrid solar plants into green hydrogen production, especially in places with high solar potential and which are also of special interest to industry, such as northern Chile.

3. Methodology

This chapter explains the steps that were followed in order to meet the proposed objectives. The methodological approach used in this study is a bottom-up approach and gathers all the information developed at the beginning of the study to produce a simulation model of a CSP+PV hybrid power plant dedicated to the production of green hydrogen. Additionally, the hybrid solar plant was compared with stand-alone plants and with a direct connection to the grid.

3.1. Simulation Tool

One of the most well-known tools for assessing many types of renewable energy systems is the System Advisor Model (SAM) provided by the National Renewable Energy Laboratory (NREL) [47]. Although this tool allows for techno-economic analysis of multiple scenarios independently (single renewable technologies), it does not allow for adapting the generation of one renewable technology in response to another (and thereby precludes analysis of hybrid systems), nor does it have a module for hydrogen production as required for this thesis. In particular, a major limitation for CSP technology is that its dispatch control is limited to only nine modes of operation in the whole year and operates only with monthly average daily values, ignoring the daily and seasonal variation of the solar resource. This gives a very simple and unsophisticated simulation model when combining technologies is required, as indicated by [45].

To overcome these types of challenges, NREL has created PySAM [48], an open-source python-based programming interface that provides access to all SAM capabilities and functionality through code blocks, but which also allows developers to implement and integrate custom scenarios of novel technologies that are not yet built into SAM. In this work, PySAM was used to build a code to achieve an operational strategy that allows an optimal interplay between PV, CSP and hydrogen production as a whole. Additionally, it was particularly useful for automating many simulations with different models and parameters in the powerful object-oriented programming language Python, something that is not possible with the traditional SAM's Graphical User Interface (GUI).

Although both SAM and PySAM are able to perform their own economic analysis of solar plants, the model used in this thesis was performed separately to obtain more realistic and country-specific results. The default model includes incentives, tax benefits and other financial assumptions that are essentially applicable for locations in the USA, which yields energy costs that are far from what is observed in Chile, as mentioned by [12]. The determination of these models is not standard, as they depend on which cost components are included or excluded, which translates into a disparity in results and a difficult comparison [49]. Finally, it must be noted that the in-house code with the scripts was developed as a means to fulfil the purpose of this thesis and not as an end in itself.

3.2. Location and Resource

The annual performance of the plants was determined by simulation models considering a meteorological database of hourly resolution in the vicinity of the city of Antofagasta (23°51'33.68"S 69°48'50.44"W). The Atacama Desert, in northern Chile, is the driest place on the planet and has the highest solar radiation in the world. Additionally, this place presents the best conditions in terms of atmospheric attenuation [36], which is very attractive for the solar industry in general and, particularly, for solar power concentration (CSP), where Direct Normal Irradiance (DNI) plays a crucial role, reaching values greater than 3000 kWh/m^2 per year [31], [38], [50].

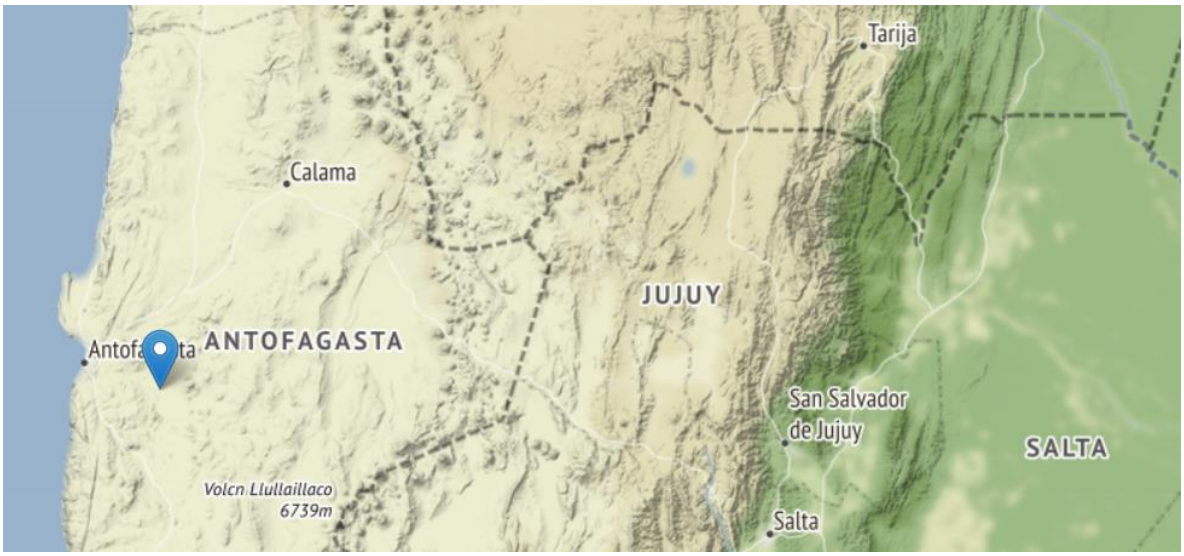

Figure 24: Analyzed Location

The Typical Meteorological Year (TMY) weather file for this study was taken from the Solar Energy Explorer of the Chilean Ministry of Energy [51]. As can be read on its official website, the Solar Explorer presents the most detailed public information currently available on the solar resource in Chile that has been generated from atmospheric models and satellite data, for the period between 2004 and 2016, with a spatial resolution of 90 meters.

3.3. System Description

In this section, the main modules used to create the Python code are presented, as well as the input parameters for the financial and technical performance evaluation for the three solar technologies (PV, CSP, and hybrid CSP+PV).

3.3.1. Case 1: Stand-alone PV

This case considers a direct coupling of an electrolyzer to a solar PV system in order to produce green hydrogen, as shown in Figure 25. The PV plant was generated and simulated through the “Pvwattsv7” module of PYSAM, which allows the creation of a PV project using a few basic inputs.

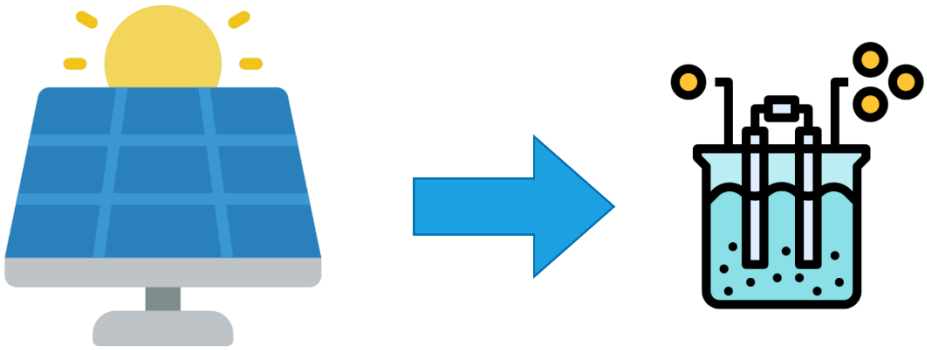

Figure 25: Electrolysis supplied directly by a PV plant

3.3.1.1. Technical Inputs

A PV array of 100 MW_{dc} capacity was chosen, with solar panels of 20.1% nominal efficiency, 1-axis backtracking and azimuth angle of 0 ° (south of the equator). To take into account the degradation in the performance of the components of the PV plant, an annual degradation rate of 0.7% and 0.5% was set for the year 2021 and 2030 respectively. In addition, 14% of total system losses were considered, mainly due to soiling, operational availability, system's life cycle, among other types of degradation.

For this configuration no inverters were considered, because the electrolyzers require DC current. In practice, the coupling of the PV array with the electrolyzer is done by means of a DC-DC converter with MPPT ("Maximum Power Point Tracking") that adapts the output voltage of the PV plant according to the input required by the electrolyzer, guaranteeing a safer and more efficient operation during the year [52].

3.3.1.2. Economic Inputs

Table 4 details the installation and operation costs of the off-grid PV system for hydrogen production:

Table 4: Cost distribution for economic evaluation of the 100 MW_e PV power plant

	Element	CAPEX 2021 (USD/Wdc)	CAPEX 2030 (USD/Wdc)	Cost Reduction
1	**Module**	0.41	0.17	58.5%
2	**Land preparation**	0.02	0.01	50%
3	**Balance of system**	0.2	0.1	50%
4	**Installation labor**	0.11	0.11	0%
5	**Contingency**	1%	1%	

Except for the contingency percentage, all economic parameters adopted for the current scenario (2021) are SAM default values, which estimate a direct investment cost that is in accordance with the information recently used for a Chile-based study [12]. The contingency percentage was set at 1% and operation and maintenance (O&M) costs equivalent to 2% of CAPEX in order to obtain a cost of energy adjusted to what was observed in the 2017/01 tender in Chile [53]. It could be argued that the cost should be lower, since the electrolyzer directly uses the DC current generated by the PV plant, which saves a lot of power electronics costs. However, it was decided to use these conservative values to absorb extra expenses on DC/DC rectifiers for the adjustment and control of the input power to the electrolyzer from the PV plant.

In order to evaluate the outlook scenario (2030), the cost of the modules was established according to a recent report issued by the Office of Energy Efficiency and Renewable Energy (EERE) [54]. The remaining items of the cost structure had the percentage reduction listed in Table 4, which manage to estimate values aligned with IRENA's projected total investment costs for utility-scale photovoltaics in 2030, ranging from USD 340 – 834 /kW_e according to its report Future of Solar Photovoltaic [55]. Additionally, the operation and maintenance costs for the year 2030 were set as 1% of the CAPEX each year due to increased efficiencies and cost savings through predictive maintenance. Although the assumed values for 2030 might seem too optimistic, these values achieve a cost of energy close to the offer made by Canadian Solar Libertador Solar Holding SpA for the National Electricity System for 15 years from 2026 [56], as will be discussed in more detail in the Results and Discussion section.

3.3.2. Case 2: Stand-alone CSP

This case considers a direct coupling of an electrolyzer to a CSP system for hydrogen production, as shown in Figure 26. A central receiver system coupled with molten-salt storage technology was chosen as the CSP technology, as it allows higher operating temperatures than those achievable by a parabolic trough plant, and therefore, better power cycle efficiencies. This system was generated and simulated using the PySAM module "TcsmoltenSalt", which creates this instance (individual object of a certain class of PySAM) and incorporates the specific attributes detailed in the following subsections.

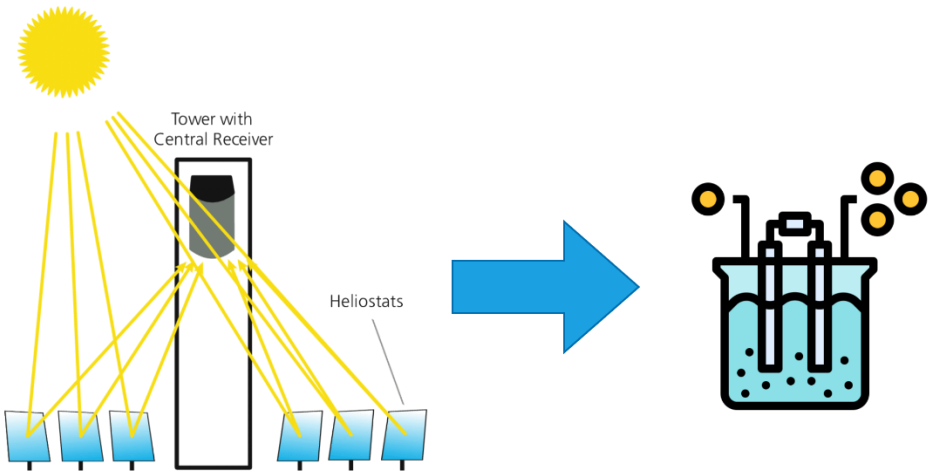

Figure 26: Electrolysis supplied directly by a CSP tower plant

3.3.2.1. Technical Inputs

The stand-alone CSP plant considers 111 MW_e of gross turbine design output (excluding parasitic losses) and a gross-to-net conversion factor of 0.9 (SAM's default value). This yields a nominal power cycle electrical output of 100 MW_e. Additionally, the CSP plant alone uses a uniform dispatch and the output fraction as the maximum output of the cycle, i.e., the turbine operates at its rated capacity throughout the year, without changing in any particular month or hour of day. To simplify the required analysis, it was assumed that the only significant technical difference between existing and future central tower plants is the annual degradation rate (0.2% and 0.1% respectively). As indicated by [57], there could be differences such as a slight temperature increase, but it would result in a minor efficiency gain. Additionally, these innovative technologies will probably not be available for commercial projects in 2030 since current CSP tower configuration is technologically mature.

3.3.2.2. Economic Inputs

Due to the relatively small global CSP market compared to PV, reliable and transparent cost data is difficult to obtain; therefore, some assumptions were made and are detailed in Table 5.

Table 5: Cost distribution for economic evaluation of the 100 MW_e CSP power plants

	Element	CAPEX 2021	CAPEX 2030	Cost Reduction
1	**Site preparation**	16 (USD/m^2)	10 (USD/m^2)	35.5%
2	**Solar field**	140 (USD/m^2)	50 (USD/m^2)	59%
3	**Tower cost fixed**	3,000,000.00	2,189,781	27%
4	**Receiver reference cost**	103,000,000.00	75,182,481.75	27%
5	**TES**	22.00 (USD/kWh_t)	10.00 (USD/kWh_t)	54.5%
6	**Power block**	1330 (USD/kW)	700 (USD/kW)	47.4%
7	**Contingencies**	5%	2%	

The total cost of the tower and the receiver were scaled according to the following equations [58]:

$$C_{tower} = C_{tower,f} exp\left[\chi_{tower}\left(h_{tower} - \frac{h_{rec}}{2} + \frac{h_h}{2}\right)\right] \quad (1)$$

$$C_{rec} = C_{rec,ref}\left(\frac{A_{rec}}{A_{rec,ref}}\right)^{\chi_{rec}} \quad (2)$$

where h_{tower}, h_{rec} and h_h are the heights of the tower, receiver and heliostats; χ_{tower} and χ_{rec} are the scaling factor of the tower and receiver; A_{rec} and $A_{rec,ref}$ are the actual and reference area of the receiver respectively.

For the current scenario (2021), SAM default values were adopted, and for the future scenario (2030) the prices were set according to the price trends reported by [54]. The economic parameters assumed are considered realistic, as in the case of the current scenario, a LCOE of less than 100 USD/MWh is achieved, in line with what was reported for this region of Chile by [38]. In the case of the future scenario, the costs are in line with the energy price offered by Likana Solar in the last Chilean electricity tender in August

2021, which could have been in place in 2030, had the tender been awarded. Although the bid submitted by Likana Solar was not the winning bidder, the price offered is a good benchmark for future prices.

3.3.3. Case 3: Hybrid CSP+PV

The hybrid CSP+PV system combines a PV subsystem with a CSP subsystem for the production of green hydrogen (Figure 27). To simulate this case, independent PV and CSP models were linked to achieve a synergistic operation that provides a base load capacity of 100 MW_e as a whole. In the operation strategy, PV has the priority of feeding over CSP, that is, when the PV plant is producing electricity, the CSP plant reduces or ceases its production, storing the residual heat from the receiver in the TES to be used in hours of low or no solar radiation.

To adapt the CSP generation to the electricity supply profile from the PV power plant, the code manipulated the TES dispatch control to allow nine different periods for each day of the year. Each of the nine periods of the day represents a different turbine output fraction, which scales the electrical output of the system up or down depending on the profile of the PV plant to achieve a more stable output for the electrolysis plant. More specific details on this approach are provided in the following section.

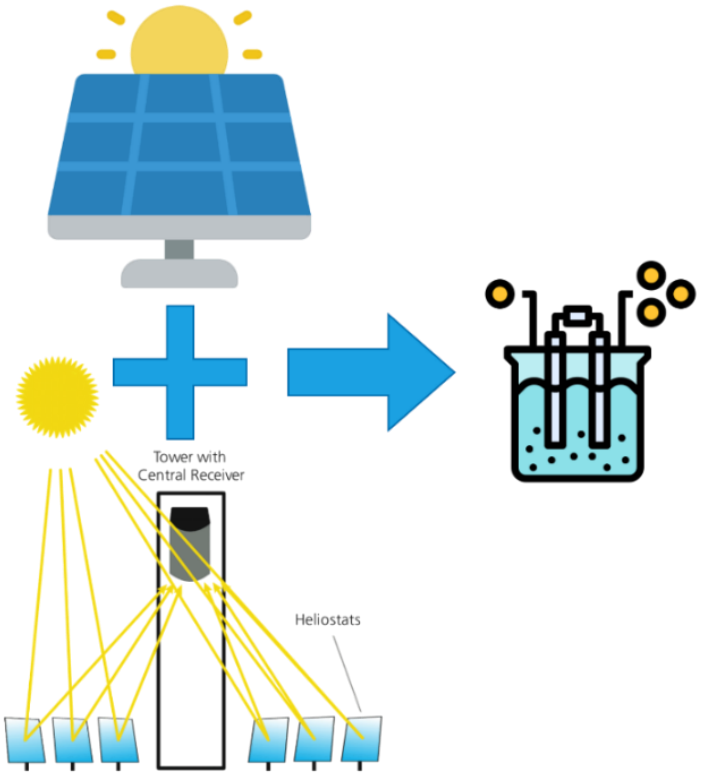

Figure 27: Electrolysis supplied directly by a hybrid CSP/PV power plant

3.3.3.1. Technical Inputs

Most of the technical parameters of the hybrid CSP plant are the same as the stand-alone CSP plant, except that the TES dispatch control matrix in the System Control must be modified to adapt the turbine output fraction. For a better understanding of the approach used in this work, the dispatch matrix used by SAM was included as a reference (Figure 28). This matrix represents a full year of operation and takes into account only one average or characteristic day for each month and has a limit of nine dispatch control periods for the whole year. These nine possible dispatch control periods or time-of-use periods are located in each box of the matrix and represent the timing of releases of energy from the thermal energy storage system to the power block. Additionally, for each of these periods, there is an associated turbine output fraction, which determines at what load level the power block runs using energy from storage during that period. In conclusion, the dispatch matrix and the turbine fractions determine the timing and quantity of energy delivered by the thermal energy storage system.

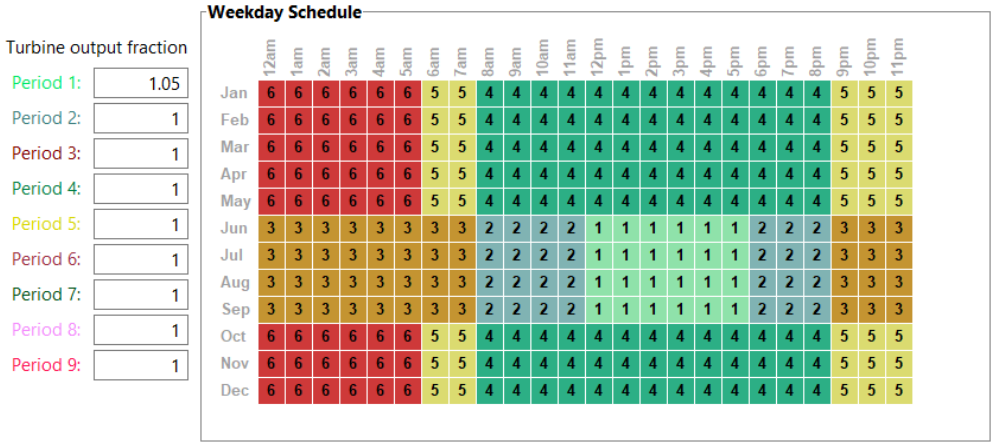

Figure 28: Reference image of the dispatch control matrix of the System Advisor Model (SAM)

To enable the simulation of the hybrid solar plant and overcome the low resolution offered by the SAM's default dispatch matrix, the new simulation model proposed for this thesis modifies the operating strategy of the original code and employs several dispatch scheduling matrices. In particular, it uses one different matrix with nine periods for each day of the year to run a sequence of hundreds of simulations iteratively until a full year's generation is reached. Further details of the methodology are described below:

- First, the hourly PV generation is subtracted from the desired 100 MW_e generation, resulting in the hourly residual generation to be supplied by the CSP plant.

- Then, this hourly residual generation is divided by the nameplate capacity (100 MW_e installed), obtaining the factors or coefficients by which the power cycle's thermal input must be weighted to scale the system's electrical output in its

respective time-of-delivery period. Although in an ideal case the division should be by the design turbine gross output (111 MW_e), it was decided to divide by the nominal capacity in order to absorb the losses in the AC/DC conversion rectifiers and other electrical losses. The latter causes the turbine outlet fractions to be slightly oversized, namely by 11%.

- Although the new simulation model improves from 9 operating modes per year (original SAM code) to 9 periods per day (proposed code), it does not achieve perfect hourly resolution (24 operating modes per day). The latter implies that the hourly resolution matrices obtained in the previous step had to be segmented and sorted into nine bins, considering equally-spaced segments between the minimum and maximum value of each day. Additionally, each of the bins was labelled with a number between 1 and 9, where 1 represents the period where the turbine operates at minimum and 9 the maximum required each day respectively.

- In addition, a technical minimum output level of 30% was set for the turbine operation, i.e., for those periods when the turbine fraction is less than 30% of the nameplate capacity, the code automatically sets it to the minimum stable output level. The purpose of this is to ensure that the system is in standby mode, i.e., that there is a minimum of energy to keep the auxiliary equipment in a hot state to be ready for a quicker start-up and to avoid the risk of failure and wear due to mechanical stress associated with temperature fluctuation.

- All the labelled data was rearranged into 31 arrays of dimension 12x24 (12 months and 24 hours), i.e., 31 arrays like the matrix shown in Figure 28, so that each array represents one day of the year. The first row of the first array represents the first day of January, the second row of the first array represents the first day of February and so on until the last day of December, which is placed in the last row of the last array.

- Finally, once all the preprocessing of the dispatch matrices was ready, the code must be executed. The approach is based on a very simple idea: execute the code by pieces or rectangular windows relative to the rows of the dispatch matrices. This iterative process was carried out using a nested for loop: an outer loop to traverse the 31 matrices (days) and an inner loop to iterate within the rows (months) of each matrix, resulting in 372 code executions. First, a window is taken and the code is run, the results for that day are selected and appended to a result vector. Subsequently, the window is moved, the code is run and the results are selected and appended again, and so on until the last row of the last matrix is reached, which completes one year of simulation.

The flow chart in Figure 29 summarizes the sequence of stages for the code execution process.

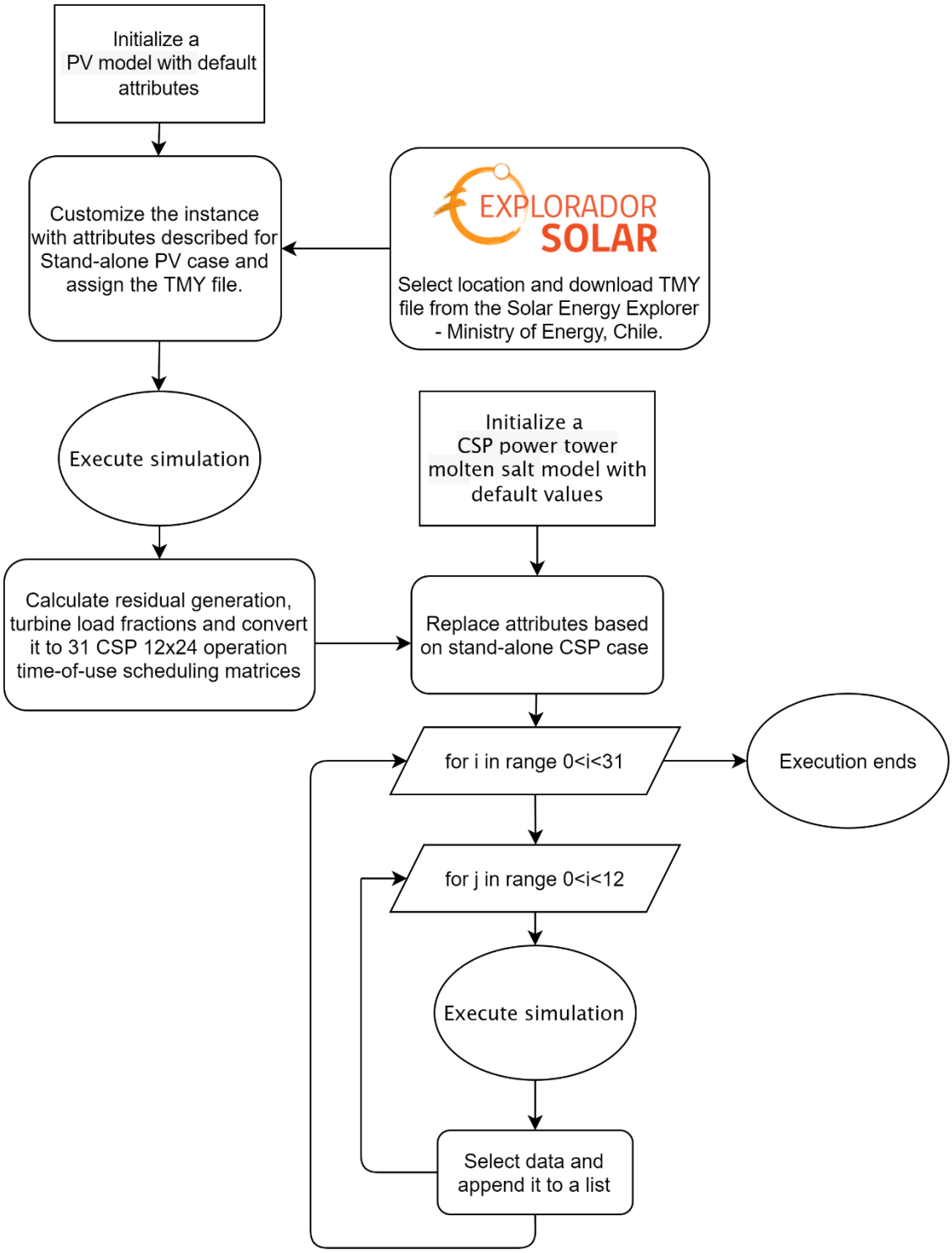

Figure 29: Program execution flowchart

3.3.4. CSP+PV Hybrid Hydrogen Production

Once the hybrid model of electricity generation was completed, the final stage was to integrate its outputs into hydrogen production. To do this, a code was generated that considers PEM (Proton Exchange Membrane or Polymer Electrolyte Membrane) electrolyzers and alkaline electrolyzers.

In order to keep the hybrid solar system powering the electrolyzers as stable as possible in 100 MW_e, a power limit (or curtailment) was applied to the sum of PV and CSP generation. This surplus energy is produced in hours of maximum solar radiation. Although the CSP hybrid code tries to operate the system so that the output of the power cycle matches the defined dispatch schedule, there are periods of high radiation, where the storage system is completely full. Because the storage tank is full and there is still solar radiation reaching the central receiver, the turbine output fraction cannot fully match what is required (low turbine fractions) and must operate at higher capacity to release energy and avoid over-charging the TES system. Energy that exceeds the needs of the electrolyzer represents a waste of energy and, in practice, could be avoided by defocusing the heliostats or, better still, injecting it into the grid. However, this is beyond the scope of this work.

3.3.4.1. Technical Inputs

Some critical technical inputs of the hybrid CSP plant connected to the PV plant feeding the hydrogen plant correspond to optimal values obtained from a parametric analysis, which is detailed as follows.

3.3.4.1.1. Parametric Analysis

A parametric study was carried out to establish the optimal combination of solar multiple and storage hours (TES capacity) for the hybrid solar plant to enhance the operation time of the electrolyzer and at the same time produce hydrogen at the minimum possible price. This analysis was conducted in terms of $LCOH_2$ and the load factor of the electrolyzer integrated to the hybrid solar plant. For this purpose, the size of the TES (in hours) and the solar multiple were considered as independent variables, due to their strong influence on energy costs and capacity factor. The evaluation range of solar multiple and TES hours was from 1 to 4 and from 5 to 20 respectively in order to better understand the influence of these design parameters on the $LCOH_2$.

Each time the solar multiple (and therefore the receiver thermal power) was changed, an optimization of the solar field was required. This procedure was performed by means of a simplified format of SolarPILOT [59], a software developed by NREL to generate and characterize tower power systems and accessible from PYSAM. The incorporation of

SolarPILOT into the code developed for this thesis ensured that the design and geometry of the heliostat field was appropriate for each new value adopted by the solar multiple.

3.3.4.1.2. Conversion Efficiency

Electrolyzer efficiency is the efficiency with which the electrolyzer converts electricity into hydrogen, assuming standard temperature and pressure of the H_2. This parameter is largely determining for power consumption and therefore the bulk of operating costs. For the parametric study carried out in this study, the most conservative current and future conversion efficiencies presented by the IEA were assumed [23]. However, the determination of the final $LCOH_2$ reported for each of the scenarios under study was done with both the lower and upper limit of the range of efficiencies, which are detailed in Table 6.

Table 6: Electrolyzer efficiencies used in this study

Parameter	2021	2030
Alkaline efficiency (%)	63 – 70	65 – 71
PEM efficiency (%)	56 – 60	63 – 68

3.3.4.2. Economic Inputs

In this study, the production of hydrogen is ensured by the two most widespread water electrolysis technologies: alkaline water electrolysis and polymer electrolyte membrane water electrolysis, with the same capacity as the renewable energy plant that powers it. The specific costs assumed for each type of electrolyzer are detailed in Table 7, based on [23].

Table 7: Electrolyzer capital costs

	Element	CAPEX 2021	CAPEX 2030	Cost Reduction
1	**PEM Electrolyzer**	1100 (USD/kW)	650 (USD/kW)	41%
2	**Alkaline Electrolyzer**	500 (USD/kW)	400 (USD/kW)	20%

The stack replacement cost is assumed to be 40% of the CAPEX of the electrolyzer for the short term (2021) and 15% for the future term (2030), using the replacement reinvestment model employed by [18] and the stack lifetime (hours of operation) indicated by [23]. Finally, it should be noted that this project was evaluated over 30 years and was calculated assuming a water price of 1.4 (USD/m^3) for the II region [60] and it was assumed that oxygen as a by-product is released into the atmosphere. However, it is left as future work to study the sale of high purity oxygen produced as a by-product of electrolysis, which is remunerative and could improve the economic results.

3.4. Technical Analysis

This section presents the main technical metrics used to quantify the performance of individual and integrated plants.

3.4.1. Load Factor

To explore and demonstrate the benefits of hydrogen production from the combination of PV and CSP technologies, the load factor of the electrolyzer was used as one of the main performance metrics, i.e., its total utilization as a fraction of the maximum possible utilization. This metric is very important in determining the amount of hydrogen that can be produced from renewable resources and its specific cost. When the electrolyzer is directly connected to the renewable electricity source as in this case (dedicated solar plants), some authors assume that the load factor of the electrolyzer is equivalent to the capacity factor of the power plant feeding it [60]–[62]. However, although the load factor of the electrolyzer is closely linked to the capacity factor of the renewable power plant, using these concepts interchangeably is not entirely accurate, as the energy produced is not always equivalent to the energy delivered to the electrolysis process.

To accurately reflect the load factor that effectively is applied to the electrolyzer operating in direct connection mode to a renewable electricity generator, it must be considered that there are hours when there is electricity production but no hydrogen production [52]. For instance, in the case of direct coupling of PV and alkaline electrolyzer, there are intervals of the day where the electrical production is not sufficient to reach the minimum percentage of the nominal capacity to start operating. On the other hand, for stand-alone CSP or hybrid + alkaline / PEM electrolysis, there are hours when electricity must be curtailed (i.e., a power limit is applied) because the electrical energy output is higher than the nominal capacity of the electrolyzer. Finally, considering the capacity factor of the renewable plant equal to the load factor of the electrolyzer is also not exact due to the type of current at which the capacity factor is measured. On the one hand, for PV systems, the capacity factor is an AC-to-DC value (system capacity is in kW DC) and for CSP, the capacity is an AC-to-AC value (system capacity is in kW AC), i.e., the capacity factors in both solar technologies are based on a different type of current. On the other hand, an electrolyzer must be supplied only with direct current (DC) because the electrodes have defined polarities [19]. Therefore, throughout this thesis, both terms were not considered equivalent.

3.4.2. Electricity and Hydrogen Production

The hourly and monthly electricity and hydrogen production of the different configurations were determined in order to observe the fluctuation of the amount of electricity and hydrogen produced throughout the year. The amount of hydrogen produced was estimated with the following equation [17]:

$$m_{H_2} = \frac{\eta_{el} E_{el}}{LHV_{H_2}} \quad (3)$$

Where LHV_{H_2} is the lower heating value of hydrogen, equal to $33.33\ (\frac{kWh}{kg_{H_2}})$, E_{el} is the electrical energy input (kWh) and η_{el} is the electrolyzer's efficiency.

The energy needed to store the hydrogen in gas or liquid form was subtracted from the total amount of electricity produced. The remaining energy is finally used to power the electrolysis plant. Currently, hydrogen is typically compressed by reciprocating compressors, and this adiabatic compression is governed by the following equation:

$$L_{e,spec} = \frac{c_{pH2} \Delta T_{12}}{\eta_m \eta_e} = \frac{T_1 \left(\beta^{\frac{k-1}{k}} - 1 \right)}{\eta_m \eta_e} \quad (4)$$

Where $L_{e,spec}\ \left(\frac{kWh_e}{kg}\right)$ is the specific energy consumption of the compressor; β is the compression ratio; T_1,T_2 are the inlet and outlet temperatures (K); η_m ,η_e are the mechanical and electrical efficiencies (are assumed constant and equal to 70% and 90%, respectively). Thus, the specific energy demand to compress the hydrogen (isothermally) from 20 bar to 350 bar requires 1.05 kWh/kg$_{H2}$.

3.4.3. CO_2 Emission Reduction Potential

The environmental benefit of the analyzed solar plants was established taking into account the abatement of CO_2 emissions. This metric was calculated according to the following equation:

$$tCO_2 \left(\frac{tCO_2\, eq}{year} \right) = EF \left(\frac{tCO_2\, eq}{MWh} \right) \cdot E \left(\frac{MWh}{year} \right) \quad (5)$$

where tCO_2 represents the CO_2 reduction resulting from the operation of a solar power project, EF is the emission factor and E represents the amount of electricity generated by the plant. The emission factor used was 0.3834 tCO_2 equivalent per MWh generated. This value corresponds to the average annual emissions factor of the National Electricity System (SEN) reported by the National Energy Commission [63]. By multiplying the generation of each solar plant by the corresponding emission factor, the emissions reduction resulting from the operation of each solar plant is obtained.

3.5. Economic Analysis

The economic analysis of hydrogen production was performed for the different pathways in the 2021 reference scenario and 2030 future scenario by means of the LCOE and $LCOH_2$, two key economic metrics for assessing the cost of an electricity and hydrogen production system respectively.

3.5.1. Levelized Cost of Energy (LCOE)

The LCOE is a measure of the average total cost to build and operate a generator over its lifetime divided by the total energy output over the lifetime of the plant. In other words, this measure allows the calculation of the minimum price necessary to sell energy in order to meet a certain hurdle rate. The simple levelized cost of energy is calculated using the following formula [64]:

$$LCOE = \frac{\sum_{t=0}^{N} \frac{CAPEX_t}{(1+i)^t} + \sum_{i=1}^{N} \frac{OPEX_t}{(1+i)^t}}{\sum_{t=1}^{N} \frac{E_t(1-d)^t}{(1+i)^t}} \quad (6)$$

Where $CAPEX_t$ is the investment expenditures in the year t, $OPEX_t$ is the operations and maintenance expenditures in the year t, E_t is the electricity generation in the year t, i is the discount rate, d is the annual degradation factor and N is the useful economic life of the system. CAPEX (capital expenditure) represents all capital or investment expenses that a company must incur in. For a CSP tower plant, the CAPEX should include items such as site preparation, solar field construction, solar tower, solar receiver, TES and power block, among other expenses. In the case of a PV plant, the cost of photovoltaic modules, inverters and site preparation should also be incorporated. It should be emphasized that depending on which cost components of the LCOE are included or excluded, different studies may lead to significant disparity in values and therefore making comparisons between them would not be correct. On the other hand, OPEX (operational expenditures) represents all those day-to-day operations and maintenance costs (O&M) that are required for the plant to operate. This item can include annual fixed costs and variable costs per generation.

3.5.2. Combined LCOE

The weighted average of the PV and the CSP plant's LCOE is calculated with the following equation [64]:

$$LCOE_{hybrid} = \frac{LCOE_{PV} \cdot E_{PV} + LCOE_{CSP} \cdot E_{CSP}}{E_{PV} + E_{CSP}} \quad (7)$$

where $LCOE_{CSP}$ and $LCOE_{PV}$ represents the levelized cost of electricity of the CSP and PV plants respectively, and E_{CSP}, E_{PV} refers to the annual energy generation of the CSP and PV plants respectively.

3.5.3. Levelized Cost of Hydrogen ($LCOH_2$)

The model is based on a straightforward calculation in which the various system costs are evaluated, and the sum is divided by the amount of hydrogen produced. According to the definition provided by GIZ [60], the $LCOH_2$ can be mathematically defined as:

$$LCOH_2 = P_{inst} \cdot CAPEX \cdot \frac{CRF + OPEX}{h \cdot f_p \cdot Q_{H_2}} + Q_{H_2O} \cdot P_{H_2O} + Q_e \cdot P_e - Q_{O_2} \cdot P_{O_2} \quad (8)$$

where P_{inst} is the installed capacity of the electrolyzer, $CAPEX$ is the investment cost according to installed capacity, CRF is the capital recovery factor as a function of the discount rate, f_p is the plant factor, $OPEX$ is the function of maintenance costs as a percentage of the investment, dependent on the plant factor, h is the number of hours in a year, Q_{H_2} is the hydrogen production capacity [kg_{H2}/h], Q_{H_2O} is the amount of water consumed [m^3/kg_{H2}], P_{H_2O} is the water price [USD/m^3], Q_e is the amount of electricity consumed [kWh/kg_{H2}], $P_e = LCOE$ is the electricity price [USD/kWh], Q_{O_2} is the sale of oxygen taking into account the quantity produced [kg_{O2}/kg_{H2}] (optional term), P_{O_2} is the oxygen selling price [USD/kg_{O2}] (optional term).

From Equation 8 it is noteworthy to mention that the capital recovery factor is a ratio used to calculate the present value of an annuity (a series of equivalent annual payments). Using an interest rate i and a system lifetime n, the capital recovery factor is:

$$CRF = \frac{i(1+i)^n}{(1+i)^n - 1} \quad (9)$$

Furthermore, it should be noted that both metrics, LCOE and $LCOH_2$, are based on the same methodology, i.e., the ratio of annualized lifetime costs over the final product produced during its lifetime, discounted to a common year using a discount rate reflecting the average cost of capital, which was set at 7% for this study.

3.5.4. Hydrogen conditioning and storage costs

Since alkaline solutions prove to be more cost competitive, the storage analysis and comparison with the solar PPA alternative were performed only with this technology. Additionally, due to the lack of reliable techno-economic data for storage in 2030, this part of the analysis was limited to the current scenario.

The two current state of the art methods of hydrogen storage technology, liquefied and compressed hydrogen, were considered. For each of these methods, a conversion or conditioning module (compressor and liquefaction unit) and a storage module (storage tanks) were taken into account, according to the techno-economic parameters reported by [17] and [65]. It should be noted that some costs assumed were adapted to the plant capacity considered in this work. The main economic parameters assumed for this study are summarized in Table 8:

Table 8: Hydrogen conditioning and storage assumptions

System	Pressure (bar)	Specific cost	Specific Energy Consumption	O&M (%CAPEX)	Depreciation Period (years)
Compressor	Up to 350 bar	3900 US$/$kW_e$	-	4%	15
GH_2 storage	Up to 350 bar	500 US$/$kg_{H2}$	1.05 kWh_e/kg_{H2}	2%	20
Liquefaction unit	82	15 kUS$/($kg_{H2}$/h)	6.4 kWh_e/kg_{H2}	8%	20
LH_2 storage	~1 bar	90 US$/$kg_{H2}$	-	2%	20

The specific CAPEX of the compressor was determined based on the maximum hydrogen flow and electricity consumption as reported by [17]. On the other hand, the specific cost of the storage tanks was considering 1 day of production as a backup, i.e., it is a "short duration" means of storage. Finally, investment and O&M costs were weighted by the capital recovery factor (Equation 9) and divided by the annual hydrogen production, in order to obtain the specific cost per kg of hydrogen that each alternative represents.

3.5.5. Power Purchase Agreement (PPA) assumptions

For the off-site or virtual PPA alternative, i.e., assuming that electricity is purchased from a solar supplier, the following base costs and plant factors were assumed:

Table 9: Electricity costs assumptions - PPA analysis

Configuration/Scenario	2021		2030	
	Base cost (USD/MWh)	Capacity factor	Base cost (USD/MWh)	Capacity factor
Solar PPA – PV (8-18h)	30	0.42	14	0.42
Solar PPA - CSP+TES (24/7)	60	1	34	1

The assumed prices were estimated from the energy bids of solar generators in the 2017 and 2021 tenders. To these prices must be added the cost for power, transmission and distribution of energy, with an approximate cost of USD 24.7 to obtain the total cost of electricity, as indicated in [60].

This part of the analysis did not consider a reduction of costs per use of the electricity transmission system by 2030 because it is very likely that overloads or congestion will occur in the northern part of the country, as the expansion of transmission infrastructure is slower than the expansion of renewable electricity generation. In other words, generation capacity will far outstrip transmission capacity, which could increase costs.

4. Results and Discussion

This chapter presents the results obtained with the simulation model and a critical discussion for the different evaluated scenarios. Firstly, the section presents the parametric analysis to identify optimal combinations of solar multiple (SM) and the number of storage hours (TES capacity) for least cost of hydrogen production. Secondly, the technical analysis is exposed, which shows the CO_2 emissions avoided, as well as the generation of electricity and hydrogen in hourly and monthly terms. Finally, the economic analysis is exhibited, where the minimum values of LCOE and $LCOH_2$ obtained for the different pathways and the additional costs of storing hydrogen are presented and analyzed in detail.

4.1. Parametric analysis for optimal combination of SM and TES size

4.1.1. $LCOH_2$ vs SM and TES Capacity: current and future scenario

The analysis of a CSP plant with TES introduces many decisions for optimal plant sizing. This subsection describes the general evolution of $LCOH_2$ as a function of solar multiple (SM) and TES full load hours, considering a stand-alone CSP plant and a hybridized CSP plant. In addition, two types of electrolyzers and time scenarios are presented. Finally, the selection of the optimal parameters that generate a minimum levelized cost of hydrogen are displayed in Table 10.

- **CSP + ALK electrolyzer**

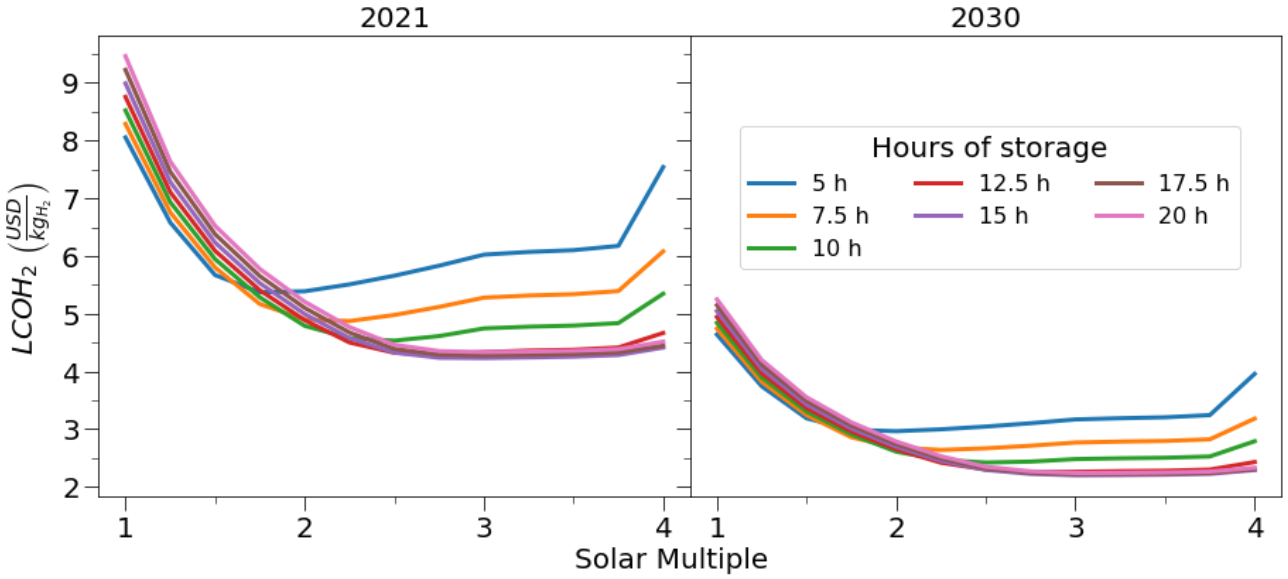

Figure 30: Variation of $LCOH_2$ with SM and TES capacity - CSP + ALK electrolyzer

From Figure 30 it can be seen that $LCOH_2$ initially decreases until it reaches a minimum and then increases again. This behavior is explained by the fact that the thermal energy collected increases with the SM, which extends the utilization of the power block. The latter initially reduces the LCOE and consequently the $LCOH_2$, owing to the lower specific energy cost and higher annual hydrogen production. However, increasing the SM and TES capacity implies an increase in the solar field leading to a strong increase in investment cost. It should be noted that, after reaching a minimum cost, the income from increased annual electricity generation (and thus annual hydrogen production) is much less than the investment cost of increasing the storage system and the solar field, and therefore there is no additional benefit from increasing the SM. A further increase in this parameter becomes too detrimental since the initial investment cost increases without compensation in electricity generation, which would explain the growth of the curves.

In Figure 30 there is also a clear downward shift of the curves in the outlook scenario (2030) due to the lower hydrogen production costs that can be achieved. One reason for the decrease in green hydrogen production costs is the increase in efficiency of the alkaline electrolyzer from 63% to 65%. In other words, it is expected that the electrolyzer will consume a smaller amount of electricity to produce one kilogram of hydrogen. Another reason is a 20% lower CAPEX investment in alkaline electrolyzers projected for the long term as a result of the increase in the learning rate as the industry grows and larger scale projects are implemented. Finally, another key factor for reducing $LCOH_2$ is lower energy prices. As will be seen in the breakdown of hydrogen costs, the levelized cost of renewable energy is one of the main parts of the hydrogen cost structure. In conclusion, the downward shift of the curves in 2030 is caused by a combination of increased efficiency, lower CAPEX investment in electrolyzers and cheaper electricity.

- **CSP + PEM electrolyzer**

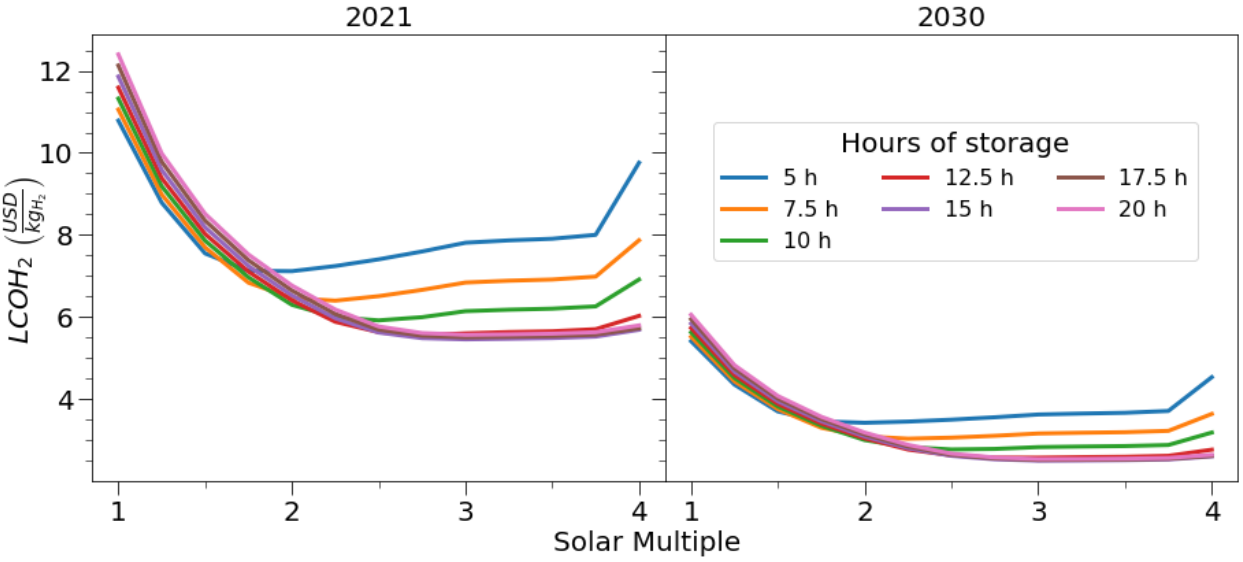

Figure 31: Variation of $LCOH_2$ with SM and TES capacity - CSP + PEM electrolyzer

Figure 31 presents the same $LCOH_2$ variation for different capacities of storage hours and solar multiples, but considering a PEM electrolyzer. The increase in the conversion efficiency assumed is from 0.56% to 0.63%, as reported by the most conservative case of the International Energy Agency [23]. Because PEM technology has fewer years of experience than the alkaline type, its investment CAPEX is higher; however, the latter is expected to have an investment cost reduction of around 41% by 2030. This combination of increased efficiency and reduced CAPEX causes the curves to shift vertically, but less than the most mature form of electrolysis (alkaline electrolysis, Figure 30).

- **Hybrid CSP + ALK electrolyzer**

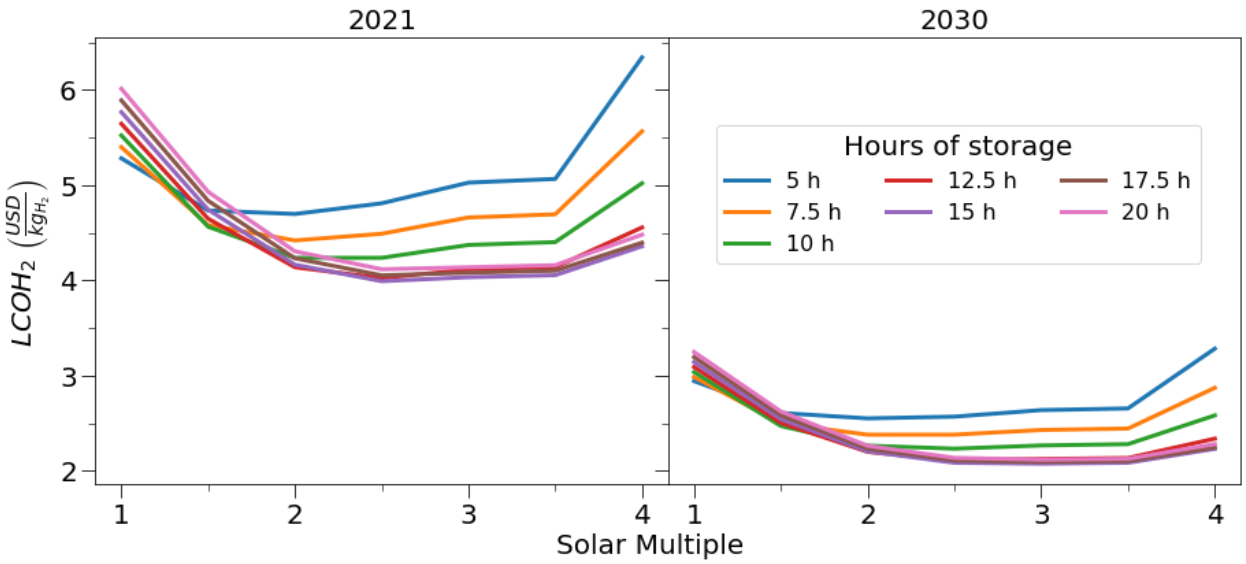

Figure 32: Variation of $LCOH_2$ with SM and TES capacity - Hybrid CSP + ALK electrolyzer

Figure 32 shows curves with a larger downward displacement than those generated by the coupling of an alkaline electrolyzer with a stand-alone or separate CSP (Figure 30). Although the conversion efficiency and electrolyzer CAPEX parameters are the same in both cases, the coupling with a hybrid solar plant offers lower electricity costs, which translates into lower specific green hydrogen production costs. This phenomenon is also evident in the integration of a PEM electrolyzer and a hybrid solar plant (Figure 33), but with higher specific hydrogen costs because the investment level of commercially available PEM electrolyzers is higher than traditional alkaline, as previously stated.

- **Hybrid CSP + PEM electrolyzer**

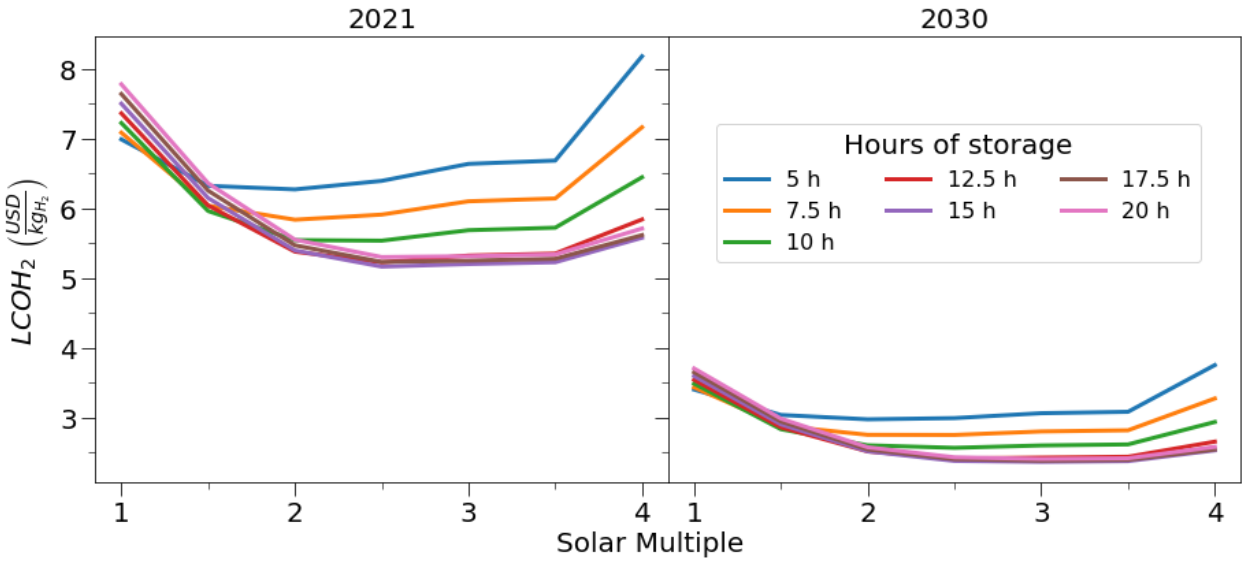

Figure 33: Variation of $LCOH_2$ with SM and TES capacity - Hybrid CSP + PEM electrolyzer

The above results provide a good visual benchmark of the impact of the solar multiple (SM) and TES capacity (hours of storage) on the specific cost of hydrogen. From these parametric studies, the optimal TES capacity and the SM are determined by minimizing the levelized costs of hydrogen ($LCOH_2$) for each scenario analyzed. The optimal parameters for each configuration are presented in the following section.

4.1.2. Optimal SM and TES system combination

Table 10 summarizes and compares the optimal design parameters for SM and TES capacity obtained from the parametric analysis, which were used to simulate the plants presented in the following sections.

Table 10: Optimal parameters of SM and TES capacity for the minimum $LCOH_2$

Configuration/Scenario	Standard cost scenario (2021)		Outlook scenario (2030)	
	Hours of Storage	Optimal SM	Hours of Storage	Optimal SM
$LCOH_2$ CSP – PEM (USD/kg_{H2})	15	3	15	3
$LCOH_2$ CSP – ALK (USD/kg_{H2})	15	3	15	3
$LCOH_2$ Hybrid – PEM (USD/kg_{H2})	15	2.5	15	3
$LCOH_2$ Hybrid – ALK (USD/kg_{H2})	15	2.5	15	3

It is worth noting that the values in Table 10 are cost-optimal parameters, i.e., they are the optimal combination of solar multiple and power plant storage hours to achieve a minimum specific cost of hydrogen and not necessarily the maximum capacity factor (technical optimal parameters). The choice of this yardstick to arrive at the best possible design parameters is because hydrogen production will not ensure market penetration unless it can ensure economic competitiveness. Interestingly, regardless of the chosen pathway, the system reaches the minimal $LCOH_2$ with 15 hours of storage. In the case of solar multiples, they remain at 3 except for the hybrid coupling case in the current scenario (2021) which is minimized with a value of 2.5. Although the similarity in parameters may seem counterintuitive, this is because the size of the solar field does not change substantially between a stand-alone CSP and a CSP hybridized to PV. The main difference lies in the dispatch schedule of the solar thermal energy, i.e., the same amount of collected and stored energy is distributed in a convenient way.

4.1.3. Load factor vs SM and TES Capacity: ALK and PEM electrolyzer

Figure 34 and Figure 35 present the variation of the two key parameters previously analyzed (solar multiple and full load storage hours) but applied to the load factor of the electrolyzers.

- **Stand-alone CSP**

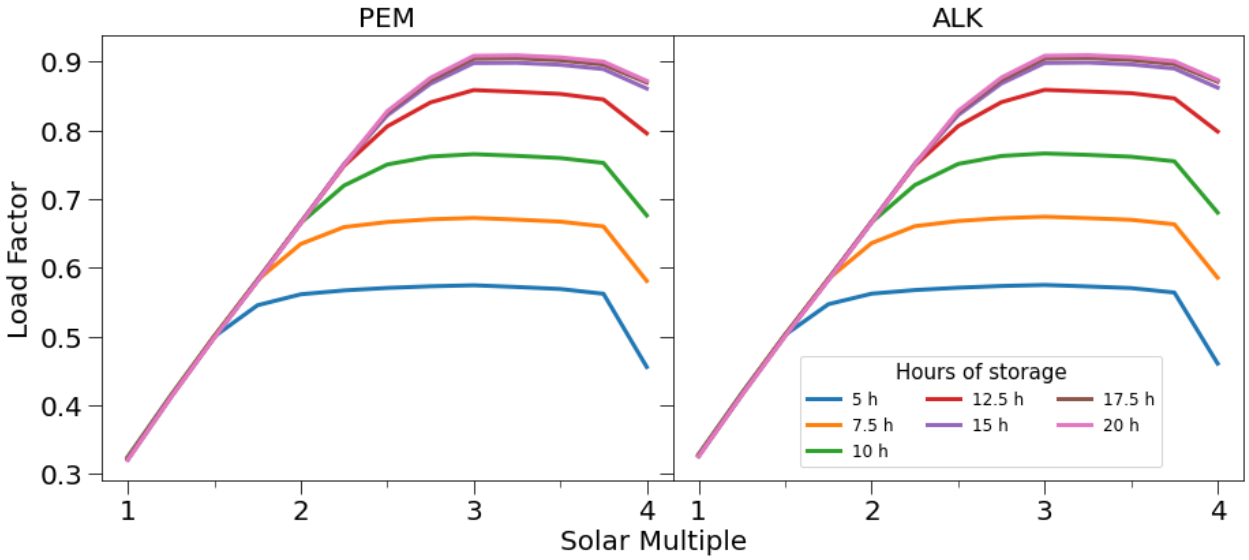

Figure 34: Variation of the Load Factor with SM and TES capacity - Stand-alone CSP

- **Hybrid CSP**

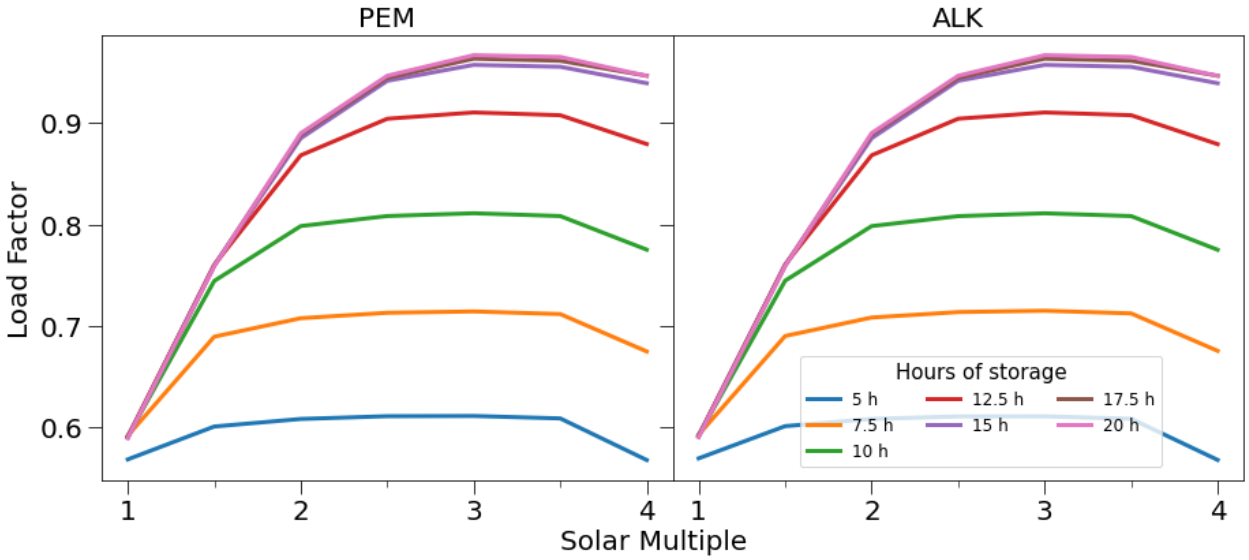

Figure 35: Variation of the Load Factor with SM and TES capacity - Hybrid CSP

From Figure 34 and 35 it can be seen that initially the load factor of the electrolyzers increases until it reaches a relatively stable zone and then decreases again, as the solar multiple rises. The initial behavior occurs because a higher solar multiple achieves a higher energy output, which leads to a high utilization of the electrolyzer. However, when the solar multiple is too high, there is a drop in the load factor. This behavior can be explained by the disturbances when the solar flux reaching the receiver is excessive with respect to the design point, and the maximum allowable power block output is exceeded. When the solar multiple is too big to be reasonable or acceptable, the solar field can collect so much energy that the mass flow rate required to maintain the design outlet temperature exceeds the upper limit. To avoid excess heat transfer fluid temperature (and a dangerous scenario) the code defocuses some collectors to reduce the amount of energy absorbed, until the maximum allowable thermal output limit is met. Another possible explanation for this drop in the load factor may be the increase of heat loss coefficients in the CSP system, which are functions of the outlet temperature from the solar field, which increases with the solar multiple.

From the previous figures, it can be also observed that the coupling of an electrolyzer to hybrid CSP plant (Figure 35) offers a higher load factor for the same solar multiple compared to a stand-alone CSP plant (Figure 34). This higher load factor for a given solar multiple is explained by the combination with PV technology. In other words, the use of a mix of solar technologies gives electrolyzer utilization rates above 90%, i.e., high operating hours.

Finally, it should be considered that an alkaline electrolyzer does not tolerate loads lower than 10% of its nominal capacity, i.e., it has a lower capacity to adapt to the variation of electrical energy. In contrast, a PEM electrolyzer is more dynamic, as it can operate at less than 10% of its nominal capacity and can therefore achieve higher load factors. This difference in the operating limits of electrolyzers becomes less evident when electrolysis is fed from CSP (stand-alone or hybridized), since they offer greater supply stability than stand-alone PV. The latter would explain the fact that there are no significant differences between the load factor variation curves between a PEM or alkaline electrolyzer and that they are virtually identical.

4.2. Technical Results

This section presents the technical performance analysis of the different pathways analyzed. Although the main focus of this thesis is on the production of green hydrogen via hybrid solar plants, it is necessary and interesting to benchmark the results against the stand-alone cases. First, the direct coupling of an electrolyzer to a stand-alone PV plant is presented (Case 1), followed by the coupling to a stand-alone CSP plant (Case 2) and finally the coupling to a hybrid solar plant (Case 3).

4.2.1. Case 1: Stand-alone PV

This case involves the direct coupling of an electrolyzer to stand-alone PV system for green hydrogen production**.**

- **Electricity and hydrogen production versus month**

Figure 36 shows the monthly electricity production of the 100 MW_e stand-alone PV plant in a stacked bar chart that differentiates the amount of electricity to power the electrolysis process and to power the hydrogen conditioning process (for storage).

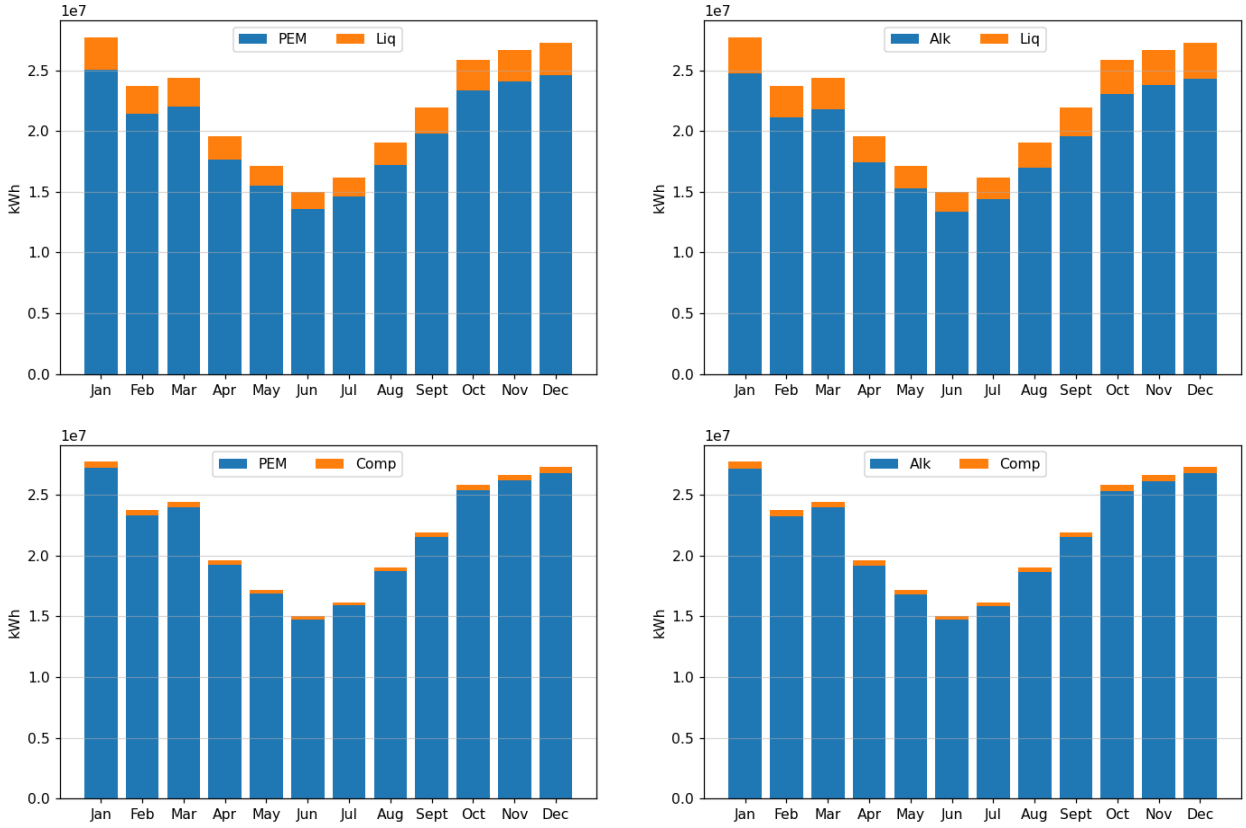

Figure 36: PV monthly electricity production

The results show a clear seasonal variability, where the months of lower electricity production coincide with the months of lower solar radiation in Chile and vice versa, due to the direct relationship between both variables. Blue shows the energy that should be used to power the electrolyzer, and orange shows the energy that powers the hydrogen conditioning units. Visually there is no significant difference between a PEM and alkaline electrolyzer, but there is a clear difference in the way that hydrogen will be stored. Closer inspection of Figure 36 shows that the hydrogen liquefaction unit is more energy intensive than a compressor, so there is a smaller amount of electrical energy that will go into hydrogen production. This difference in the monthly amount of hydrogen produced according to the different pathways is shown in Figure 37 and Figure 38, for the year 2021 and 2030 respectively.

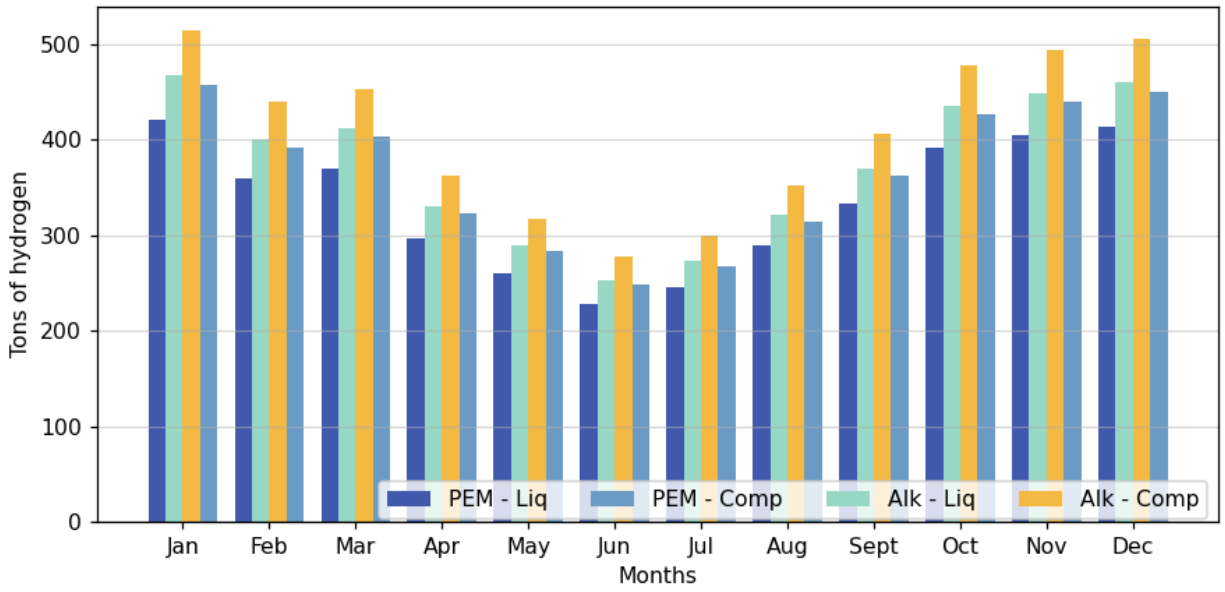

Figure 37: PV - driven monthly hydrogen production 2021

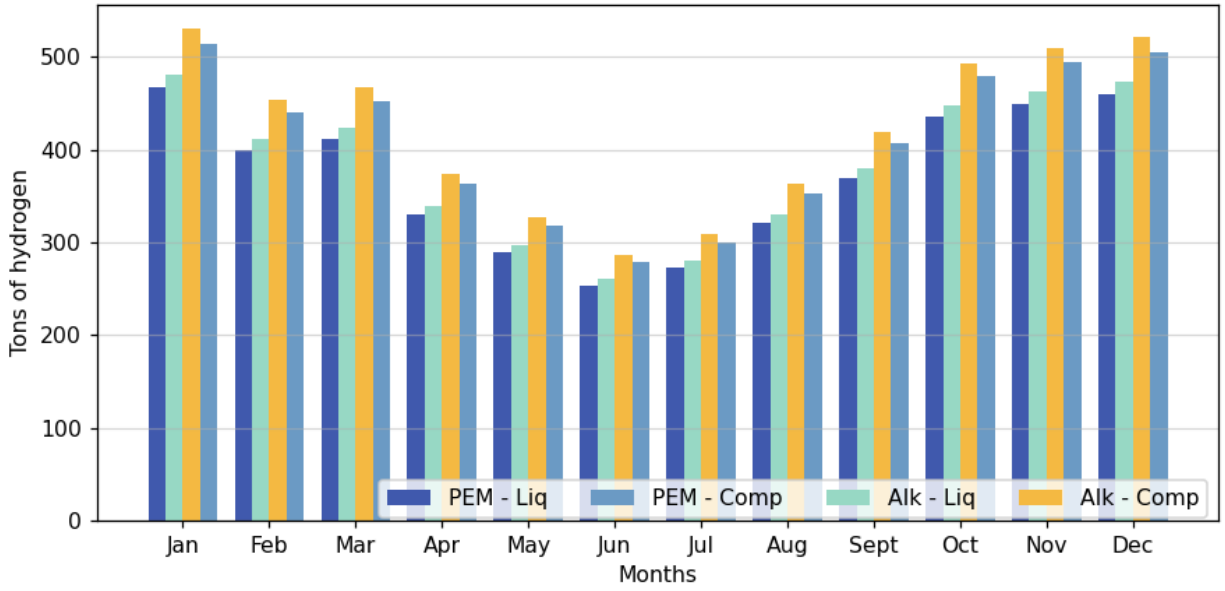

Figure 38: PV - driven monthly hydrogen production 2030

Figure 37 and Figure 38 show that the monthly hydrogen generation follows the same distribution pattern of solar radiation and electricity production because the production of hydrogen depends directly on these variables. As can be seen in the figures, the highest hydrogen production occurs in November, December and January. On the other hand, June represents the month with the lowest hydrogen production, which was an expected result since it is the month with the lowest solar irradiance of the year (winter season in Chile).

The combination of technologies that produces the most hydrogen is an alkaline electrolyzer with storage in the form of compressed gas. In contrast, a PEM electrolyzer with liquid hydrogen storage produces on average 12% less hydrogen per month than the best combination of technologies, a situation that remains largely unchanged by 2030. This difference in the monthly amount of hydrogen production is explained by the higher efficiency reported by an alkaline electrolyzer compared to a PEM electrolyzer. In addition, liquefaction is energy-intensive, so approximately 10% of the energy produced each month is used to bring the hydrogen to a temperature of around 20º K (-253ºC). Thus, this increased amount of energy for conditioning is at the expense of the electrolysis process.

- **Electrical power output vs time (hrs) over a year**

Figure 39 presents the electricity generation profile of the 100 MW_e PV plant over a year:

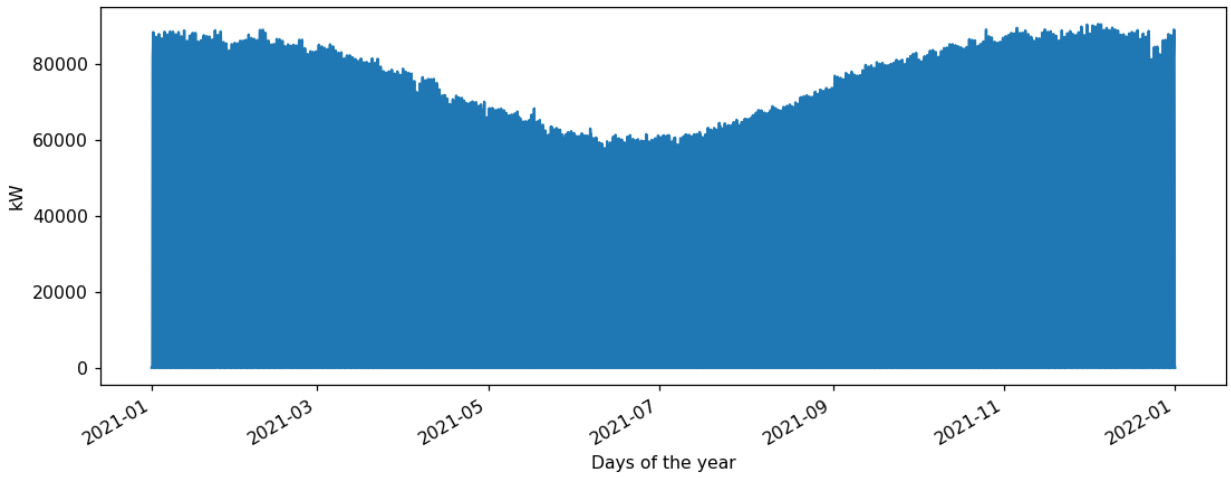

Figure 39: Energy generation profile of the PV system

From Figure 39, a clear seasonality during a generation year is observed, with low generation peaks during the winter months. In addition, it is interesting to note that the electricity power is at most 90% of the rated output without reaching the 100 MW_e design capacity at any time, because some of the standard test conditions are not achieved in practice.

- **Daily variation in electrical power against time for December 18-23**

Figure 40 and Figure 41 provide a good understanding of the daily variability in PV plant performance for some summer and winter days respectively.

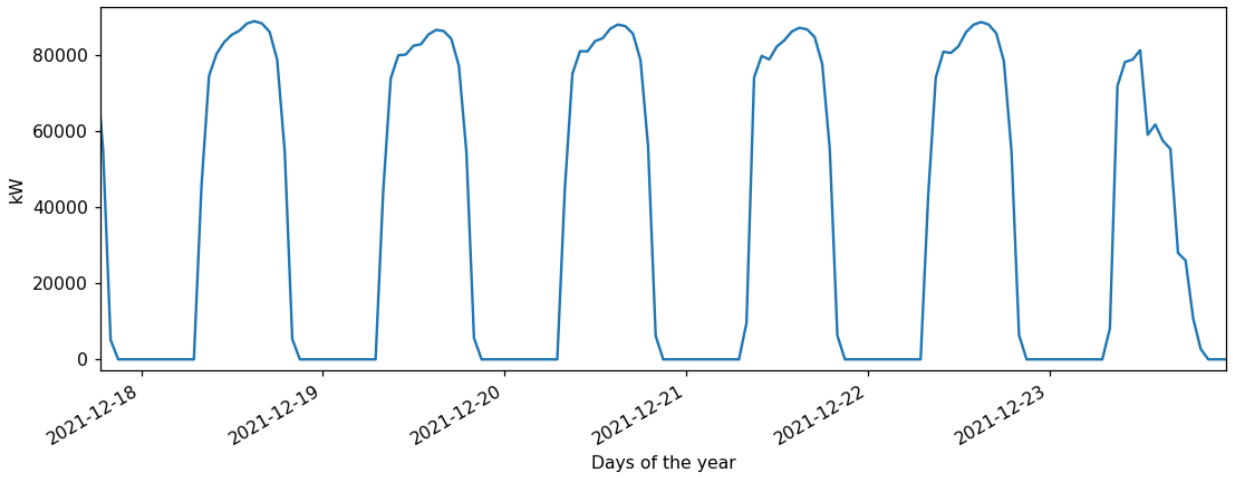

Figure 40: Daily energy production profile of the PV system - Summer time

- **Daily variation in electrical power against time for June 18-23**

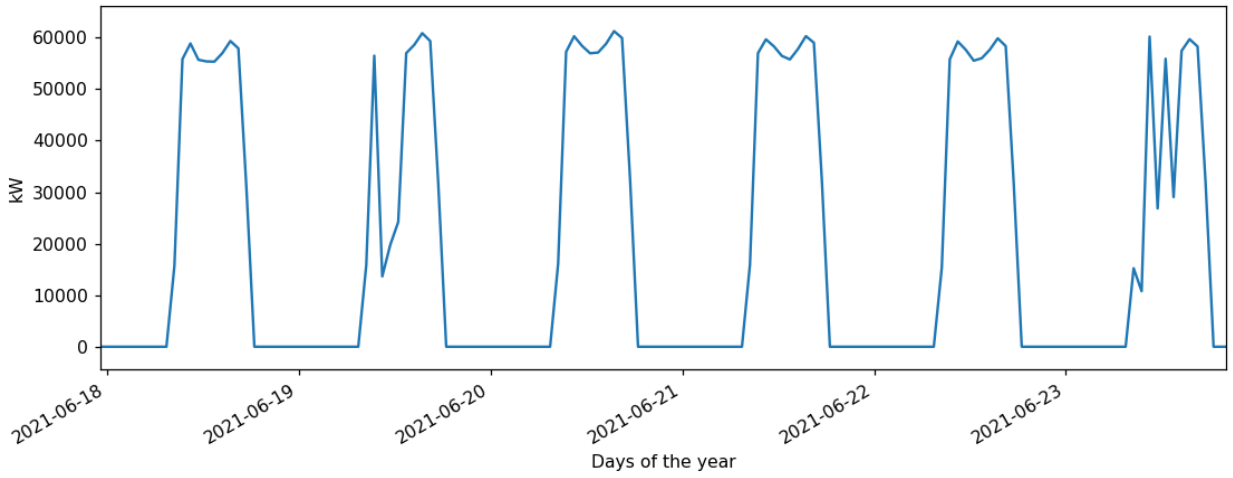

Figure 41: Daily energy production profile of the PV system - Winter time

The figures above show the variability and intermittency of PV technology. A good understanding of these power fluctuations is extremely important, as the production of hydrogen via PV coincides with the solar production profile of this technology. Clearly, PV technology alone is not capable of feeding the electrolyzer in a continuous and reliable manner, because given its natural variability, it does not manage to extend the running of

the electrolyzer and increases its frequent start-up/shutdown. The latter could have detrimental effects on electrolyzers due to early degradation.

4.2.2. Case 2: Stand-alone CSP

This case involves the direct coupling of an electrolyzer to stand-alone CSP system for green hydrogen production**.**

- **Electricity and hydrogen production versus month**

Figure 42 shows the monthly electricity production of the 100 MW_e stand-alone CSP plant in a stacked bar chart that differentiates the amount of electricity to power the electrolysis process and to power the hydrogen conditioning process (for storage).

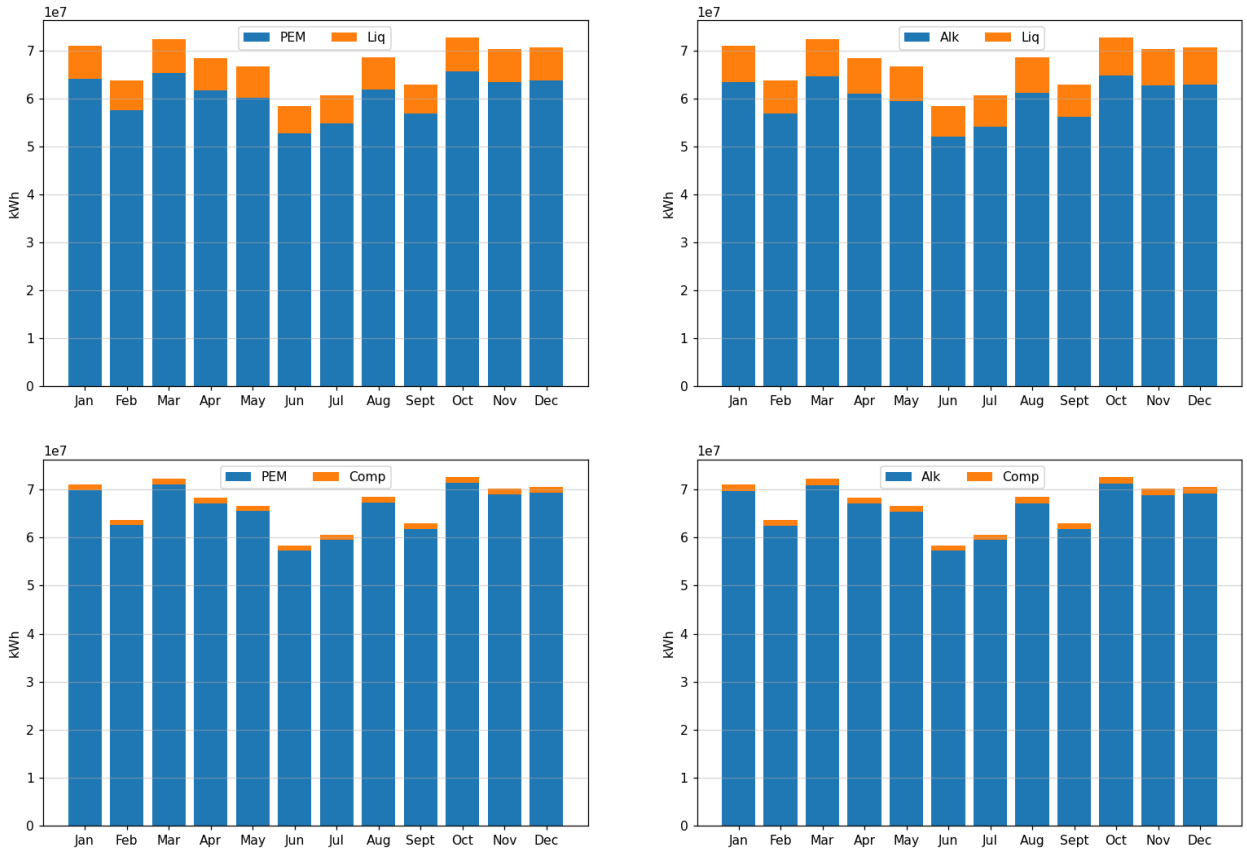

Figure 42: CSP monthly electricity production

As shown in Figure 42, the monthly electricity production of the stand-alone CSP plant is considerably higher than that of a stand-alone PV plant (Figure 36). The CSP plant can deliver about 150% more energy to the electrolysis process in January and about 300%

more in June, because the generation is not limited only to the hours of solar radiation. Additionally, it is evident that monthly generation is more constant (or flatter) throughout the year compared to PV generation, with only a small drop in winter and in February. The latter is attributable to the Altiplano winter phenomenon, hence, higher rate of clouds during the month. In conclusion, a CSP plant offers the advantage of delivering power for a longer number of hours, so that the electrolysis process can be maintained for a longer period of time. This higher level of equipment utilization implies an increase in the volumes of hydrogen produced with the same installed capacity, as shown in Figure 43 and Figure 44.

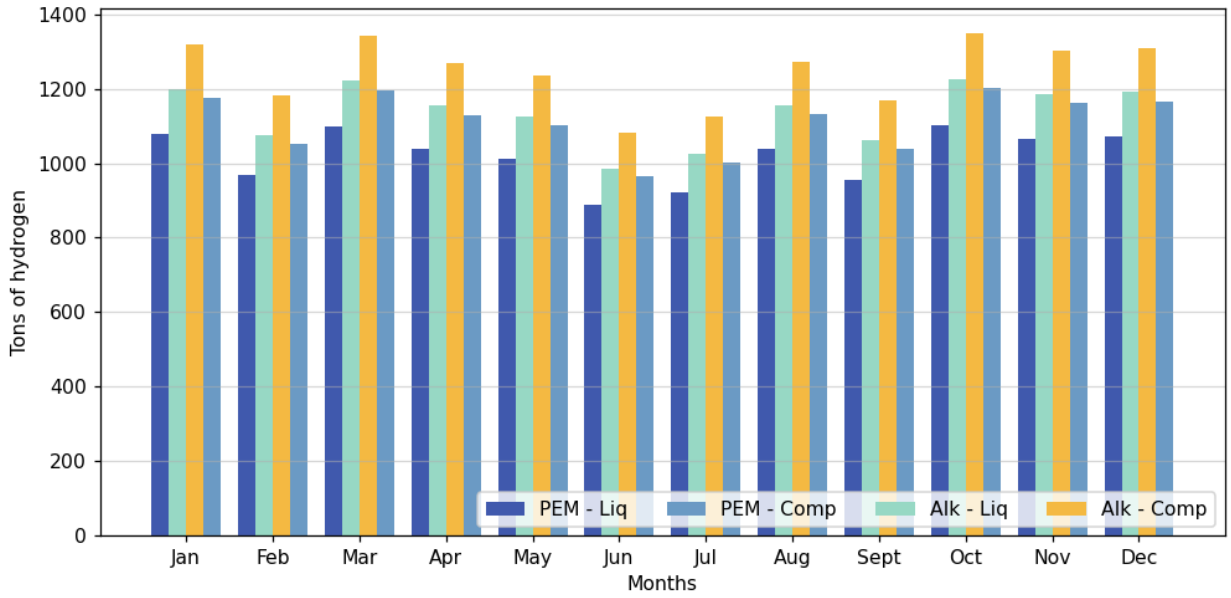

Figure 43: CSP - driven monthly hydrogen production 2021

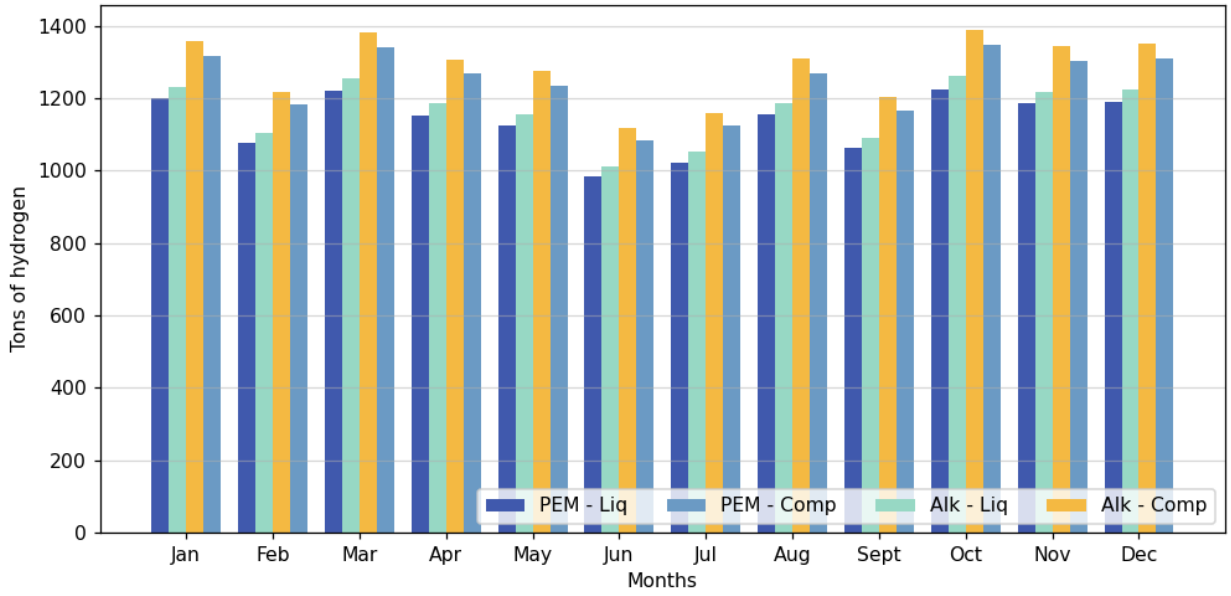

Figure 44: CSP - driven monthly hydrogen production 2030

- **Electrical power output vs time (hrs) over a year**

Figure 45 presents the electricity generation profile of the 100 MW_e CSP plant over the year.

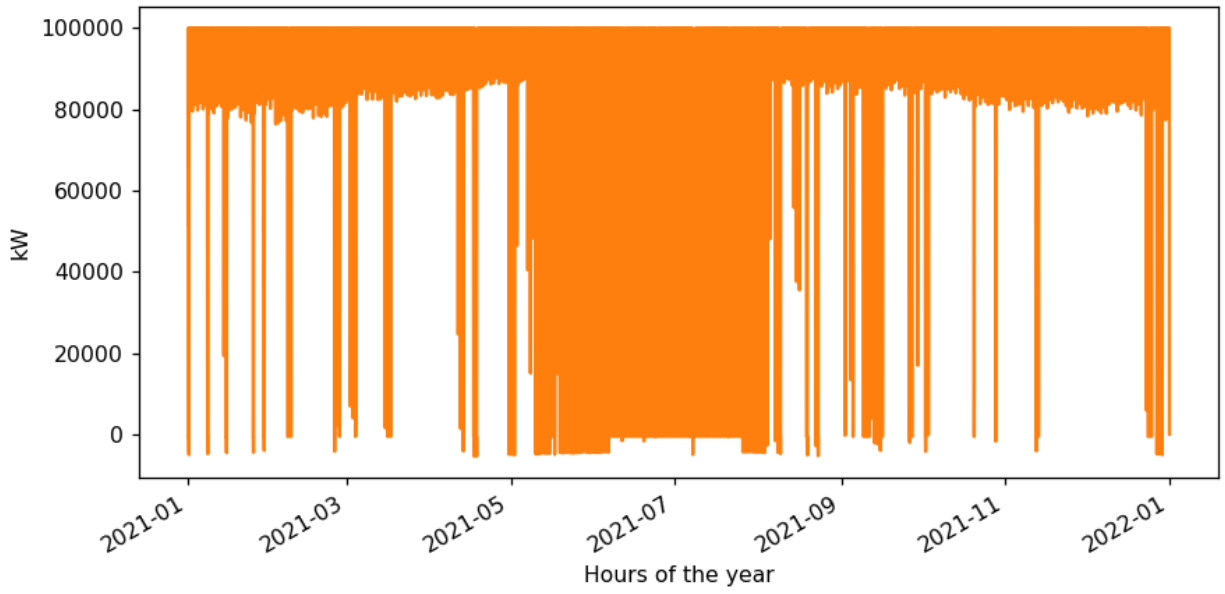

Figure 45: Energy generation profile of the CSP system

From the previous figure it is possible to observe that during the winter season the production of the stand-alone CSP plant is not enough to cover the base load. The complete discharge of the TES system and the frequent shut down of the power block during some hours of the night, explains the higher color concentration in the center of the figure. In contrast, in the seasons of higher solar radiation, even though the rated output drops in some early morning hours, the turbine is not completely shut down in most cases, as shown below.

- **Daily variation in electrical power against time for December 19-23**

Figure 46 and Figure 47 provide a good understanding of the daily generation profile for 100 MW_e CSP (15h storage) for some summer and winter days respectively.

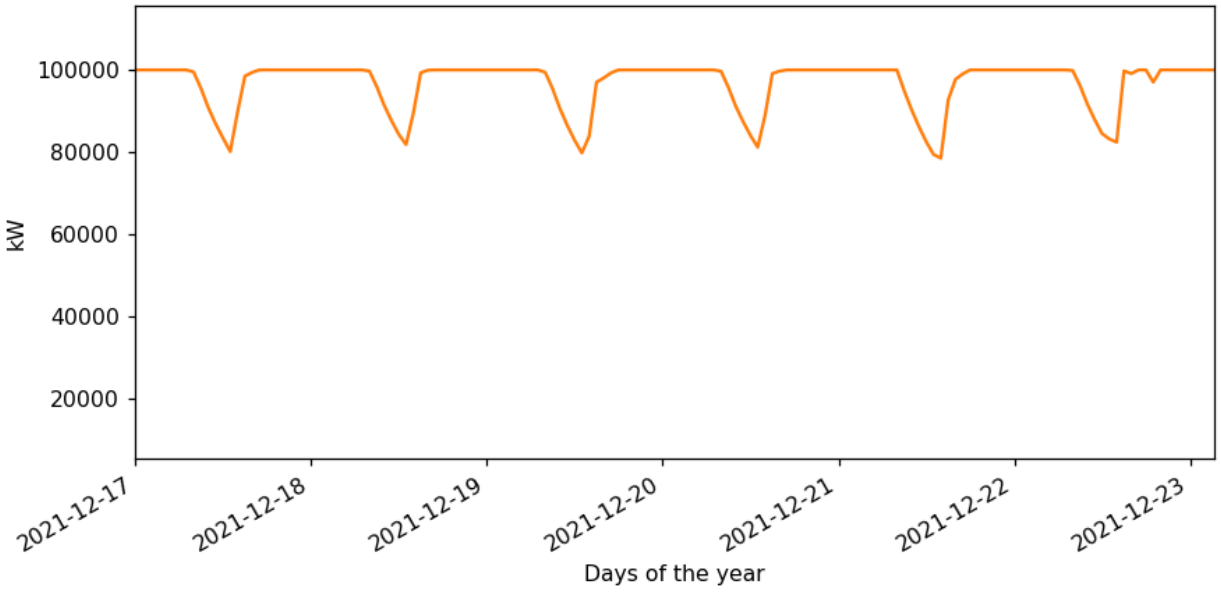

Figure 46: Daily energy production profile of the CSP system - Summer time

On typically good days for CSP production (summer days), as shown in Figure 46, the CSP and TES system can supply power to the electrolyzer during all hours, but with load reductions at night. These dips in rated power from 100 MW_e to about 80 MW_e are explained by the fact that the level of molten salts left in storage in the early morning is no longer sufficient to run the turbine at full capacity and thus ensure completely flat generation. However, stand-alone CSP is able to provide smoother power output and greater stability to the electrolysis process than stand-alone PV, which significantly increases hydrogen production. It should be noted that PV-based hydrogen production suffers from discontinuous power supply regardless of the season of the year and unpredictable production due to weather conditions (Figure 40).

- **Daily variation in electrical power against time for June 18-23**

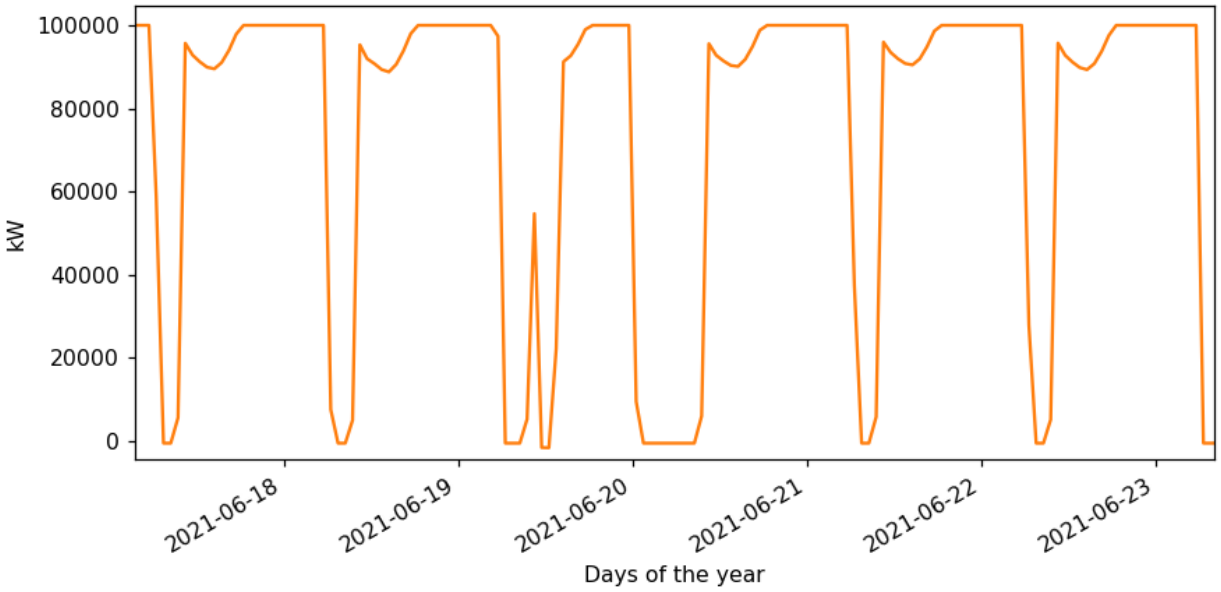

Figure 47: Daily energy production profile of the CSP system - Winter time

As can be seen in Figure 47, although during the winter the output of the CSP plant is higher than the PV plant, the TES system is not sufficient to generate electricity continuously. The latter implies that the electrolyzer will also operate intermittently, shutting down for a few hours in the early morning until the minimum technical power is reached for the CSP plant to start operating again.

4.2.3. Case 3: Hybrid CSP+PV

This case involves the production of green hydrogen powered by a hybrid solar plant.

- **Electricity and hydrogen production versus month**

Figure 48 shows the monthly electricity production of the 100 MW_e hybrid CSP+PV plant in a stacked bar chart that differentiates the amount of electricity to power the electrolysis process and to power the hydrogen conditioning process (for storage).

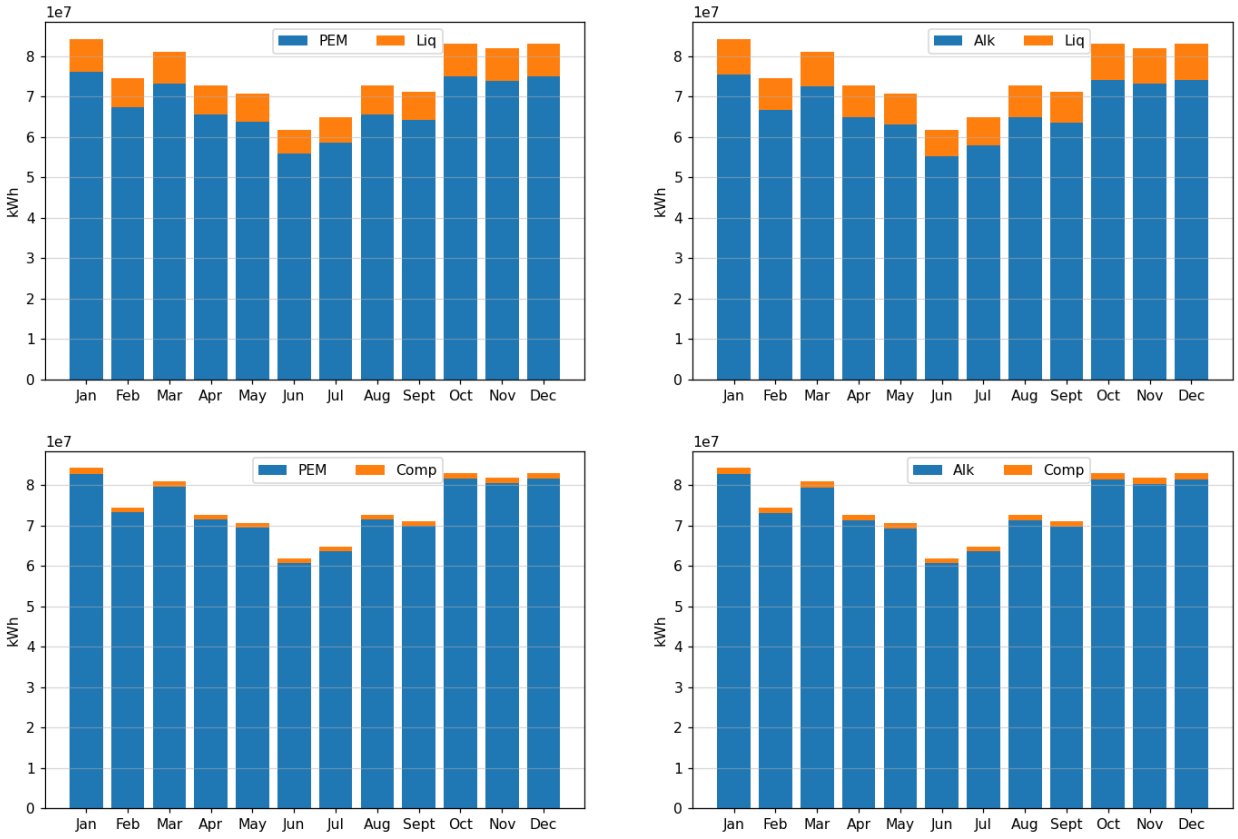

Figure 48: Hybrid CSP+PV monthly electricity production

Figure 49 and Figure 50 show the monthly hydrogen production from hybrid solar plants for the year 2021 and 2030 respectively.

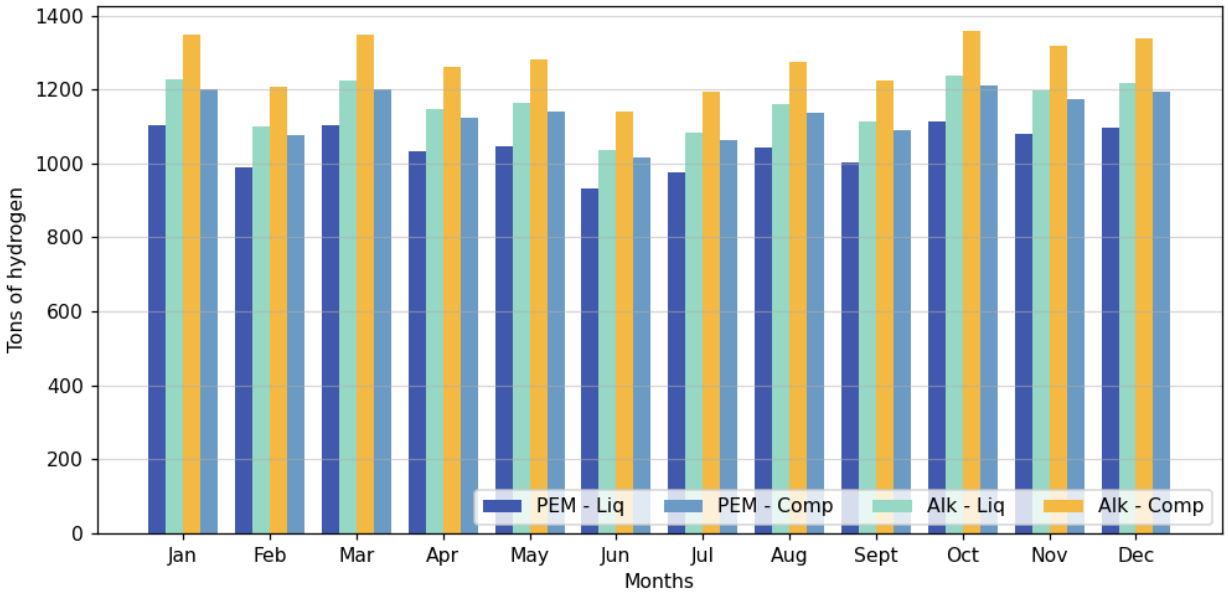

Figure 49: Hybrid CSP+PV - driven monthly hydrogen production 2021

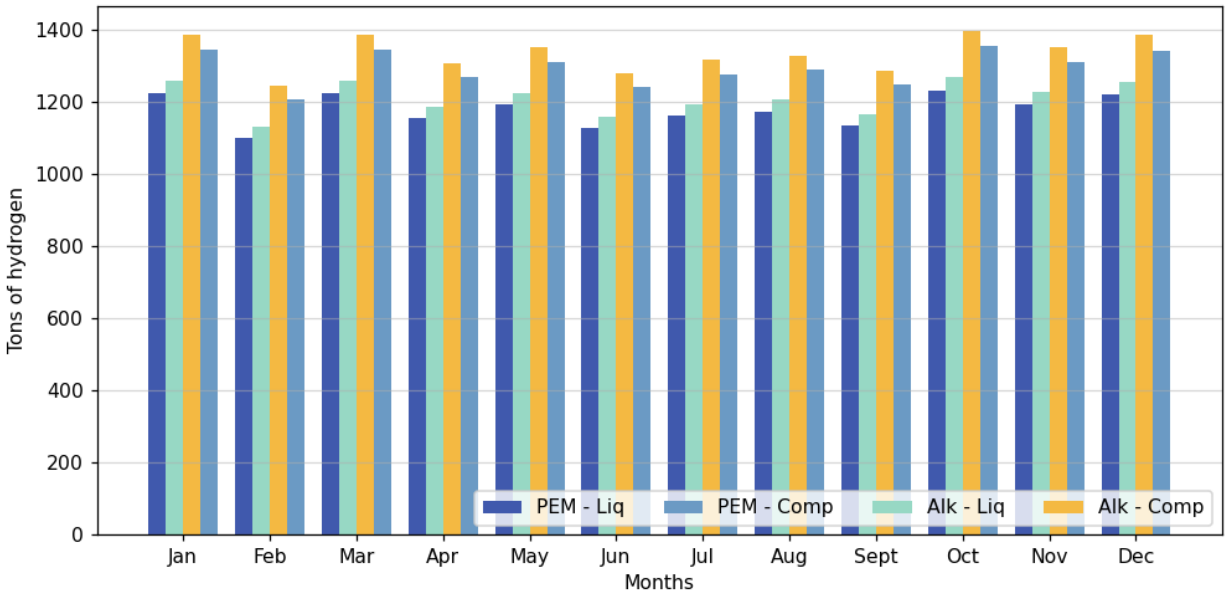

Figure 50: Hybrid CSP+PV - driven monthly hydrogen production 2030

In contrast to stand-alone solar technologies, the evolution of the monthly hydrogen production from a solar system is more uniform across seasons, i.e., there is less inter-annual variability due to the flexibility and stability that CSP brings to the electrolyzer's power supply. Hydrogen production from a hybrid solar plant achieves on average 1.24 and 1.28 Ton-hrs more hydrogen production than a PV plant in 2021 and 2030 respectively by means of an alkaline electrolyzer, the most efficient electrolyzer.

- **Electrical power output vs time (hrs) over a year**

Figure 51 shows the annual electricity generation profile of the PV (in blue) and CSP (in orange) technologies combined to achieve a nominal target of 100 MW_e.

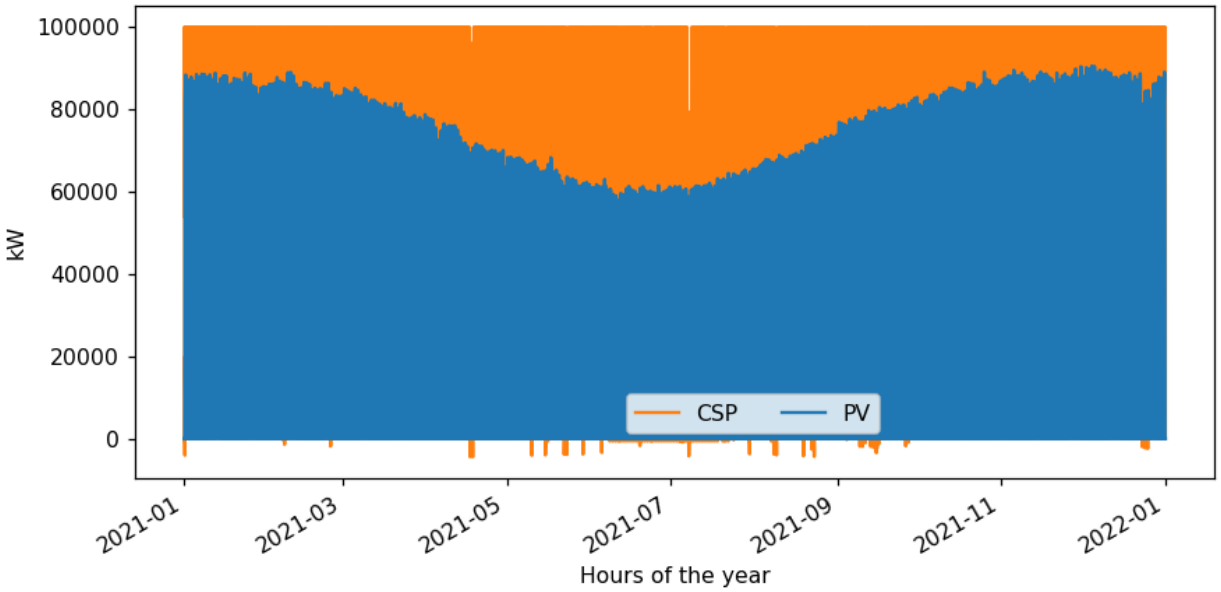

Figure 51: Energy generation profile of the PV + CSP system

- **Daily variation in electrical power against time for December 19-23**

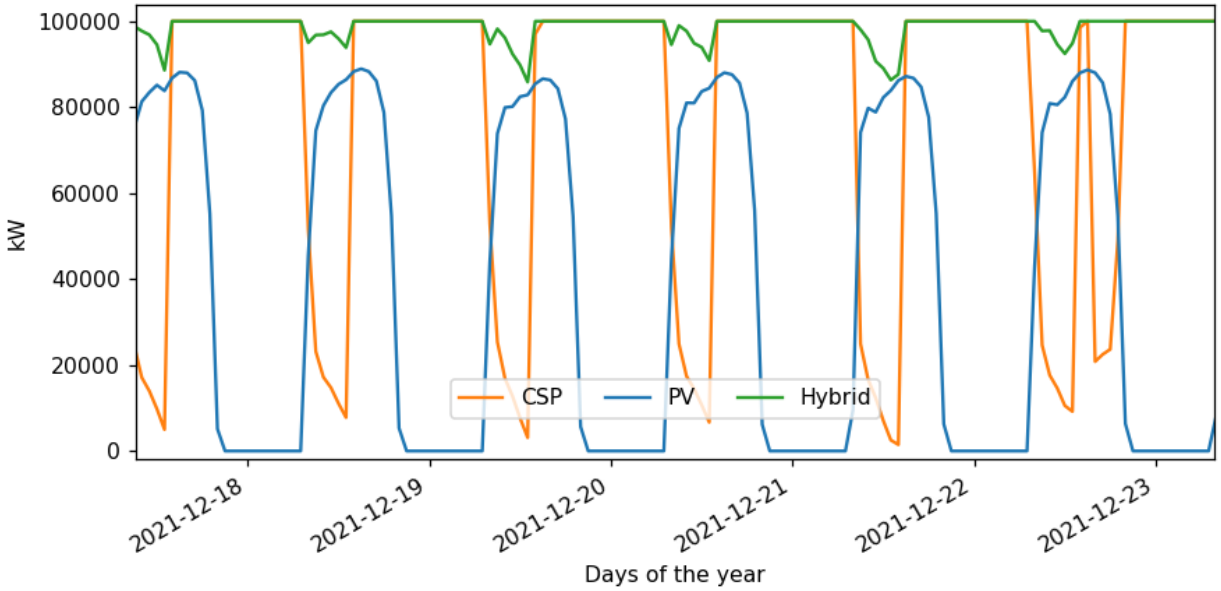

Figure 52: Daily energy production profile of the PV + CSP system - Summer time

Figure 52 shows the dynamics in the operation of the hybridized plant. It illustrates how the CSP output (orange line) adapts to the PV production (blue line) to provide a smoother combined output (green line). In other words, there is a clear temporal complementarity between the two technologies, which produces 24/7 generation during the months of highest solar radiation. This complementarity is achieved because CSP with TES is a dispatchable technology, i.e., it can increase or decrease the energy it delivers in response to the generation of PV, which is intermittent, non-dispatchable and relies exclusively on solar radiation. Summing up, at this time of the year, a hybrid solar plant significantly reduces the stops and start-ups of the electrolyzer.

- **Daily variation in electrical power against time for June 19-23**

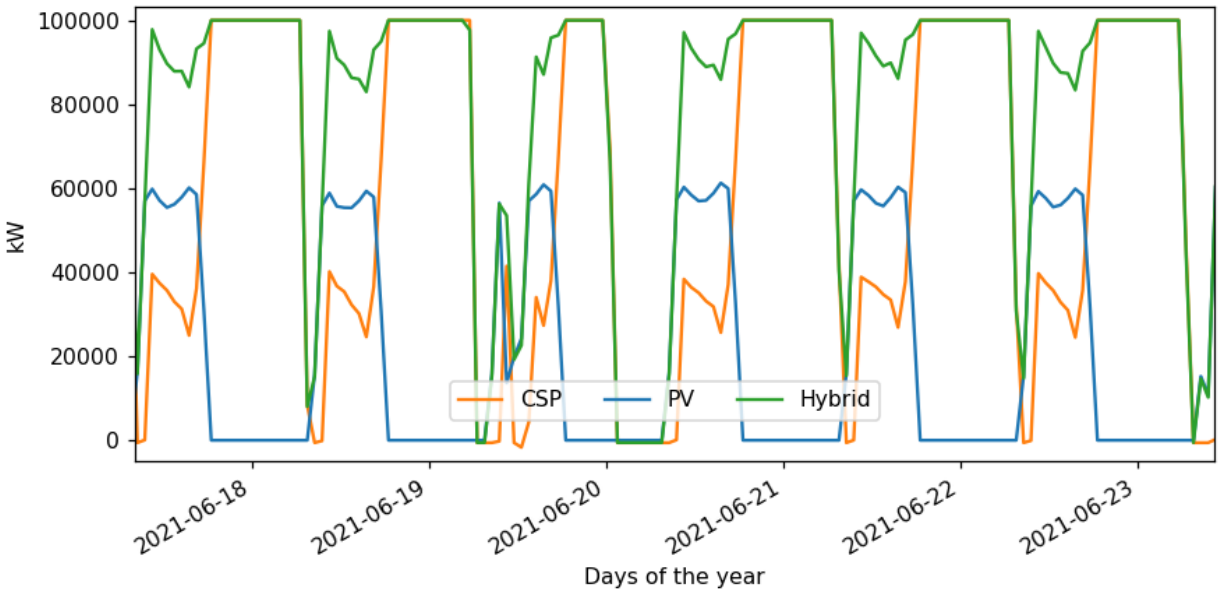

Figure 53: Daily energy production profile of the PV + CSP system - Winter time

Figure 53 shows that while during the winter there is no flat generation (CSP does not fill the gaps where PV generation is less than 100 MW_e), there is still a better performance of the combined plant compared to what each achieves on its own. In conclusion, in a hybrid solar plant, the PV energy covers the electricity production during daylight hours and the CSP acts as a "solar battery", which stores energy to power the electrolyzer during hours of low or no solar radiation. In a location with good solar radiation such as northern Chile, this could be the optimal combination for green hydrogen production, as an overly dynamic operation (many starts and stops) could increase the degradation of the electrolyzer, compromising its functionality, durability and lifetime. Additionally, there are economic benefits of this integration, as one of the ways to ensure a lower cost for green hydrogen is to keep the electrolyzers running as close to 24 hours a day as possible. The latter will be detailed in the economic results section.

4.2.4. Overall comparison for the three cases

Table 11 presents a comparison of technical parameters of the different configurations analyzed:

Table 11: Performance comparison of the different pathways

Configuration	LF Electrolyzer	GWh/year	Ton H_2/year	ktCO_2 avoided/year
PV - ALK	30%	263.48	4985 (2021) 5143 (2030)	101
PV - PEM	30.1%	264.41	4447 (2021) 5003 (2030)	101
CSP - ALK	89.8%	786.08	14872 (2021) 15344 (2030)	301
CSP - PEM	89.8%	786.08	13220 (2021) 14872 (2030)	301
Hybrid - ALK	95.7 %	837.92	15853 (2021) 16355 (2030)	321
Hybrid - PEM	95.7 %	837.92	14091 (2021) 15853 (2030)	321

From Table 11 it is clear that the hybridization of a PV and CSP plant offers the highest load factor of the electrolyzers (95.7%), i.e., this scenario increases the degree of utilization of the electrolyzers with a stable, secure and sustainable electricity supply throughout the year. These load factors are equivalent to the fact that hydrogen production powered by a hybrid plant can operate on average ~23 hrs/day (8383 hrs/year), by a stand-alone CSP ~22 hrs/day (7867 hrs/year) and by a stand-alone PV ~7 hrs/day (2628 hrs/year), in that order. The stand-alone PV technology is more sensitive to daily and seasonal variations in solar radiation, so the electrolyzer utilization is significantly lower than the stand-alone CSP plant and the hybridization of technologies. On the other hand, the stand-alone CSP technology achieves a higher yield compared to the stand-alone PV plant, as it increases the hydrogen production time during cloudy periods or at night, but less than a hybridized plant.

The load factor of the electrolyzer is proportional to the mass of hydrogen gas produced. In that sense, a hybrid solar plant ensures a massive production of hydrogen gas on an annual basis, with 15853 and 14091 tons of hydrogen via alkaline and PEM electrolysis in the current scenario (2021). Similarly, a production of 16355 and 15853 tons of hydrogen via alkaline and PEM electrolysis are projected in the future scenario (2030). It is important to highlight that these values consider the electrical energy actually fed into

the electrolyzer (excluding energy for storage) and not necessarily the total energy generated by the plant, which may be curtailed in order to ensure the operating limits of the electrolyzer. If the total annual energy generated by the hybrid solar plant were considered, it would be 966.18(GWh), which would avoid 370 ktCO_2 per year.

The synergetic operation of solar technologies in a hybrid plant also achieves a greater displacement of fossil fuels, which offers a considerable reduction in CO_2 equivalent emissions, and thus a better environmental protection. In other words, combined plants contribute more to the annual CO_2 equivalent abatement than stand-alone technologies, compared to a reference scenario that considers an average emission factor of the National Electricity System (SEN) in Chile. This metric is particularly valuable, as all actions the world is taking are aimed to achieve carbon neutrality by 2050, in line with the Paris Agreement's ambitious target to limit global temperature rise to 1.5°C.

Finally, it is worth mentioning that these differences in technical performance occur even though all solar plants have the same installed capacity or rated power (100 MW_e), but not the same electricity generation. The latter is explained by the fact that the nominal power of solar plants indicates only the maximum electrical power they can produce under specific conditions, while the electricity generation is the amount of electricity produced by the plant during a specific period of time (in this case, one year).

4.3. Economic Results

This section presents the main results obtained from the economic analysis. First, the LCOE results are presented, followed by the $LCOH_2$ of dedicated off-grid installations and their breakdown. Finally, the $LCOH_2$ obtained from grid electricity is presented, followed by the potential costs of storing hydrogen.

4.3.1. Levelized Cost of Energy (LCOE)

Table 12 shows the minimum LCOE value achieved for the different solar technologies analyzed.

Table 12: Minimum LCOE values achieved

Configuration/Scenario	Standard cost scenario (2021)	Outlook scenario (2030)
LCOE PV (USD/MWh)	30.61	14.23
LCOE CSP (USD/MWh)	69.96	35.44
LCOE Hybrid (USD/MWh)	65.84	33.42

From Table 12 it can be seen that in both the current and future scenarios, PV technology achieves the lowest specific cost of energy with a reduction of 54% between both time scenarios, mainly due to its low investment costs. In the second place is the estimated cost of energy achieved by a hybrid solar plant, and in the last place the cost of energy of a CSP plant. It is worth noting that both stand-alone and hybrid CSP generation show a percentage cost reduction of 49% between the current and future scenarios, mainly because CSP is expected to have a similar scale effect as PV had years ago, so its costs could fall further as installed capacity worldwide increases.

The LCOE results for solar PV and CSP in the current scenario are within the ranges of values reported by the IEA [66]. Similarly, the projected LCOE values for 2030 are close to the prices offered in Chile's last electricity supply tender (August 2021), which would take effect from 2026 for a period of 15 years. In this tender, Canadian Libertador Solar Holding SpA submitted the lowest bid for a PV project in Chile's last clean energy auction, which submitted a price of 13.32 (USD/MWh), setting the record as the lowest bid in Latin America [67]. In addition, the CSP project Likana Solar, broke the world record price for its bid in the last electricity supply tender with a price of 34 (USD/MWh). The project lost the tender, even though it could have provided 100% renewable, firm and dispatchable all-solar generation at a record price for 24/7.

4.3.2. Levelized Cost of Hydrogen ($LCOH_2$)

Table 13 shows the range of $LCOH_2$ values achieved according to the different pathways analyzed.

Table 13: Minimum $LCOH_2$ values achieved

Configuration/Scenario	Standard cost scenario (2021)		Outlook scenario (2030)	
	ALK	PEM	ALK	PEM
$LCOH_2$ PV (USD/kg_{H2})	2.38 - 2.65	4.05 - 4.34	1.39 - 1.52	1.92 - 2.07
$LCOH_2$ CSP (USD/kg_{H2})	3.81 - 4.23	5.10 - 5.46	2.02 - 2.19	2.32 - 2.50
$LCOH_2$ Hybrid (USD/kg_{H2})	3.59 - 3.99	4.81 - 5.16	1.90 - 2.07	2.20 - 2.36

Table 13 confirms that from a purely economic point of view the production of green hydrogen based on stand-alone PV reaches the lowest hydrogen production costs due to its low CAPEX, which is mainly attributed to the emergence of China as a major player in this industry. Next, in ascending order of cost, are hybrid plants and, lastly, hydrogen production based on stand-alone CSP. The costs achieved for the current scenario are not the same for all pathways analyzed; however, they are clearly not competitive with fuel-based or “grey” hydrogen today, regardless of the case under analysis. For the next decade, this situation is projected to change, as PV-based generation (PEM and alkaline) and hybrid plant generation (alkaline) could reach, under certain favorable conditions, the

range of competitive values, below USD 2 per kg of hydrogen (fossil fuel range, its main competitor in the market).

The levelized cost of hydrogen in the current scenario for PV-ALK is consistent with the cost reported by the IEA for Chile in the Global Hydrogen Review 2021 [25]. It is worth noting that all costs found for 2021 are also in accordance with the levelized cost of hydrogen based on renewable energies as reported by the IEA in its report The Future of Hydrogen, which fluctuates between 3 and 7.5 USD/kg_{H2} [23]. In addition, the hydrogen production cost estimates for the next decade are in general accord with recent studies indicating that by 2030, renewable hydrogen's cost will range from ~USD1.3 - 3.5/kg_{H2} (broader range). These sources include Bloomberg New Energy Finance (BNEF) [68], [69], International Renewable Energy Agency (IRENA) [62], International Energy Agency (IEA) [25] and the Hydrogen Council (H_2 Council) [70].

To put the levelized hydrogen costs shown above into perspective and to see the effect of different system components, Figure 54, Figure 55 and Figure 56 present the breakdown for the lower limit of each pathway.

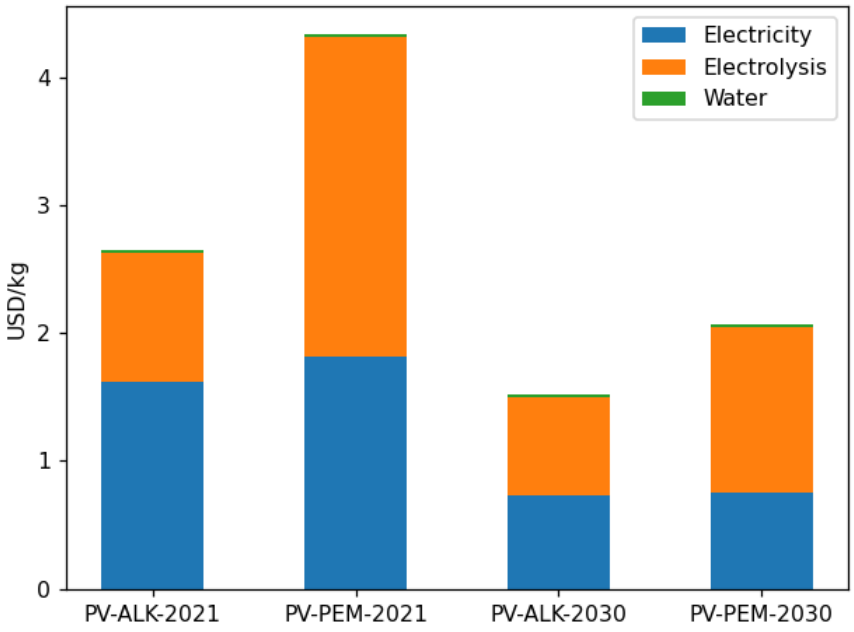

Figure 54: $LCOH_2$ breakdown, PV – electrolysis

As shown in Figure 54, for the current scenario (2021), about 61% of hydrogen production costs are related to the cost of PV electricity, 38% to the cost of the alkaline electrolyzer and less than 1% to the cost of water. On the other hand, in the PV-PEM case, the electricity cost drops to about 42% of the total cost, the electrolyzer rises to 57.5% and water is almost negligible at 0.5%. This difference in the breakdown is due to the higher

CAPEX investment of a PEM electrolyzer. In contrast, when the system has an alkaline electrolyzer, the cost of hydrogen production is highly dependent on the cost of energy to produce it. For the 2030 outlook scenario, in the PV-ALK case, about 50.5% of the levelized cost of hydrogen production is expected to be due to the cost of the electrolyzer, 48% due to the cost of electricity and 1.5% due to the cost of water. In the same time scenario, but for the PV-PEM case, 62% of the cost of producing one kilogram of hydrogen comes from the cost of the electrolyzer, 36% from the cost of electricity and less than 2% from the cost of water.

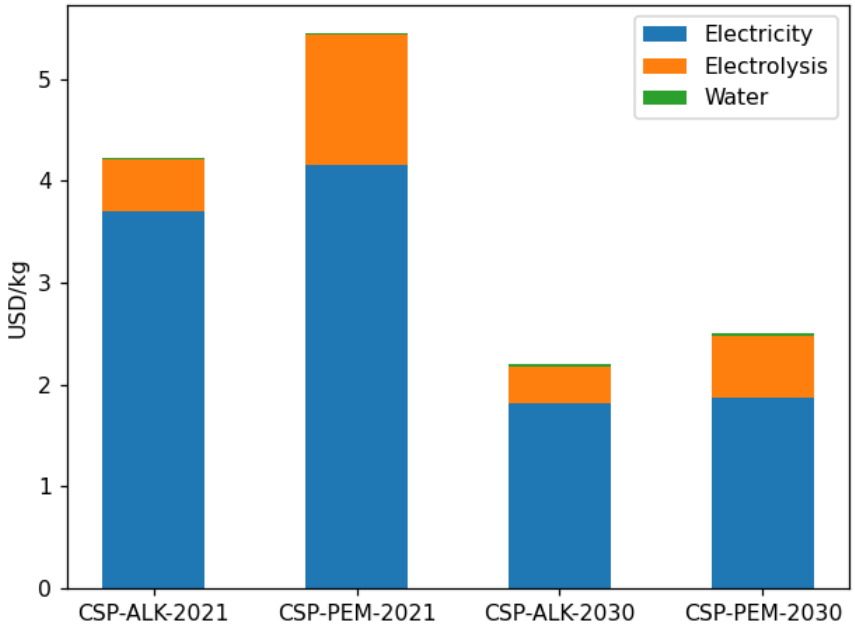

Figure 55: $LCOH_2$ breakdown, CSP – electrolysis

Figure 55 presents the breakdown of the specific hydrogen costs based on CSP alone. In this figure, clearly the cost of electricity dominates the cost of hydrogen production in all scenarios. In 2021, CSP-ALK 87.4% of the total comes from the cost of electricity, 12% from the cost of the electrolyzer and only 0.56% is attributed to the cost of water. In the CSP-PEM case, the cost of electricity drops to 76.2%, the electrolyzer rises to 23.4% and the cost of water is almost negligible at 0.4%. In the 2030 scenario the situation does not change substantially. For the CSP-ALK case, 82.5% of the cost corresponds to the cost of energy, 16.4% to the cost of the electrolyzer and 1.1% to the cost of water. In the CSP-PEM case, 74.8% of the cost corresponds to the cost of energy, 24.3% to the cost of the electrolyzer and 0.9% to the cost of water.

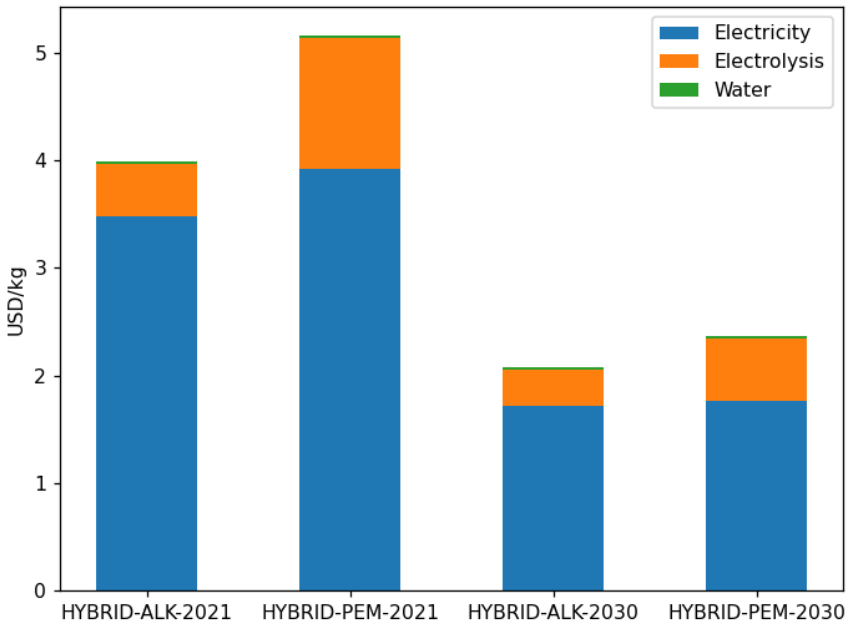

Figure 56: $LCOH_2$ breakdown, Hybrid plant – electrolysis

From Figure 56 it is clear that for a hybrid solar plant, the cost of energy is by far the most important component in the cost breakdown of green hydrogen production (greater than 50%), when compared to the cost of electrolyzers and the cost of water. The cost breakdown by major components of the specific cost of hydrogen production allows to detect where efforts should be focused in order to reduce hydrogen production costs and make it more cost-effective. In that sense, more efforts should be focused on reducing the investment costs of CSP technology to make it more attractive as an energy source for the hydrogen-based economy. In the particular case of Chile, CSP technology could increase the learning rate due to the higher cumulative installed capacity that will be available in the near future, considering the CSP projects already in operation, under construction and under environmental assessment.

The reader may have noticed that in stand-alone (Figure 55) and hybrid (Figure 56) CSP-based hydrogen production (which allow for more operating hours), the impact of electrolysis CAPEX costs on $LCOH_2$ decreases and the impact of electricity costs increases (there is a larger portion of the bar in blue than orange). In other words, with increasing electrolyzer operating hours, electricity cost is the major cost component, accounting for more than 50% of the production cost of each kg of green hydrogen. Therefore, the specific cost of energy offered by CSP still presents considerable margin for improvement and a clear opportunity for cost reduction in the long term.

4.3.3. Indirect on-grid connection to the electrolyzer: PPA mechanism

Table 14 shows the specific cost of hydrogen when electricity is considered to be supplied by an off-site PPA mechanism.

Table 14: $LCOH_2$ supplied through a PPA mechanism

Configuration/Scenario	Standard cost scenario (2021)	Outlook scenario (2030)
$LCOH_2$ - PPA (PV based) (USD/kg_{H2})	3.66	2.56
$LCOH_2$ - PPA (CSP based) (USD/kg_{H2})	4.96	3.36

From the results, it is possible to conclude that using an off-site PV-based PPA mechanism results in costs 35% and 68% higher than a direct connection in the years 2021 and 2030 respectively. Similarly, considering a CSP-based PPA mechanism results in costs 17% and 80% higher than a direct connection in the years 2021 and 2030 respectively. This increase in costs is explained by the additional electricity transmission costs that have to be paid when the electricity generation and the hydrogen production plants are decoupled (indirect connection). In this case, there is no physical exchange of energy, as the generation plant could be hundreds of kilometers away from the point of consumption, so there is an additional charge for the use of the grid. If electrolysis plants did not have to face these extra costs, grid-connected operation would be a more attractive case for an investor.

It is important to bear in mind that because there is no physical exchange of energy in this production pathway and the generation plant may be far from the point of consumption, the electrolyzer is powered by the nearest electrons and not necessarily those coming from the renewable plant. Despite having a grid-connected solar PPA, electrolysis will not necessarily work with 100% green electricity, and therefore, there is no certainty that it is effectively green hydrogen. The renewable generator injects the equivalent of the energy purchased by the buyer (the electrolysis plant), but the electricity that is taken from the grid to power the electrolyzer still comes from the same general "pool" of energy, where there is clean and dirty energy. In short, if "green" hydrogen is produced using the electricity grid, where electrons generated from different sources are mixed, it is not possible to ensure that there is any real benefit to the environment. In contrast, a direct on-site connection between a renewable plant and the electrolysis plant provides a guarantee of green origin, which is highly valued in the international markets.

4.3.4. Hydrogen Storage Cost

To quantify the storage cost per kg of hydrogen, the levelized cost methodology was used, i.e., the total storage cost divided by the hydrogen output. CAPEX costs include conditioning modules (compressor or liquefaction unit) to bring the hydrogen to the physical conditions necessary for storage, as well as steel storage tanks, which have a volume equivalent to the average daily production of each configuration. Table 15 presents an overview of post-processing (or conditioning) and storage of hydrogen in the currently most feasible options for hydrogen storage, i.e., compressed and liquid hydrogen.

Table 15: Levelized Cost of Hydrogen Storage

Configuration/Scenario	Hydrogen Storage	
	Compressed H_2 (GH_2)	Liquid H_2 (LH_2)
PV (USD/kg$_{H2}$)	0.37	3.03
CSP (USD/kg$_{H2}$)	0.24	1.14
Hybrid (USD/kg$_{H2}$)	0.23	1.09

The specific costs of the two storage options analyzed differ significantly because the effect of differences in CAPEX. On the one hand, the results show that the lowest specific storage costs are achieved for the compressed gas method (350 bar) with hydrogen production based on a hybrid solar plant, followed by stand-alone CSP production and finally stand-alone PV. On the other hand, liquid storage is a significantly more expensive alternative, exceeding by more than 300% the specific cost achieved for gaseous storage of hydrogen produced with dispatchable solar energy (stand-alone CSP and hybrid) and by more than 700% for variable solar energy (stand-alone PV). To store hydrogen in liquid form, high CAPEX costs must be incurred, making it the least cost-effective option of the two stationary systems analyzed.

It is interesting to highlight that the order of specific hydrogen storage costs changed with respect to the specific cost of production, showing that a hybrid plant could achieve the lowest specific cost of storage, even though the daily production volume in a hybrid solar plant is higher, which implies a larger and more expensive steel storage tank. This is explained precisely by the higher number of operating hours and consequently higher hydrogen production. When there is a high utilization of the electrolyzer, the specific CAPEX and OPEX share of the tanks and conditioning units per kg of hydrogen is reduced. To put it simply, there is a higher amortization of the investment per kilogram of hydrogen produced, as the investments are diluted by a higher quantity of product output, which is directly proportional to the load factor of the electrolyzer. To sum up, the higher the load factor of the electrolyzer, the lower the levelized cost of hydrogen storage.

4.4. Global Results Synthesis

Taken together, the results obtained in this thesis indicate that a hybrid CSP+PV plant dedicated to power the electrolysis process offers a promising pathway to stabilize hydrogen production at a price that could be less than USD 2 per kg_{H2} by 2030 (alkaline electrolysis). Although the lowest cost was achieved by PV-based hydrogen generation, considering only the LCOE and $LCOH_2$ is not sufficient to measure the real benefits of each system. The LCOE does not take into account that hybrid solar plants provide dispatchable renewable electricity due to the CSP plant with storage, and therefore, offer an added value that standalone PV does not offer. Consequently, value should be placed on the flexibility and storage that CSP offers to hydrogen production.

Stability in hydrogen supply is a key point to consider. Potential consumers of green hydrogen, such as mining companies or ammonia, methanol, and steel companies, cannot work with fluctuating supply of hydrogen, so a stand-alone PV plant would require a reserve of electricity generation capacity (back-up capacity) or an oversizing, which must be included in the production costs. It is precisely this capacity - stabilization in the electrolysis process - that makes a hybrid solar plant attractive, especially when production volumes and specific storage costs are taken into account. This idea is in agreement with what the IEA stated in its latest report, Global Hydrogen Review 2021 [25], where it is clearly stated that considering only the levelized cost of hydrogen production ignores other important factors, such as the number of electrolyzer operating hours; the volume of hydrogen produced throughout the year; and the costs that may arise from the need to smooth out fluctuations in renewable hydrogen supply (daily or seasonal). In addition, the same report adds that hydrogen users (consuming hydrogen directly or converting it into other fuels and feedstocks) require stability of supply, i.e., they must be assured of constancy of supply.

In summary, this thesis argues that solar hydrogen projects should be comprehensively evaluated, assigning additional value to solar plants when they offer flexibility or storage of renewable energy, which helps to stabilize and control the energy output that feeds the electrolysis process. This is also aligned with what the Chile's National Green Hydrogen Strategy proposes, which seeks not only to produce hydrogen at the best price, but also to achieve large volumes of green hydrogen production to become the world's leading producer of green hydrogen by electrolysis in 2030 [3]. In this sense, the techno-economic analysis carried out in this thesis supports the idea that there is a clear need to combine renewable energy sources, in particular PV and CSP, to allow the deployment of large-scale green hydrogen production that can position Chile as one of the most efficient and competitive producers of green hydrogen in the world.

5. Conclusions

This thesis set out to assess the technical and economic feasibility of large-scale green hydrogen production based on a hybrid solar plant in the Atacama Desert, in northern Chile. For a better understanding of the potential benefits of integrating such technologies, it was also necessary to study the performance of the stand-alone plants and a grid-connection via a PPA mechanism. The analysis of the different pathways was conducted by means of a simulation tool created for this thesis, which was based on PySAM, a Python interface that allowed to modify the source code of the National Renewable Energy Laboratory's System Advisor Model (SAM). The main conclusions of this thesis were as follows:

First, from an economic point of view, this thesis has identified that none of the solar hydrogen production pathways achieve costs lower than 2 (USD/kg_{H2}) in the current scenario (2021). Therefore, it can be concluded that today it is impossible for green hydrogen to compete economically with fossil-based hydrogen production. This situation would change in the next decade (2030), when green hydrogen generation directly coupled to stand-alone PV would reach the lowest specific cost among the analyzed pathways (1.39 USD/kg_{H2}). Furthermore, given certain favorable conditions, green hydrogen produced from hybrid solar plants and an alkaline electrolyzer could reach a cost of 1.90 USD/kg_{H2}, i.e., within the range of fossil-fuel based hydrogen, its closest competitor.

Second, the competitive range of costs that a hybrid solar plant could achieve in the next ten years demystifies the perception that CSP is too expensive as a renewable energy generation technology to produce hydrogen via electrolysis and the idea that PV and CSP are competing with each other. A hybridization of the two solar systems provides a reliable and more stable source of carbon-free electricity to produce hydrogen, which could reach a cost-competitive range in 2030, because the higher load factor of CSP over electrolysis (hence increasing the number of operating hours of the electrolyzers) offsets the investment costs of the project.

Third, from a technical point of view, a hybrid solar plant offers complementary or added benefits such as greater stability and reliability in hydrogen production, as it is more flexible and less dependent on the daily and seasonal variation of the solar resource. Although stand-alone PV-based hydrogen production is the cheapest alternative, it may not provide the necessary volumes for some demand cases (around 218% less annual production than a hybrid solar plant). In contrast, a hybrid solar plant can produce not only greater amounts of electricity and hydrogen, but also avoid the emission of about 220 $ktCO_2$ more than a stand-alone PV plant per year, making it also a better environmental option.

Fourth, this thesis has shown that the ranking order of economic merit obtained in production changes when the specific cost of storing daily hydrogen production is analyzed. The lowest specific or unit cost of storage is achieved with a hybrid solar plant that stores hydrogen as a high-pressure gas (0.23 USD/kg_{H2}). The latter is explained by the higher utilization of the electrolyzer, and therefore, the higher amortization of the investment in conditioning units and storage tanks for each kg of hydrogen produced.

Moreover, the results of this study support the idea that a direct connection or coupling between an electrolyzer and a renewable generation plant is more cost-effective than an indirect connection via a PPA mechanism. Although an off-site PPA mechanism stabilizes the hydrogen production, the additional transmission charges make the cost of energy higher than a direct connection, making hydrogen production between 35% and 68% more expensive, depending on the solar technology. Additionally, an off-site solar PPA contract does not ensure that the energy consumed at the hydrogen production site is actually 100% renewable and therefore that the hydrogen is effectively green.

In conclusion, if each pathway is analyzed holistically, the hybridization of solar technologies would not only be feasible, but also imperative to achieve a balance between a competitive price (not necessarily the lowest) and greater potential for large-scale solar hydrogen production (vast amounts of hydrogen) compared to stand-alone technologies with comparable power rating in 2030. Dedicated green hydrogen projects from the combination of PV and CSP can leverage the advantages that each technology has separately, so it could be an auspicious alternative if it is judged on its merits, i.e., its value is better recognized, especially in one of the locations with the highest solar energy potential worldwide: the Atacama Desert in northern Chile.

6. Limitations and Outlook for Future Work

The scope of this study was limited to the first four stages of the hydrogen value chain: energy source, production, conditioning and storage. Additionally, this study was limited to the production of pure green hydrogen, in liquid and gaseous state, but the study did not evaluate the use of another type of compound such as ammonia, synthetic methane or synthetic liquid fuels. An additional uncontrolled factor was the origin of the water used for the electrolysis process and its implications for water scarcity in northern Chile. Finally, it should be noted that the code generated for this thesis substantially improved the resolution of the SAM software for combining PV and CSP plants, as explained in the methodology. However, the new code does not achieve hourly resolution, i.e., the turbine can change nine times during the day, but not twenty-four, which would represent a perfect match between both solar technologies.

In spite of its limitations, the insights gained from this study may be useful as an input for future research, investors and policy makers in Chile and the world, because although green hydrogen is becoming already a reality, there is still many uncertainties to produce green hydrogen at a more competitive cost and on a large scale. Another important practical implication is that the code developed for this thesis can be easily adapted and manipulated to evaluate different scenarios, locations and parameters of both combined and stand-alone technologies.

These findings provide the following insights for future research:

- A natural progression of this work is to analyze the stages of the green hydrogen value chain that were not considered for this study, such as transport and applications in end-use sectors. Additionally, it would be interesting to study the sale of by-product oxygen from electrolysis and the potential for reducing the specific cost of hydrogen production by electrolysis.

- More broadly, research is also needed to determine optimal parameters through multi-objective optimization, which might be able to not only minimize costs, but also optimize water consumption, land use, electrolyzer utilization time, among other interesting aspects to be evaluated as a whole.

- Future work should analyze in detail other forms of solar hydrogen production that can be integrated into CSP technology, such as solar hydrogen by high-temperature electrolysis using solid oxide electrolyzers (SOEC) or also thermochemical water splitting.

- A further study could also assess the effects on the competitiveness of solar hydrogen production if carbon taxes are increased. That is, to impose a high annual tax on carbon dioxide (CO_2) emissions into the air that are produced during electricity generation and also in steam methane reforming (SMR), which is currently prevalent for hydrogen production in the industrial sector.

- Due to the constant changes the hydrogen industry is facing, further research should be undertaken to explore how the main drivers of the levelized cost of hydrogen will vary according to updated reports. For example, faster progress in cost reduction of PV technologies, CSP, electrolyzers or higher efficiency in their performance. It is recommended to follow the information published by leading institutions such as the International Energy Agency (IEA), the International Renewable Energy Agency (IRENA) or the Hydrogen Council.

7. Bibliography

[1] "The clean hydrogen future has already begun – Analysis - IEA." https://www.iea.org/commentaries/the-clean-hydrogen-future-has-already-begun (accessed Nov. 29, 2021).

[2] N. Barhorst, *Green hydrogen*, vol. 2. 2016.

[3] M. de Energía, "Estrategia nacional de hidrógeno verde."

[4] A. Starke, J. M. Cardemil, R. Escobar, and S. Colle, "Assessing the performance of hybrid CSP+PV plants in northern Chile," *AIP Conf. Proc.*, vol. 1734, no. May 2016, 2016, doi: 10.1063/1.4949230.

[5] M. Petrollese and D. Cocco, "Optimal design of a hybrid CSP-PV plant for achieving the full dispatchability of solar energy power plants," *Sol. Energy*, vol. 137, pp. 477–489, 2016, doi: 10.1016/j.solener.2016.08.027.

[6] C. Parrado, A. Girard, F. Simon, and E. Fuentealba, "2050 LCOE (Levelized Cost of Energy) projection for a hybrid PV (photovoltaic)-CSP (concentrated solar power) plant in the Atacama Desert, Chile," *Energy*, vol. 94, pp. 422–430, 2016, doi: 10.1016/j.energy.2015.11.015.

[7] R. Zhai, H. Liu, Y. Chen, H. Wu, and Y. Yang, "The daily and annual technical-economic analysis of the thermal storage PV-CSP system in two dispatch strategies," *Energy Convers. Manag.*, vol. 154, no. June, pp. 56–67, 2017, doi: 10.1016/j.enconman.2017.10.040.

[8] A. Zurita, C. Mata-Torres, C. Valenzuela, J. M. Cardemil, and R. A. Escobar, "Techno-economic analysis of a hybrid CSP+PV plant integrated with TES and BESS in Northern Chile," *AIP Conf. Proc.*, vol. 2033, no. November, 2018, doi: 10.1063/1.5067185.

[9] A. R. Starke, J. M. Cardemil, R. Escobar, and S. Colle, "Multi-objective optimization of hybrid PTC+PV system using genetic algorithm," *AIP Conf. Proc.*, vol. 2033, no. November, 2018, doi: 10.1063/1.5067183.

[10] A. Zurita, C. Mata-Torres, J. M. Cardemil, and R. A. Escobar, "Evaluating different operation modes of a hybrid CSP+PV+TES+BESS plant varying the dispatch priority," *AIP Conf. Proc.*, vol. 2126, no. July, 2019, doi: 10.1063/1.5117609.

[11] A. Zurita, C. Mata-Torres, J. M. Cardemil, and R. A. Escobar, "Assessment of time resolution impact on the modeling of a hybrid CSP-PV plant: A case of study in Chile," *Sol. Energy*, vol. 202, no. April 2019, pp. 553–570, 2020, doi: 10.1016/j.solener.2020.03.100.

[12] C. Hernández Moris, M. T. Cerda Guevara, A. Salmon, and A. Lorca, "Comparison between Concentrated Solar Power and Gas-Based Generation in Terms of Economic and Flexibility-Related Aspects in Chile," *Energies*, vol. 14, no. 4, p. 1063, 2021, doi: 10.3390/en14041063.

[13] C. Mata-Torres, R. A. Escobar, and J. M. Cardemil, "Techno-economic analysis of

CSP+PV+MED plant: Electricity and water production for mining industry in Northern Chile," *AIP Conf. Proc.*, vol. 2033, no. November, 2018, doi: 10.1063/1.5067179.

[14] J. M. Cardemil, A. R. Starke, A. Zurita, C. Mata-Torres, and R. Escobar, "Integration schemes for hybrid and polygeneration concentrated solar power plants," *Wiley Interdiscip. Rev. Energy Environ.*, no. May, pp. 1–22, 2021, doi: 10.1002/wene.412.

[15] J. M. Zolezzi, A. Garay, and M. Reveco, "Large scale hydrogen production from wind energy in the Magallanes area for consumption in the central zone of Chile," *J. Power Sources*, vol. 195, no. 24, pp. 8236–8243, 2010, doi: 10.1016/j.jpowsour.2009.12.060.

[16] P. M. Heuser, D. S. Ryberg, T. Grube, M. Robinius, and D. Stolten, "Techno-economic analysis of a potential energy trading link between Patagonia and Japan based on CO2 free hydrogen," *Int. J. Hydrogen Energy*, vol. 44, no. 25, pp. 12733–12747, 2019, doi: 10.1016/j.ijhydene.2018.12.156.

[17] F. I. Gallardo, A. Monforti Ferrario, M. Lamagna, E. Bocci, D. Astiaso Garcia, and T. E. Baeza-Jeria, "A Techno-Economic Analysis of solar hydrogen production by electrolysis in the north of Chile and the case of exportation from Atacama Desert to Japan," *Int. J. Hydrogen Energy*, vol. 46, no. 26, pp. 13709–13728, 2020, doi: 10.1016/j.ijhydene.2020.07.050.

[18] J. Armijo and C. Philibert, "Flexible production of green hydrogen and ammonia from variable solar and wind energy: Case study of Chile and Argentina," *Int. J. Hydrogen Energy*, vol. 45, no. 3, pp. 1541–1558, 2020, doi: 10.1016/j.ijhydene.2019.11.028.

[19] WMO - World Meteorological Organization, *Global Climate Report - August 2020 | State of the Climate*. 2020.

[20] "Hydrogen Solutions | Renewable Energy | Siemens Energy Global." https://www.siemens-energy.com/global/en/offerings/renewable-energy/hydrogen-solutions.html (accessed Jun. 05, 2021).

[21] Ministerio de Energía, "Guía de apoyo para solicitud de autorización de Proyectos Especiales de Hidrógeno," 2021.

[22] N. Ortiz, "Cuantificación del encadenamiento industrial y laboral para el desarrollo del hidrógeno en Chile Reporte final," 2020.

[23] "The Future of Hydrogen," *Futur. Hydrog.*, no. June, 2019, doi: 10.1787/1e0514c4-en.

[24] M. Rivarolo, G. Riveros-Godoy, L. Magistri, and A. F. Massardo, "Clean hydrogen and ammonia synthesis in paraguay from the Itaipu 14 GW hydroelectric plant," *ChemEngineering*, vol. 3, no. 4, pp. 1–11, 2019, doi: 10.3390/chemengineering3040087.

[25] "Global Hydrogen Review 2021," *Glob. Hydrog. Rev. 2021*, 2021, doi: 10.1787/39351842-en.

[26] S. Briefs and I. N. Energy, *Solar Based H2 Prod Systems*. .

[27] W. Law, *The sustainable hydrogen production process*. 2008.

[28] M. A. Valenzuela and B. Zapata, “Hydrogen production,” *Hydroprocessing Heavy Oils Residua*, pp. 313–338, 2007, doi: 10.1299/jsmemag.119.1169_182.

[29] S. S. Srinivasan, P. C. Sharma, E. K. Stefanakos, and D. Y. Goswami, *Nanomaterials for hydrogen storage*, no. January. 2014.

[30] C. Philibert, “Materials and Fuels,” 2017.

[31] R. A. Escobar *et al.*, “Estimating the potential for solar energy utilization in Chile by satellite-derived data and ground station measurements,” *Sol. Energy*, vol. 121, pp. 139–151, 2015, doi: 10.1016/j.solener.2015.08.034.

[32] IRENA, “Power Purchase Agreements for Variable Renewable Energy,” no. August, p. 13, 2018, [Online]. Available: https://www.irena.org/-/media/Files/IRENA/Agency/Events/2018/Aug/Renewable-Energy-PPAs.pdf.

[33] “Capacidad instalada – Energía Abierta | Comisión Nacional de Energía.” http://energiaabierta.cl/visualizaciones/capacidad-instalada/ (accessed Dec. 28, 2021).

[34] Ministerio de Energía and GIZ, *El Potencial Eólico, Solar E Hidroeléctrico De Arica a Chiloé*. 2014.

[35] M. S. Raboaca *et al.*, “Concentrating solar power technologies,” *Energies*, vol. 12, no. 6, pp. 1–17, 2019, doi: 10.3390/en19061048.

[36] A. Marzo *et al.*, “Solar extinction map in Chile for applications in solar power tower plants, comparison with other places from sunbelt and impact on LCOE,” *Renew. Energy*, vol. 170, no. October 2015, pp. 197–211, 2021, doi: 10.1016/j.renene.2021.01.126.

[37] G. Kolb, S. Power, and T. Systems, “An Evaluation of Possible Next-Generation High-Temperature Molten-Salt Power Towers,” no. January 2011, 2016, doi: 10.2172/1035342.

[38] C. Hernández, R. Barraza, A. Saez, M. Ibarra, and D. Estay, “Potential map for the installation of concentrated solar power towers in Chile,” *Energies*, vol. 13, no. 9, pp. 1–15, 2020, doi: 10.3390/en13092131.

[39] M. F. Eceiza and F. Torres, “SOLAR TOWER LCOE IN CHILE : COMPARATIVE STUDY,” 2021.

[40] A. Green, C. Diep, R. Dunn, and J. Dent, “High Capacity Factor CSP-PV Hybrid Systems,” *Energy Procedia*, vol. 69, pp. 2049–2059, 2015, doi: 10.1016/j.egypro.2015.03.218.

[41] G. Electricity, G. Heat, and G. Hydrogen, “Concentrated Solar Power | CSP Solar power around the clock,” 2021.

[42] “Generadoras de Chile - Cerro Dominador se adjudica fondos para desarrollo de proyectos de hidrógeno verde.” http://generadoras.cl/prensa/cerro-dominador-se-adjudica-fondos-para-desarrollo-de-proyectos-de-hidrogeno-verde (accessed Nov. 25, 2021).

[43] W. J. Platzer, “Combined solar thermal and photovoltaic power plants - An approach to 24h solar electricity?,” *AIP Conf. Proc.*, vol. 1734, no. May 2016, 2016, doi: 10.1063/1.4949173.

[44] D. Cocco, L. Migliari, and M. Petrollese, “A hybrid CSP-CPV system for improving the dispatchability of solar power plants,” *Energy Convers. Manag.*, vol. 114, pp. 312–323, 2016, doi: 10.1016/j.enconman.2016.02.015.

[45] C. A. Pan and F. Dinter, “Combination of PV and central receiver CSP plants for base load power generation in South Africa,” *Sol. Energy*, vol. 146, pp. 379–388, 2017, doi: 10.1016/j.solener.2017.02.052.

[46] F. M. Aprà, S. Smit, R. Sterling, and T. Loureiro, “Overview of the Enablers and Barriers for a Wider Deployment of CSP Tower Technology in Europe,” *Clean Technol.*, vol. 3, no. 2, pp. 377–394, 2021, doi: 10.3390/cleantechnol3020021.

[47] “Home - System Advisor Model (SAM).” https://sam.nrel.gov/ (accessed Oct. 17, 2021).

[48] “NREL-PySAM — NREL-PySAM 2.2.4 documentation.” https://nrel-pysam.readthedocs.io/en/master/ (accessed Sep. 02, 2021).

[49] L. Miller, R. Carriveau, S. Harper, and S. Singh, “Evaluating the link between LCOE and PPA elements and structure for wind energy,” *Energy Strateg. Rev.*, vol. 16, pp. 33–42, 2017, doi: 10.1016/j.esr.2017.02.006.

[50] Deutsche Gesellschaft fur Internationale Zusammenarbeit (GIZ) and Ministerio de Energía, “Potencial industrial de Chile para el desarrollo de una industria de concentración solar.” 2018.

[51] “Explorador Solar.” http://solar.minenergia.cl/inicio (accessed Sep. 13, 2021).

[52] D. Contreras Bilbao, “Valorization of the waste heat given off in a system alkaline electrolyzer-photovoltaic array to improve hydrogen production performance: Case study Antofagasta, Chile,” *Int. J. Hydrogen Energy*, vol. 46, no. 61, pp. 31108–31121, 2021, doi: 10.1016/j.ijhydene.2021.07.016.

[53] A. Romero, “Licitaciones de Suministro en Chile,” 2017, [Online]. Available: https://investchile.gob.cl/wp-content/uploads/2017/04/CNE-Licitaciones-Andrés-Romero_Abr-17.pdf.

[54] “2030 Solar Cost Targets | Department of Energy.” https://www.energy.gov/eere/solar/articles/2030-solar-cost-targets (accessed Sep. 03, 2021).

[55] IRENA, *Future of solar photovoltaic: Deployment, investment, technology, grid integration and socio-economic aspects (A Global Energy Transformation: paper)*, vol. November. 2019.

[56] A. D. O. Económicas, “Licitación 2021/01,” 2021.

[57] J. Dersch, S. Dieckmann, K. Hennecke, R. Pitz-Paal, M. Taylor, and P. Ralon, “LCOE reduction potential of parabolic trough and solar tower technology in G20 countries until 2030,” *AIP Conf. Proc.*, vol. 2303, 2020, doi: 10.1063/5.0028883.

[58] P. Gilman, N. Blair, M. Mehos, C. Christensen, S. Janzou, and C. Cameron, “Solar Advisor Model: User Guide for Version 2.0,” no. August, p. 133, 2008, [Online]. Available: http://www.nrel.gov/docs/fy08osti/43704.pdf.

[59] “Solar Power Tower Integrated Layout and Optimization Tool | Concentrating Solar Power | NREL.” https://www.nrel.gov/csp/solarpilot.html (accessed Oct. 18, 2021).

[60] D. G. für I. Z. (GIZ) G. Rodrigo Vásquez, Felipe Salinas, “Tecnologías del Hidrógeno y perspectivas para Chile,” p. 135, 2018, [Online]. Available: https://4echile-datastore.s3.eu-central-1.amazonaws.com/wp-content/uploads/2020/07/23185348/LIBRO-TECNOLOGIAS-H2-Y-PERSPECTIVAS-CHILE.pdf.

[61] T. H. Ruggles, J. A. Dowling, N. S. Lewis, and K. Caldeira, “Opportunities for flexible electricity loads such as hydrogen production from curtailed generation,” *Adv. Appl. Energy*, vol. 3, no. June, p. 100051, 2021, doi: 10.1016/j.adapen.2021.100051.

[62] IRENA, *Hydrogen: a Renewable Energy Perspective*, no. September. 2019.

[63] “Factores de Emisión – Energía Abierta | Comisión Nacional de Energía.” http://energiaabierta.cl/visualizaciones/factor-de-emision-sic-sing/ (accessed Oct. 17, 2021).

[64] L. Bousselamti and M. Cherkaoui, “Modelling and Assessing the Performance of Hybrid PV-CSP Plants in Morocco: A Parametric Study,” *Int. J. Photoenergy*, vol. 2019, 2019, doi: 10.1155/2019/5783927.

[65] M. Reuß, T. Grube, M. Robinius, P. Preuster, P. Wasserscheid, and D. Stolten, “Seasonal storage and alternative carriers: A flexible hydrogen supply chain model,” *Appl. Energy*, vol. 200, pp. 290–302, 2017, doi: 10.1016/j.apenergy.2017.05.050.

[66] N. C. for D. C. (NCDC), “2020 Edition,” *Natl. Guidel. Infect. Prev. Control Viral Hemorrhagic Fevers*, no. January, p. 112, 2020, [Online]. Available: https://ncdc.gov.ng/themes/common/docs/protocols/111_1579986179.pdf.

[67] I. E. Agency, “Renewables,” 2021.

[68] SNAM, “Global Gas Report 2020,” *Glob. Gas Rep. 2020*, p. 76, 2020, [Online]. Available: https://www.igu.org/app/uploads-wp/2020/08/GGR_2020.pdf.

[69] “‘Green’ Hydrogen to Outcompete ‘Blue’ Everywhere by 2030 | BloombergNEF.” https://about.bnef.com/blog/green-hydrogen-to-outcompete-blue-everywhere-by-2030/ (accessed Nov. 15, 2021).

[70] Hydrogen Council, “Hydrogen Insights,” no. February, p. 58, 2021, [Online]. Available: https://hydrogencouncil.com/wp-content/uploads/2021/02/Hydrogen-Insights-2021.pdf.

Annexes

Annexed A. Python code – Stand-alone PV

```
# # **1. PVWatts 100MW - Single Owner**

import pandas as pd
import numpy as np
import matplotlib.pyplot as plt
get_ipython().run_line_magic('matplotlib', 'inline')

# **1.1   Model Initialization**

import PySAM.Pvwattsv7 as pv
import PySAM.Singleowner as so
system_model = pv.default('PVWattsSingleOwner')

# **1.2   SystemDesign Group**

system_model.SystemDesign.system_capacity=100000 #kW
system_model.SystemDesign.module_type=1
system_model.SystemDesign.array_type=3
system_model.SystemDesign.tilt=0
system_model.SystemDesign.azimuth=0

# **1.3   SolarResource Group**

system_model.SolarResource.solar_resource_file="Antofagasta.csv"

# **1.4.   Outputs Group**

system_model.execute()
gen_pv=np.array(system_model.Outputs.dc)/1000
month_pv=system_model.Outputs.dc_monthly

get_ipython().run_line_magic('store', 'gen_pv')
get_ipython().run_line_magic('store', 'month_pv')

# **CF - PV**

system_model.Outputs.capacity_factor
gen_pv_limit=np.array(gen_pv)
for i in range(0,8760):
  if (gen_pv_limit[i]<100000*0.1):
    gen_pv_limit[i]=0

# **CF - ALK - PV**

CF_pv_alk=sum(gen_pv_limit)/(100000*8760)
CF_pv_alk

# **CF - PEM - PV**

CF_pv_PEM=sum(gen_pv)/(100000*8760)
CF_pv_PEM

def LCOE_pv(d,Module,Balance,Land_prep,Installation_labor,Contingency,percent_opex):
    Sum1=0
    Sum2=0
    t=0.07
    for i in range(1,31):
        Sum1 = Sum1 + (((1-d)**i)/((1+t)**i))
        Sum2 = Sum2 + (1/((1+t)**i))
```

```
    Production_pv=sum(gen_pv)
    CAPEX= ((Module + Installation_labor+Balance)*Contingency +
Land_prep)*system_model.SystemDesign.system_capacity*1000
    OPEX=percent_opex*CAPEX
    LCOE_pv=((CAPEX+OPEX*Sum2)/(Production_pv*Sum1))*1000
    return LCOE_pv

# **LCOE 2021**

LCOE_pv_2021=LCOE_pv(0.7/100,0.41,0.2,0.02,0.11,101/100,2/100) #USD/MWh
get_ipython().run_line_magic('store', 'LCOE_pv_2021')
LCOE_pv_2021

# **LCOE 2030**

LCOE_pv_2030=LCOE_pv(0.5/100,0.17,0.1,0.01,0.11,101/100,1/100) #USD/MWh
get_ipython().run_line_magic('store', 'LCOE_pv_2030')
LCOE_pv_2030

def LCOH(I,LCOE,f_p,eff,stack_lifetime=90000,percent_remp=0.4):
    P_inst=100 #Installed power of the electrolyser [MW]
    i=0.07
    h=8760 #Hours in a year
    N_rep=stack_lifetime/(f_p*h)
    I=I+I*percent_remp*(1-i)**N_rep
    n=30
    FRC=(i*((1+i)**n))/(((1+i)**n)-1)  #Capital Recovery Factor
    M=0.017 #Maintenance cost function as a percentage of investment, dependent on plant
factor
    Q_h2=20.3 #Hydrogen production capacity [kg/h]
    Q_H2O=0.017  #Amount of water consumed [m3/kg of hydrogen]
    P_H2O=1.4 #Water price [USD/m3]
    Q_e=33.3/eff  #Amount of electricity consumed [kWh/kg of hydrogen]
    P_e=LCOE
    Q_O2=7.8 #Sale of oxygen taking into account the quantity produced [kgO2/kg of hydrogen]
(optional term)
    P_O2=0.03 #Selling price of oxygen [USD/kgO2] (optional term)
    #LCOH_2 = P_inst*I*((FRC+M)/(h*f_p*Q_h2))+Q_H2O*P_H2O+Q_e*P_e-Q_O2*P_O2
    LCOH = I*(FRC+M)*33.3/(h*f_p*eff)+Q_H2O*P_H2O+Q_e*P_e
    Water=Q_H2O*P_H2O
    Electricity=Q_e*P_e
    Electrolysis=I*(FRC+M)*33.3/(h*f_p*eff)

      return(LCOH,Water,Electricity,Electrolysis)

# **LCOH - PV - ALK - 2021**

LCOH_pv_alk_2021=LCOH(500,LCOE_pv_2021/1000,CF_pv_alk,0.63,100000)[0]
LCOH_pv_alk_2021

# **LCOH - PV - PEM - 2021**

LCOH_pv_PEM_2021=LCOH(1100,LCOE_pv_2021/1000,CF_pv_PEM,0.56)[0]
LCOH_pv_PEM_2021

# **LCOH - PV - ALK - 2030**

LCOH_pv_alk_2030=LCOH(400,LCOE_pv_2030/1000,CF_pv_alk,0.65,100000,0.15)[0]
LCOH_pv_alk_2030

# **LCOH - PV - PEM - 2030**

LCOH_pv_PEM_2030=LCOH(650,LCOE_pv_2030/1000,CF_pv_PEM,0.63,percent_remp=0.2)[0]
LCOH_pv_PEM_2030

labels = ['PV-ALK-2021',"PV-PEM-2021","PV-ALK-2030","PV-PEM-2030"]
```

```
W =
[LCOH(500,LCOE_pv_2021/1000,CF_pv_alk,0.63,100000)[1],LCOH(1100,LCOE_pv_2021/1000,CF_pv_PEM,
0.56)[1],LCOH(400,LCOE_pv_2030/1000,CF_pv_alk,0.65,100000,0.15)[1],LCOH(650,LCOE_pv_2030/100
0,CF_pv_PEM,0.63,percent_remp=0.2)[1]]
Electri =
[LCOH(500,LCOE_pv_2021/1000,CF_pv_alk,0.63,100000)[2],LCOH(1100,LCOE_pv_2021/1000,CF_pv_PEM,
0.56)[2],LCOH(400,LCOE_pv_2030/1000,CF_pv_alk,0.65,100000,0.15)[2],LCOH(650,LCOE_pv_2030/100
0,CF_pv_PEM,0.63,percent_remp=0.2)[2]]
Electro =
[LCOH(500,LCOE_pv_2021/1000,CF_pv_alk,0.63,100000)[3],LCOH(1100,LCOE_pv_2021/1000,CF_pv_PEM,
0.56)[3],LCOH(400,LCOE_pv_2030/1000,CF_pv_alk,0.65,100000,0.15)[3],LCOH(650,LCOE_pv_2030/100
0,CF_pv_PEM,0.63,percent_remp=0.2)[3]]
width = 0.5       # the width of the bars: can also be len(x) sequence

fig, ax = plt.subplots()

bars = np.add(Electri, Electro).tolist()

ax.bar(labels, Electri, width, label='Electricity')
ax.bar(labels, Electro, width, bottom=Electri,label='Electrolysis')
ax.bar(labels, W, width, bottom=bars,label='Water')
ax.legend()

ax.set_ylabel("USD/kg")
#ax.set_title('Levelised Cost of Hydrogen - PV')

#ax.bar(labels, women_means, width, bottom=men_means,label='Women')

i=3
Agua=W[i]*100/(W[i]+Electri[i]+Electro[i])
Agua

Electricidad=Electri[i]*100/(W[i]+Electri[i]+Electro[i])
Electricidad

Electrolizador=Electro[i]*100/(W[i]+Electri[i]+Electro[i])
Electrolizador

fig, ax = plt.subplots(figsize=(10, 4), tight_layout=True, facecolor='w')
ax.plot(pd.date_range(start='1/1/2021', end='01/01/2022',periods=8760),gen_pv)
ax.set_ylabel('kW')
ax.set_xlabel('Days of the year')
fig.autofmt_xdate()

LHV=33.3 #(kWh/KgH2)
eff_PEM=0.56
eff_ALK=0.63
df1=pd.DataFrame(np.array(system_model.Outputs.dc_monthly))
df1["PEM"]=(df1[0]/(LHV/eff_PEM + 6.4))*(LHV/eff_PEM)
df1["Liq"]=(df1[0]/(LHV/eff_PEM + 6.4))*6.4
df1["Alk"]=(df1[0]/(LHV/eff_ALK + 6.4))*(LHV/eff_ALK)
df1["Liq1"]=(df1[0]/(LHV/eff_ALK + 6.4))*6.4
df1["PEM1"]=(df1[0]/(LHV/eff_PEM + 1.05))*(LHV/eff_PEM)
df1["Comp"]=(df1[0]/(LHV/eff_PEM + 1.05))*1.05
df1["Alk1"]=(df1[0]/(LHV/eff_ALK + 1.05))*(LHV/eff_ALK)
df1["Comp1"]=(df1[0]/(LHV/eff_ALK + 1.05))*1.05

Months=["Jan","Feb","Mar","Apr","May","Jun","Jul","Aug","Sept","Oct","Nov","Dec"]
df1.index=Months
df1.columns=["Energy", "PEM","Liq","Alk","Liq1","PEM1","Comp","Alk1","Comp1"]

x=range(12)
fig, ax = plt.subplots(2, 2,constrained_layout=False)
fig.set_size_inches(15, 10)

ax[0, 0].bar(x=range(12),
       height=df1["PEM"],
```

```
        label='PEM',
        width=0.8, bottom=0, align='center',
        color=None, edgecolor=None, linewidth=None);
ax[0, 0].bar(x=range(12),
        height=df1["Liq"],
        bottom=df1["PEM"],
        label='Liq',
        #width=0.8, bottom=0, align='center',
         color=None, edgecolor=None, linewidth=None);
ax[0, 0].set_ylabel('kWh')
#ax[0, 0].set_xlabel('Months')
#ax[0, 0].set_title('Monthly system power generated')
ax[0, 0].legend(loc=1, ncol=3, bbox_to_anchor=(0.65, 1))
ax[0, 0].set_xticklabels(Months)
ax[0, 0].set_xticks(range(12))
ax[0, 0].grid(alpha=0.5,axis='y')

ax[0, 1].bar(x=range(12),
        height=df1["Alk"],
        label='Alk',
        width=0.8, bottom=0, align='center',
        color=None, edgecolor=None, linewidth=None);
ax[0, 1].bar(x=range(12),
        height=df1["Liq1"],
        bottom=df1["Alk"],
        label='Liq',
        #width=0.8, bottom=0, align='center',
        color=None, edgecolor=None, linewidth=None);
ax[0, 1].set_ylabel('kWh')
#ax[0, 1].set_xlabel('Months')
#ax[0, 1].set_title('Monthly system power generated')
ax[0, 1].legend(loc=1, ncol=3, bbox_to_anchor=(0.65, 1))
ax[0, 1].set_xticklabels(Months)
ax[0, 1].set_xticks(x)
ax[0, 1].grid(alpha=0.5,axis='y')

ax[1, 0].bar(x=range(12),
        height=df1["PEM1"],
        label='PEM',
        width=0.8, bottom=0, align='center',
        color=None, edgecolor=None, linewidth=None);
ax[1, 0].bar(x=range(12),
        height=df1["Comp"],
        bottom=df1["PEM1"],
        label='Comp',
        #width=0.8, bottom=0, align='center',
        color=None, edgecolor=None, linewidth=None);
ax[1, 0].set_ylabel('kWh')
#ax[1, 0].set_xlabel('Months')
#ax[1, 0].set_title('Monthly system power generated')
ax[1, 0].legend(loc=1, ncol=3, bbox_to_anchor=(0.65, 1))
ax[1, 0].set_xticklabels(Months)
ax[1, 0].set_xticks(x)
ax[1, 0].grid(alpha=0.5,axis='y')

ax[1, 1].bar(x=range(12),
        height=df1["Alk1"],
        label='Alk',
        width=0.8, bottom=0, align='center',
        color=None, edgecolor=None, linewidth=None);
ax[1, 1].bar(x=range(12),
        height=df1["Comp1"],
        bottom=df1["Alk1"],
        label='Comp',
        #width=0.8, bottom=0, align='center',
        color=None, edgecolor=None, linewidth=None);
ax[1, 1].set_ylabel('kWh')
```

```
#ax[1, 1].set_xlabel('Months')
#ax[1, 1].set_title('Monthly system power generated')
ax[1, 1].legend(loc=1, ncol=3, bbox_to_anchor=(0.65, 1))
ax[1, 1].set_xticklabels(Months)
ax[1, 1].set_xticks(x)
ax[1, 1].grid(alpha=0.5,axis='y')

#2021
LHV=33.3 #(kWh/KgH2)
eff_PEM=0.56
eff_ALK=0.63
H2_PEM_Liq=(np.array(system_model.Outputs.dc_monthly)/(LHV/eff_PEM+6.4))*(1/1000)
H2_PEM_Comp=(np.array(system_model.Outputs.dc_monthly)/(LHV/eff_PEM+1.05))*(1/1000)
H2_Alk_Liq=(np.array(system_model.Outputs.dc_monthly)/(LHV/eff_ALK+6.4))*(1/1000)
H2_Alk_Comp=(np.array(system_model.Outputs.dc_monthly)/(LHV/eff_ALK+1.05))*(1/1000)

fig, ax = plt.subplots(figsize=(8, 4), tight_layout=True, facecolor='w')
y=np.arange(12)
width1 = 0.2
ax.bar(y - 1.5*width1,
       height=H2_PEM_Liq,
       label="PEM - Liq",
       width=0.2, color="#4059AD");

ax.bar(y +1.5*width1,
       height=H2_PEM_Comp,
       label='PEM - Comp',
       width=0.2,color="#6B9AC4");

ax.bar(y-0.5*width1,
       height=H2_Alk_Liq,
       label='Alk - Liq',
       width=0.2,color="#97D8C4");

ax.bar(y + 0.5*width1,
       height=H2_Alk_Comp,
       label='Alk - Comp',
       width=0.2, color="#F4B942");

ax.set_ylabel('Tons of hydrogen')
ax.set_xlabel('Months')
#ax.set_title('Monthly Hydrogen Production 2021')
ax.legend(loc=1, ncol=4, bbox_to_anchor=(1, 0.1))
ax.set_xticklabels(Months)
ax.set_xticks(y)
ax.grid(alpha=0.5,axis='y')

#2030
LHV=33.3 #(kWh/KgH2)
eff_PEM=0.63
eff_ALK=0.65
H2_PEM_Liq=(np.array(system_model.Outputs.dc_monthly)/(LHV/eff_PEM+6.4))*(1/1000)
H2_PEM_Comp=(np.array(system_model.Outputs.dc_monthly)/(LHV/eff_PEM+1.05))*(1/1000)
H2_Alk_Liq=(np.array(system_model.Outputs.dc_monthly)/(LHV/eff_ALK+6.4))*(1/1000)
H2_Alk_Comp=(np.array(system_model.Outputs.dc_monthly)/(LHV/eff_ALK+1.05))*(1/1000)

fig, ax = plt.subplots(figsize=(8, 4), tight_layout=True, facecolor='w')
y=np.arange(12)
width1 = 0.2
ax.bar(y - 1.5*width1,
       height=H2_PEM_Liq,
       label="PEM - Liq",
       width=0.2,color="#4059AD");

ax.bar(y +1.5*width1,
       height=H2_PEM_Comp,
       label='PEM - Comp',
```

```
        width=0.2,color="#6B9AC4");

ax.bar(y-0.5*width1,
        height=H2_Alk_Liq,
        label='Alk - Liq',
        width=0.2,color="#97D8C4");

ax.bar(y + 0.5*width1,
        height=H2_Alk_Comp,
        label='Alk - Comp',
        width=0.2,color="#F4B942");

ax.set_ylabel('Tons of hydrogen')
ax.set_xlabel('Months')
#ax.set_title('Monthly Hydrogen Production 2030')
ax.legend(loc=1, ncol=4, bbox_to_anchor=(1, 0.1))
ax.set_xticklabels(Months)
ax.set_xticks(y)
ax.grid(alpha=0.5,axis='y')

day_prod=(sum(gen_pv)/365)*0.63/33.3

flow_max=gen_pv.max()*0.63/33.3

#Compressed hydrogen gas storage system

i=0.07
n_conversion=15
n_storage=20

FRC_conversion=(i*((1+i)**n_conversion))/(((1+i)**n_conversion)-1)
FRC_storage=(i*((1+i)**n_storage))/(((1+i)**n_storage)-1)

M_storage=2/100
M_conversion=4/100

storage_module=500*day_prod*((FRC_storage+M_storage)/(sum(gen_pv_limit)*0.63/33.3))  #USD
conversion_module=3900*flow_max*1.05*((FRC_conversion+M_conversion)/(sum(gen_pv_limit)*0.63/33.3))

GH2=storage_module+conversion_module

#Liquid hydrogen

i=0.07
n_conversion=20
n_storage=20

FRC_conversion=(i*((1+i)**n_conversion))/(((1+i)**n_conversion)-1)
FRC_storage=(i*((1+i)**n_storage))/(((1+i)**n_storage)-1)

M_storage=2/100
M_conversion=8/100

storage_module=90*day_prod*((FRC_storage+M_storage)/(sum(gen_pv_limit)*0.63/33.3))  #USD
conversion_module=50000*flow_max*((FRC_conversion+M_conversion)/(sum(gen_pv_limit)*0.63/33.3))
LH2=storage_module+conversion_module

LCOH_pv_PPA_2021=LCOH(500,54.7/1000,0.42,0.63,100000)[0]
LCOH_pv_PPA_2021

LCOH_pv_PPA_2030=LCOH(400,38.7/1000,0.42,0.65,100000,0.15)[0]
LCOH_pv_PPA_2030
```

Annexed B. Python code – Stand-alone CSP

```
# # **2. Power Tower Molten Salt 100MW - Single Owner**

import pandas as pd
import numpy as np
import matplotlib.pyplot as plt
import math
get_ipython().run_line_magic('matplotlib', 'inline')

# **2.1   Model Initialization**

import PySAM.Solarpilot as sp
import PySAM.TcsmoltenSalt as tcs
system_model_csp = tcs.default('MSPTSingleOwner')

# **2.2   SystemDesign Group**

P_ref=111 #[MW]
Cycle_th_eff=0.412
S_M=3
Cycle_th_P=P_ref/Cycle_th_eff
tshours=15
system_model_csp.SystemDesign.P_ref=P_ref
system_model_csp.SystemDesign.solarm=S_M

model_opt1=sp.from_existing(system_model_csp)
model_opt1.SolarPILOT.helio_optical_error=0.00153
model_opt1.SolarPILOT.q_design=round(S_M*Cycle_th_P)
model_opt1.SolarPILOT.rec_aspect=21.6029/17.65
model_opt1.SolarPILOT.solar_resource_file="Antofagasta.csv"
model_opt1.execute()

system_model_csp.SystemDesign.tshours=tshours
system_model_csp.HeliostatField.helio_positions=model_opt1.Outputs.heliostat_positions
system_model_csp.TowerAndReceiver.h_tower=model_opt1.Outputs.h_tower_opt
system_model_csp.TowerAndReceiver.rec_height=model_opt1.Outputs.rec_height_opt
system_model_csp.HeliostatField.N_hel=model_opt1.Outputs.number_heliostats
system_model_csp.TowerAndReceiver.D_rec=model_opt1.Outputs.rec_height_opt/model_opt1.Outputs
.rec_aspect_opt
#system_model_csp.HeliostatField.A_sf_in=model_opt1.Outputs.area_sf
system_model_csp.HeliostatField.A_sf_in=model_opt1.SolarPILOT.helio_width*model_opt1.SolarPI
LOT.dens_mirror*model_opt1.SolarPILOT.helio_height*model_opt1.Outputs.number_heliostats

system_model_csp.SystemControl.f_turb_tou_periods=(1.0, 1.0, 1.0, 1.0, 1.0, 1.0, 1.0, 1.0,
1.0)
system_model_csp.SystemControl.weekday_schedule=12*[list(np.ones(24))]
system_model_csp.SystemControl.weekend_schedule=12*[list(np.ones(24))]

# **2.3   SolarResource Group**

system_model_csp.SolarResource.solar_resource_file="Antofagasta.csv"

# **2.4 Outputs Group**

system_model_csp.execute()

# **CF - CSP**

print(system_model_csp.Outputs.capacity_factor)

prod=list(np.array(system_model_csp.Outputs.gen)*0.96)

for i in range(0,8760):
```

```
    if (prod[i]>100000):
        prod[i]=100000

# **CF - ELECT - CSP**

CF_elect_csp=sum(prod)/(8760*0.9*111000)
CF_elect_csp

gen_csp_limit=prod

for i in range(0,8760):
    if (gen_csp_limit[i]<100000*0.1):
        gen_csp_limit[i]=0

CF_elect_csp_alk=sum(gen_csp_limit)/(8760*0.9*111000)

def LCOE_csp(d1,Site_prep,Solar_field,Fixed_tower_cost,Receiver_reference_cost,TES,Power_block,Contigencies,OM_fix,OM_var):
    Sum1=0
    Sum2=0
    t1=7/100
    for i in range(1,41):
        Sum1 = Sum1 + (((1-d1)**i)/((1+t1)**i))
        Sum2 = Sum2 + (1/((1+t1)**i))
    Production_csp=system_model_csp.Outputs.annual_energy
    Site_prep=Site_prep*system_model_csp.HeliostatField.A_sf_in
    Solar_field=Solar_field*system_model_csp.HeliostatField.A_sf_in
    Fixed_tower_cost=Fixed_tower_cost
    Tower_scaling_exp=0.0113
    Total_tower_cost=Fixed_tower_cost*math.exp(Tower_scaling_exp*(system_model_csp.TowerAndReceiver.h_tower-system_model_csp.TowerAndReceiver.rec_height/2+model_opt1.SolarPILOT.helio_height/2))
    Receiver_reference_cost=Receiver_reference_cost
    Receiver_area=math.pi*system_model_csp.TowerAndReceiver.D_rec*system_model_csp.TowerAndReceiver.rec_height
    Receiver_reference_area=1571
    Receiver_scaling_exponent=0.7
    Solar_receiver=Receiver_reference_cost*(Receiver_area/Receiver_reference_area)**Receiver_scaling_exponent
    #TES Thermal Capacity = Hours of Storage at Power Cycle Full Load × Cycle Thermal Input Power at Design
    #Cycle Thermal Power (MWt) = Design Turbine Gross Output (MWe) ÷ Cycle Thermal Efficiency
    Storage_capacity=(tshours*1000*P_ref)/Cycle_th_eff
    TES=TES*Storage_capacity
    #Balance_of_plant=290.00
    #Power_cycle_cost=1040.00
      #Power_block=(Balance_of_plant+Power_cycle_cost)*1000*P_ref
      Power_block=Power_block*1000*P_ref
      #Contigencies=5%

      CAPEX1=(Site_prep+Solar_field+Total_tower_cost+Solar_receiver+TES+Power_block)*Contigencies

      OPEX1=OM_fix*P_ref*1000+OM_var*Production_csp*(1/1000)

      LCOE_csp_standalone=((CAPEX1+OPEX1*Sum2)/(Production_csp*Sum1))*1000
      return(LCOE_csp_standalone)

  # **LCOE 2021**

  LCOE_csp_standalone_2021=LCOE_csp(0.2/100,16.00,140,3000000.00,103000000.00,22,1330,105/100,66,3.5)
  LCOE_csp_standalone_2021

  # **LCOE 2030**
```

```
117.
118.  LCOE_csp_standalone_2030=LCOE_csp(0.1/100,10,50,2189781,75182481.75,10,700,102/100,44,2.3)
119.  LCOE_csp_standalone_2030
120.
121.  def LCOH(I,LCOE,f_p,eff,stack_lifetime=90000,percent_remp=0.4):
122.      P_inst=100 #Installed power of the electrolyser [MW]
123.      i=0.07
124.      h=8760 #Hours in a year
125.      N_rep=stack_lifetime/(f_p*h)
126.      I=I+I*percent_remp*(1-i)**N_rep
127.      n=30
128.      FRC=(i*((1+i)**n))/(((1+i)**n)-1)  #Capital Recovery Factor
129.      M=0.05 #Maintenance cost function as a percentage of investment, dependent on plant
    factor
130.      Q_h2=20.3 #Hydrogen production capacity [kg/h]
131.      Q_H2O=0.017  #Amount of water consumed [m3/kg of hydrogen]
132.      P_H2O=1.4 #Water price [USD/m3]
133.      Q_e=33.3/eff  #Amount of electricity consumed [kWh/kg of hydrogen]
134.      P_e=LCOE
135.      Q_O2=7.8 #Sale of oxygen taking into account the quantity produced [kgO2/kg of
    hydrogen] (optional term)
136.      P_O2=0.03 #Selling price of oxygen [USD/kgO2] (optional term)
137.      LCOH = I*(FRC+M)*33.3/(h*f_p*eff)+Q_H2O*P_H2O+Q_e*P_e
138.
139.      Water=Q_H2O*P_H2O
140.      Electricity=Q_e*P_e
141.      Electrolysis=I*(FRC+M)*33.3/(h*f_p*eff)
142.      return(LCOH,Water,Electricity,Electrolysis)
143.
144.  # **LCOH - CSP - ALK - 2021**
145.
146.  LCOH_csp_alk_2021=LCOH(500,LCOE_csp_standalone_2021/1000,CF_elect_csp_alk,0.7,100000)[0]
147.  LCOH_csp_alk_2021
148.
149.  # **LCOH - CSP - PEM - 2021**
150.
151.  LCOH_csp_PEM_2021=LCOH(1100,LCOE_csp_standalone_2021/1000,CF_elect_csp,0.6)[0]
152.  LCOH_csp_PEM_2021
153.
154.  # **LCOH - CSP - ALK - 2030**
155.
156.  LCOH_csp_alk_2030=LCOH(400,LCOE_csp_standalone_2030/1000,CF_elect_csp_alk,0.71,100000,0.15
    )[0]
157.  LCOH_csp_alk_2030
158.
159.  # **LCOH - CSP - PEM - 2030**
160.
161.  LCOH_csp_PEM_2030=LCOH(650,LCOE_csp_standalone_2030/1000,CF_elect_csp,0.68,percent_remp=0.
    15)[0]
162.  LCOH_csp_PEM_2030
163.
164.  LCOH_CSP_PPA_2021=LCOH(500,84.7/1000,1,0.63,100000)[0]
165.  LCOH_CSP_PPA_2021
166.
167.  LCOH_pv_PPA_2030=LCOH(400,58.7/1000,1,0.65,100000,0.15)[0]
168.  LCOH_pv_PPA_2030
169.
170.  labels = ['CSP-ALK-2021',"CSP-PEM-2021","CSP-ALK-2030","CSP-PEM-2030"]
171.  W =
    [LCOH(500,LCOE_csp_standalone_2021/1000,CF_elect_csp,0.63,100000)[1],LCOH(1100,LCOE_csp_stan
    dalone_2021/1000,CF_elect_csp,0.56)[1],LCOH(400,LCOE_csp_standalone_2030/1000,CF_elect_csp,0
    .65,100000,0.15)[1],LCOH(650,LCOE_csp_standalone_2030/1000,CF_elect_csp,0.63,percent_remp=0.
    15)[1]]
172.  Electri =
    [LCOH(500,LCOE_csp_standalone_2021/1000,CF_elect_csp,0.63,100000)[2],LCOH(1100,LCOE_csp_stan
    dalone_2021/1000,CF_elect_csp,0.56)[2],LCOH(400,LCOE_csp_standalone_2030/1000,CF_elect_csp,0
```

```
    .65,100000,0.15)[2],LCOH(650,LCOE_csp_standalone_2030/1000,CF_elect_csp,0.63,percent_remp=0.
    15)[2]]
173.  Electro =
    [LCOH(500,LCOE_csp_standalone_2021/1000,CF_elect_csp,0.63,100000)[3],LCOH(1100,LCOE_csp_stan
    dalone_2021/1000,CF_elect_csp,0.56)[3],LCOH(400,LCOE_csp_standalone_2030/1000,CF_elect_csp,0
    .65,100000,0.15)[3],LCOH(650,LCOE_csp_standalone_2030/1000,CF_elect_csp,0.63,percent_remp=0.
    15)[3]]
174.  width = 0.5       # the width of the bars: can also be len(x) sequence
175.
176.  fig, ax = plt.subplots()
177.
178.  bars = np.add(Electri, Electro).tolist()
179.
180.  ax.bar(labels, Electri, width, label='Electricity')
181.  ax.bar(labels, Electro, width, bottom=Electri,label='Electrolysis')
182.  ax.bar(labels, W, width, bottom=bars,label='Water')
183.  ax.legend()
184.
185.  ax.set_ylabel("USD/kg")
186.  #ax.set_title('Levelised Cost of Hydrogen - CSP')
187.  #ax.bar(labels, women_means, width, bottom=men_means,label='Women')
188.
189.  i=3
190.  Agua=W[i]*100/(W[i]+Electri[i]+Electro[i])
191.  Agua
192.
193.  Electricidad=Electri[i]*100/(W[i]+Electri[i]+Electro[i])
194.  Electricidad
195.
196.  Electrolizador=Electro[i]*100/(W[i]+Electri[i]+Electro[i])
197.  Electrolizador
198.
199.  fig, ax = plt.subplots(figsize=(8, 4), tight_layout=True, facecolor='w')
200.
201.  ax.plot(pd.date_range(start='1/1/2021',
    end='01/01/2022',periods=8760),prod,c="tab:orange")
202.  ax.set_ylabel('kW')
203.  ax.set_xlabel('Hours of the year')
204.  #ax.set_title('Hourly energy generated by the CSP system and hydrogen production')
205.  #ax.legend(loc=2, ncol=3, bbox_to_anchor=(0.7, 0.2))
206.  fig.autofmt_xdate()
207.  #ax2 = ax.twinx()
208.  #ax2.set_ylabel('kg/h')  # we already handled the x-label with ax1
209.  #ax2.plot(pd.date_range(start='1/1/2021',
    end='01/01/2022',periods=8760),np.array(prod)*0.7/33.3,label='Hydrogen',c="tab:orange")
210.
211.  gen_csp=list(np.array(system_model_csp.Outputs.gen)*0.96)
212.  Sum_Enero=sum(gen_csp[0:744])
213.  Sum_Febrero=sum(gen_csp[744:1416])
214.  Sum_Marzo=sum(gen_csp[1416:2160])
215.  Sum_Abril=sum(gen_csp[2160:2880])
216.  Sum_Mayo=sum(gen_csp[2880:3624])
217.  Sum_Junio=sum(gen_csp[3624:4344])
218.  Sum_Julio=sum(gen_csp[4344:5088])
219.  Sum_Agosto=sum(gen_csp[5088:5832])
220.  Sum_Septiembre=sum(gen_csp[5832:6552])
221.  Sum_Octubre=sum(gen_csp[6552:7296])
222.  Sum_Noviembre=sum(gen_csp[7296:8016])
223.  Sum_Diciembre=sum(gen_csp[8016:8760])
224.
225.  Production =[Sum_Enero, Sum_Febrero, Sum_Marzo, Sum_Abril, Sum_Mayo, Sum_Junio, Sum_Julio,
    Sum_Agosto, Sum_Septiembre, Sum_Octubre, Sum_Noviembre,Sum_Diciembre]
226.
227.  LHV=33.3 #(kWh/KgH2)
228.  eff_PEM=0.56
229.  eff_ALK=0.63
230.
```

```
df1=pd.DataFrame(Production)
df1["PEM"]=(df1[0]/(LHV/eff_PEM + 6.4))*(LHV/eff_PEM)
df1["Liq"]=(df1[0]/(LHV/eff_PEM + 6.4))*6.4
df1["Alk"]=(df1[0]/(LHV/eff_ALK + 6.4))*(LHV/eff_ALK)
df1["Liq1"]=(df1[0]/(LHV/eff_ALK + 6.4))*6.4
df1["PEM1"]=(df1[0]/(LHV/eff_PEM + 1.05))*(LHV/eff_PEM)
df1["Comp"]=(df1[0]/(LHV/eff_PEM + 1.05))*1.05
df1["Alk1"]=(df1[0]/(LHV/eff_ALK + 1.05))*(LHV/eff_ALK)
df1["Comp1"]=(df1[0]/(LHV/eff_ALK + 1.05))*1.05

Months=["Jan","Feb","Mar","Apr","May","Jun","Jul","Aug","Sept","Oct","Nov","Dec"]
df1.index=Months
df1.columns=["Energy", "PEM","Liq","Alk","Liq1","PEM1","Comp","Alk1","Comp1"]

x=range(12)
fig, ax = plt.subplots(2, 2, constrained_layout=False)

fig.set_size_inches(15, 10)

ax[0, 0].bar(x=range(12),
       height=df1["PEM"],
       label='PEM',
       width=0.8, bottom=0, align='center',
       color=None, edgecolor=None, linewidth=None);
ax[0, 0].bar(x=range(12),
       height=df1["Liq"],
       bottom=df1["PEM"],
       label='Liq',
       #width=0.8, bottom=0, align='center',
       color=None, edgecolor=None, linewidth=None);
ax[0, 0].set_ylabel('kWh')
#ax[0, 0].set_xlabel('Months')
#ax[0, 0].set_title('Monthly system power generated')
ax[0, 0].legend(loc=1, ncol=3, bbox_to_anchor=(0.65, 1))
ax[0, 0].set_xticklabels(Months)
ax[0, 0].set_xticks(range(12))
ax[0, 0].grid(alpha=0.5,axis='y')

ax[0, 1].bar(x=range(12),
       height=df1["Alk"],
       label='Alk',
       width=0.8, bottom=0, align='center',
       color=None, edgecolor=None, linewidth=None);
ax[0, 1].bar(x=range(12),
       height=df1["Liq1"],
       bottom=df1["Alk"],
       label='Liq',
       #width=0.8, bottom=0, align='center',
       color=None, edgecolor=None, linewidth=None);
ax[0, 1].set_ylabel('kWh')
#ax[0, 1].set_xlabel('Months')
#ax[0, 1].set_title('Monthly system power generated')
ax[0, 1].legend(loc=1, ncol=3, bbox_to_anchor=(0.65, 1))
ax[0, 1].set_xticklabels(Months)
ax[0, 1].set_xticks(x)
ax[0, 1].grid(alpha=0.5,axis='y')

ax[1, 0].bar(x=range(12),
       height=df1["PEM1"],
       label='PEM',
       width=0.8, bottom=0, align='center',
       color=None, edgecolor=None, linewidth=None);
ax[1, 0].bar(x=range(12),
       height=df1["Comp"],
       bottom=df1["PEM1"],
       label='Comp',
       #width=0.8, bottom=0, align='center',
```

```
        color=None, edgecolor=None, linewidth=None);
ax[1, 0].set_ylabel('kWh')
#ax[1, 0].set_xlabel('Months')
#ax[1, 0].set_title('Monthly system power generated')
ax[1, 0].legend(loc=1, ncol=3, bbox_to_anchor=(0.65, 1))
ax[1, 0].set_xticklabels(Months)
ax[1, 0].set_xticks(x)
ax[1, 0].grid(alpha=0.5,axis='y')

ax[1, 1].bar(x=range(12),
        height=df1["Alk1"],
        label='Alk',
        width=0.8, bottom=0, align='center',
        color=None, edgecolor=None, linewidth=None);
ax[1, 1].bar(x=range(12),
        height=df1["Comp1"],
        bottom=df1["Alk1"],
        label='Comp',
        #width=0.8, bottom=0, align='center',
        color=None, edgecolor=None, linewidth=None);
ax[1, 1].set_ylabel('kWh')
#ax[1, 1].set_xlabel('Months')
#ax[1, 1].set_title('Monthly system power generated')
ax[1, 1].legend(loc=1, ncol=3, bbox_to_anchor=(0.65, 1))
ax[1, 1].set_xticklabels(Months)
ax[1, 1].set_xticks(x)
ax[1, 1].grid(alpha=0.5,axis='y')

#2021
LHV=33.3 #(kWh/KgH2)
eff_PEM=0.56
eff_ALK=0.63
H2_PEM_Liq=(np.array(Production)/(LHV/eff_PEM+6.4))*(1/1000)
H2_PEM_Comp=(np.array(Production)/(LHV/eff_PEM+1.05))*(1/1000)
H2_Alk_Liq=(np.array(Production)/(LHV/eff_ALK+6.4))*(1/1000)
H2_Alk_Comp=(np.array(Production)/(LHV/eff_ALK+1.05))*(1/1000)

fig, ax = plt.subplots(figsize=(8, 4), tight_layout=True, facecolor='w')
y=np.arange(12)
width1 = 0.2
ax.bar(y - 1.5*width1,
        height=H2_PEM_Liq,
        label="PEM - Liq",
        width=0.2, color="#4059AD");

ax.bar(y +1.5*width1,
        height=H2_PEM_Comp,
        label='PEM - Comp',
        width=0.2,color="#6B9AC4");

ax.bar(y-0.5*width1,
        height=H2_Alk_Liq,
        label='Alk - Liq',
        width=0.2,color="#97D8C4");

ax.bar(y + 0.5*width1,
        height=H2_Alk_Comp,
        label='Alk - Comp',
        width=0.2, color="#F4B942");

ax.set_ylabel('Tons of hydrogen')
ax.set_xlabel('Months')
#ax.set_title('Monthly Hydrogen Production 2021')
ax.legend(loc=1, ncol=4, bbox_to_anchor=(1, 0.1))
ax.set_xticklabels(Months)
ax.set_xticks(y)
ax.grid(alpha=0.5,axis='y')
```

```
365.
366.  #2030
367.  LHV=33.3 #(kWh/KgH2)
368.  eff_PEM=0.63
369.  eff_ALK=0.65
370.  H2_PEM_Liq=(np.array(Production)/(LHV/eff_PEM+6.4))*(1/1000)
371.  H2_PEM_Comp=(np.array(Production)/(LHV/eff_PEM+1.05))*(1/1000)
372.  H2_Alk_Liq=(np.array(Production)/(LHV/eff_ALK+6.4))*(1/1000)
373.  H2_Alk_Comp=(np.array(Production)/(LHV/eff_ALK+1.05))*(1/1000)
374.
375.  fig, ax = plt.subplots(figsize=(8, 4), tight_layout=True, facecolor='w')
376.  y=np.arange(12)
377.  width1 = 0.2
378.  ax.bar(y - 1.5*width1,
379.         height=H2_PEM_Liq,
380.         label="PEM - Liq",
381.         width=0.2, color="#4059AD");
382.
383.  ax.bar(y +1.5*width1,
384.         height=H2_PEM_Comp,
385.         label='PEM - Comp',
386.         width=0.2,color="#6B9AC4");
387.
388.  ax.bar(y-0.5*width1,
389.         height=H2_Alk_Liq,
390.         label='Alk - Liq',
391.         width=0.2,color="#97D8C4");
392.
393.  ax.bar(y + 0.5*width1,
394.         height=H2_Alk_Comp,
395.         label='Alk - Comp',
396.         width=0.2, color="#F4B942");
397.
398.  ax.set_ylabel('Tons of hydrogen')
399.  ax.set_xlabel('Months')
400.  #ax.set_title('Monthly Hydrogen Production 2021')
401.  ax.legend(loc=1, ncol=4, bbox_to_anchor=(1, 0.1))
402.  ax.set_xticklabels(Months)
403.  ax.set_xticks(y)
404.  ax.grid(alpha=0.5,axis='y')
405.
406.  day_prod=(sum(prod)/365)*0.63/33.3
407.  flow_max=np.array(prod).max()*0.63/33.3
408.
409.  #Compressed hydrogen gas storage system
410.
411.  i=0.07
412.  n_conversion=15
413.  n_storage=20
414.
415.  FRC_conversion=(i*((1+i)**n_conversion))/(((1+i)**n_conversion)-1)
416.  FRC_storage=(i*((1+i)**n_storage))/(((1+i)**n_storage)-1)
417.
418.  M_storage=2/100
419.  M_conversion=4/100
420.
421.  storage_module=500*day_prod*((FRC_storage+M_storage)/(sum(prod)*0.63/33.3))  #USD
422.  conversion_module=3900*flow_max*1.05*((FRC_conversion+M_conversion)/(sum(prod)*0.63/33.3))
423.
424.  GH2=storage_module+conversion_module
425.
426.  #Liquid hydrogen
427.
428.  i=0.07
429.  n_conversion=20
430.  n_storage=20
431.
```

```
FRC_conversion=(i*((1+i)**n_conversion))/(((1+i)**n_conversion)-1)
FRC_storage=(i*((1+i)**n_storage))/(((1+i)**n_storage)-1)

M_storage=2/100
M_conversion=8/100

storage_module=90*day_prod*((FRC_storage+M_storage)/(sum(prod)*0.63/33.3))  #USD
conversion_module=50000*flow_max*((FRC_conversion+M_conversion)/(sum(prod)*0.63/33.3))
LH2=storage_module+conversion_module
```

Annexed C. Python code – Hybrid CSP + PV

```
 # # **3. 100 MW hybrid solar plant (CSP + PV)**

import pandas as pd
import numpy as np
import matplotlib.pyplot as plt
import math

get_ipython().run_line_magic('store', '-r gen_pv')
get_ipython().run_line_magic('store', '-r Production_pv')
get_ipython().run_line_magic('store', '-r LCOE_pv_2021')
get_ipython().run_line_magic('store', '-r LCOE_pv_2030')
get_ipython().run_line_magic('store', '-r month_pv')

# **3.1.Defining Dispatch Schedules**

gen_residual=100000-np.array(gen_pv)
T_fraction=gen_residual/(100*1000)

Table_Jan=pd.DataFrame(T_fraction[0:744].reshape([31,24])).round(3)
Table_Feb=pd.DataFrame(T_fraction[744:1416].reshape([28,24])).round(3)
Table_Mar=pd.DataFrame(T_fraction[1416:2160].reshape([31,24])).round(3)
Table_Apr=pd.DataFrame(T_fraction[2160:2880].reshape([30,24])).round(3)
Table_May=pd.DataFrame(T_fraction[2880:3624].reshape([31,24])).round(3)
Table_Jun=pd.DataFrame(T_fraction[3624:4344].reshape([30,24])).round(3)
Table_Jul=pd.DataFrame(T_fraction[4344:5088].reshape([31,24])).round(3)
Table_Aug=pd.DataFrame(T_fraction[5088:5832].reshape([31,24])).round(3)
Table_Sept=pd.DataFrame(T_fraction[5832:6552].reshape([30,24])).round(3)
Table_Oct=pd.DataFrame(T_fraction[6552:7296].reshape([31,24])).round(3)
Table_Nov=pd.DataFrame(T_fraction[7296:8016].reshape([30,24])).round(3)
Table_Dec=pd.DataFrame(T_fraction[8016:8760].reshape([31,24])).round(3)

Table_annual=[Table_Jan,Table_Feb,Table_Mar,Table_Apr,Table_May,Table_Jun,Table_Jul,Table_Au
g,Table_Sept,Table_Oct,Table_Nov,Table_Dec]

def Prod_Day(i):
  Day=[Table_Jan.iloc[i],Table_Feb.iloc[i],Table_Mar.iloc[i],Table_Apr.iloc[i],Table_May.ilo
c[i],Table_Jun.iloc[i],Table_Jul.iloc[i],Table_Aug.iloc[i],Table_Sept.iloc[i],Table_Oct.iloc
[i],Table_Nov.iloc[i],Table_Dec.iloc[i]]
  Day=pd.DataFrame(Day)
  Day.index=range(0,12)
  return Day

Daily_factors=[]
for i in range(0,28):
  Daily_factors.append(Prod_Day(i))

Prod_28=[Table_Jan.iloc[28],np.zeros_like(Table_Jan.iloc[28]),Table_Mar.iloc[28],Table_Apr.i
loc[28],Table_May.iloc[28],Table_Jun.iloc[28],Table_Jul.iloc[28],Table_Aug.iloc[28],Table_Se
pt.iloc[28],Table_Oct.iloc[28],Table_Nov.iloc[28],Table_Dec.iloc[28]]
```

```
Prod_28=pd.DataFrame(Prod_28)
Prod_28.index=range(0,12)
Daily_factors.append(Prod_28)

Prod_29=[Table_Jan.iloc[29],np.zeros_like(Table_Jan.iloc[29]),Table_Mar.iloc[29],Table_Apr.iloc[29],Table_May.iloc[29],Table_Jun.iloc[29],Table_Jul.iloc[29],Table_Aug.iloc[29],Table_Sept.iloc[29],Table_Oct.iloc[29],Table_Nov.iloc[29],Table_Dec.iloc[29]]
Prod_29=pd.DataFrame(Prod_29)
Prod_29.index=range(0,12)
Daily_factors.append(Prod_29)

Prod_30=[Table_Jan.iloc[30],np.zeros_like(Table_Jan.iloc[30]),Table_Mar.iloc[30],np.zeros_like(Table_Jan.iloc[30]),Table_May.iloc[30],np.zeros_like(Table_Jan.iloc[30]),Table_Jul.iloc[30],Table_Aug.iloc[30],np.zeros_like(Table_Jan.iloc[30]),Table_Oct.iloc[30],np.zeros_like(Table_Jan.iloc[30]),Table_Dec.iloc[30]]
Prod_30=pd.DataFrame(Prod_30)
Prod_30.index=range(0,12)
Daily_factors.append(Prod_30)

def Dispatch_Control(day,Daily_factors):
  Daily_factors_T=Daily_factors[day].T
  df1=pd.DataFrame()
  df2=pd.DataFrame()
  df3=pd.DataFrame()
  for i in range(0,12):
    min=Daily_factors_T[i].min()
    max=Daily_factors_T[i].max()
    delta=(max-min)/8
    if min!=0 and max!=0 :
      df1[i]=pd.cut(Daily_factors_T[i], bins=[min-delta,min,min+delta,min+2*delta,min+3*delta,min+4*delta,min+5*delta,min+6*delta,min+7*delta,max],
      labels=[min,min+delta,min+2*delta,min+3*delta,min+4*delta,min+5*delta,min+6*delta,min+7*delta,max])
      df2[i]=pd.cut(Daily_factors_T[i], bins=[min-delta,min,min+delta,min+2*delta,min+3*delta,min+4*delta,min+5*delta,min+6*delta,min+7*delta,max], labels=[1,2,3,4,5,6,7,8,9])
      df3[i]=[min,min+delta,min+2*delta,min+3*delta,min+4*delta,min+5*delta,min+6*delta,min+7*delta,max]
    else:
      df1[i]=np.ones(24)
      df2[i]=np.ones(24)
      df3[i]=np.ones(9)
  df1=df1.T
  df2=df2.T
  return [df1,df2,df3]

List_1=[] #List of standardized values
List_2=[] # Dispatch control
List_3=[] # f_turb values
for i in range(0,31):
  df=Dispatch_Control(i,Daily_factors)
  df1=df[0]
  df2=df[1]
  df3=df[2]
  List_1.append(df1)
  List_2.append(df2)
  List_3.append(df3)

for i in range(31):
  List_3[i] = List_3[i].apply(lambda x: [y if y >= 0.3 else 0.3 for y in x])

# **3.2 Model Initialization**

import PySAM.Solarpilot as sp
import PySAM.TcsmoltenSalt as tcs
system_model_hybrid = tcs.default('MSPTSingleOwner')
```

```
get_ipython().run_line_magic('matplotlib', 'inline')

# **3.3 SolarResource Group**

system_model_hybrid.SolarResource.solar_resource_file="Antofagasta.csv"

# **3.4 System Design Group**

P_ref=111 #[MW]
Cycle_th_eff=0.412
S_M=2.5
Cycle_th_P=P_ref/Cycle_th_eff
tshours=15
system_model_hybrid.SystemDesign.P_ref=P_ref
system_model_hybrid.SystemDesign.solarm=S_M

model_opt1=sp.from_existing(system_model_hybrid)
model_opt1.SolarPILOT.helio_optical_error=0.00153
model_opt1.SolarPILOT.q_design=round(S_M*Cycle_th_P)
model_opt1.SolarPILOT.rec_aspect=21.6029/17.65
model_opt1.execute()

system_model_hybrid.SystemDesign.tshours=tshours
system_model_hybrid.HeliostatField.helio_positions=model_opt1.Outputs.heliostat_positions
system_model_hybrid.TowerAndReceiver.h_tower=model_opt1.Outputs.h_tower_opt
system_model_hybrid.TowerAndReceiver.rec_height=model_opt1.Outputs.rec_height_opt
system_model_hybrid.HeliostatField.N_hel=model_opt1.Outputs.number_heliostats
system_model_hybrid.TowerAndReceiver.D_rec=model_opt1.Outputs.rec_height_opt/model_opt1.Outputs.rec_aspect_opt
#system_model_hybrid.HeliostatField.A_sf_in=model_opt1.Outputs.area_sf
system_model_hybrid.HeliostatField.A_sf_in=model_opt1.SolarPILOT.helio_width*model_opt1.SolarPILOT.dens_mirror*model_opt1.SolarPILOT.helio_height*model_opt1.Outputs.number_heliostats

Jan_gen=[]
Feb_gen=[]
Mar_gen=[]
Apr_gen=[]
May_gen=[]
Jun_gen=[]
Jul_gen=[]
Aug_gen=[]
Sept_gen=[]
Oct_gen=[]
Nov_gen=[]
Dec_gen=[]

j=0
for i in range(0,31):
  system_model_hybrid.SystemControl.weekday_schedule=List_2[i].values.tolist()
  system_model_hybrid.SystemControl.weekend_schedule=List_2[i].values.tolist()
  for k in range(0,12):
    system_model_hybrid.SystemControl.f_turb_tou_periods=List_3[i].round(3)[k].values.tolist()
    system_model_hybrid.execute()
    if k==0:
      Jan=system_model_hybrid.Outputs.gen[0:744]
      Jan_gen.append(Jan[j:j+24])
    if k==1 and i!=28 and i!=29 and i!=30:
      Feb=system_model_hybrid.Outputs.gen[744:1416]
      Feb_gen.append(Feb[j:j+24])
    if k==2:
      Mar=system_model_hybrid.Outputs.gen[1416:2160]
      Mar_gen.append(Mar[j:j+24])
    if k==3 and i!=30:
      Apr=system_model_hybrid.Outputs.gen[2160:2880]
      Apr_gen.append(Apr[j:j+24])
    if k==4:
```

```
        May=system_model_hybrid.Outputs.gen[2880:3624]
        May_gen.append(May[j:j+24])
      if k==5 and i!=30:
        Jun=system_model_hybrid.Outputs.gen[3624:4344]
        Jun_gen.append(Jun[j:j+24])
      if k==6:
        Jul=system_model_hybrid.Outputs.gen[4344:5088]
        Jul_gen.append(Jul[j:j+24])
      if k==7:
        Aug=system_model_hybrid.Outputs.gen[5088:5832]
        Aug_gen.append(Aug[j:j+24])
      if k==8 and i!=30:
        Sept=system_model_hybrid.Outputs.gen[5832:6552]
        Sept_gen.append(Sept[j:j+24])
      if k==9:
        Oct=system_model_hybrid.Outputs.gen[6552:7296]
        Oct_gen.append(Oct[j:j+24])
      if k==10 and i!=30:
        Nov=system_model_hybrid.Outputs.gen[6552:7296]
        Nov_gen.append(Nov[j:j+24])
      if k==11:
        Dec=system_model_hybrid.Outputs.gen[8016:8760]
        Dec_gen.append(Dec[j:j+24])
    j=j+24

  # **3.6. Outputs Group**

  gen_total=pd.DataFrame(Jan_gen+Feb_gen+Mar_gen+Apr_gen+May_gen+Jun_gen+Jul_gen+Aug_gen+Sept_gen+Oct_gen+Nov_gen+Dec_gen)

  gen_comb=[]
  for i in range(0,365):
    gen_comb=gen_comb+gen_total.iloc[i].tolist()

  def LCOE_csp(d1,Site_prep,Solar_field,Fixed_tower_cost,Receiver_reference_cost,TES,Power_block,Contigencies,OM_fix,OM_var):
      Sum1=0
      Sum2=0
      t1=7/100
      for i in range(1,41):
          Sum1 = Sum1 + (((1-d1)**i)/((1+t1)**i))
          Sum2 = Sum2 + (1/((1+t1)**i))
      Production_csp_adapted=sum(np.array(gen_comb))
      Site_prep=Site_prep*system_model_hybrid.HeliostatField.A_sf_in
      Solar_field=Solar_field*system_model_hybrid.HeliostatField.A_sf_in
      Fixed_tower_cost=Fixed_tower_cost
      Tower_scaling_exp=0.0113
      Total_tower_cost=Fixed_tower_cost*math.exp(Tower_scaling_exp*(system_model_hybrid.TowerAndReceiver.h_tower-
  system_model_hybrid.TowerAndReceiver.rec_height/2+model_opt1.SolarPILOT.helio_height/2))
      Receiver_reference_cost=Receiver_reference_cost
      Receiver_area=math.pi*system_model_hybrid.TowerAndReceiver.D_rec*system_model_hybrid.TowerAndReceiver.rec_height
      Receiver_reference_area=1571
      Receiver_scaling_exponent=0.7
      Solar_receiver=Receiver_reference_cost*(Receiver_area/Receiver_reference_area)**Receiver_scaling_exponent
      #TES Thermal Capacity = Hours of Storage at Power Cycle Full Load × Cycle Thermal Input Power at Design
      #Cycle Thermal Power (MWt) = Design Turbine Gross Output (MWe) ÷ Cycle Thermal Efficiency
      Storage_capacity=(tshours*1000*P_ref)/Cycle_th_eff
      TES=TES*Storage_capacity
      #Balance_of_plant=290.00
      #Power_cycle_cost=1040.00
      #Power_block=(Balance_of_plant+Power_cycle_cost)*1000*P_ref
```

```
222.      Power_block=Power_block*1000*P_ref
223.      #Contigencies=5%
224.
225.      CAPEX1=(Site_prep+Solar_field+Total_tower_cost+Solar_receiver+TES+Power_block)*Contige
    ncies
226.
227.      OPEX1=OM_fix*P_ref*1000+OM_var*Production_csp_adapted*(1/1000)
228.
229.      LCOE_csp_adapted=((CAPEX1+OPEX1*Sum2)/(Production_csp_adapted*Sum1))*1000
230.      return(LCOE_csp_adapted)
231.
232.  LCOE_csp_adapted_2021=LCOE_csp(0.2/100,16.00,140,3000000.00,103000000.00,22,1330,105/100,6
    6,3.5)
233.  LCOE_csp_adapted_2030=LCOE_csp(0.1/100,10,50,2189781,75182481.75,10,700,102/100,44,2.3)
234.
235.  # **LCOE 2021**
236.
237.  LCOE_hybrid_2021=(LCOE_csp_adapted_2021*sum(np.array(gen_comb))+LCOE_pv_2021*Production_pv
    )/(sum(np.array(gen_comb))+Production_pv)
238.  LCOE_hybrid_2021
239.
240.  # **LCOE 2030**
241.
242.  LCOE_hybrid_2030=(LCOE_csp_adapted_2030*sum(np.array(gen_comb))+LCOE_pv_2030*Production_pv
    )/(sum(np.array(gen_comb))+Production_pv)
243.  LCOE_hybrid_2030
244.
245.  gen_with_curtailment=np.array(gen_pv)+np.array(gen_comb)*0.96
246.
247.  for i in range(0,8760):
248.    if (gen_with_curtailment[i]>100000):
249.      gen_with_curtailment[i]=100000
250.
251.  # **CF - ELECT - HYBRID**
252.
253.  CF_hybrid=(sum(gen_with_curtailment))/(8760*0.9*111000)
254.  CF_hybrid
255.
256.  gen_hybrid_limit=np.array(gen_with_curtailment)
257.
258.  for i in range(0,8760):
259.      if (gen_hybrid_limit[i]<100000*0.1):
260.          gen_hybrid_limit[i]=0
261.
262.  CF_elect_hybrid_alk=sum(gen_hybrid_limit)/(8760*0.9*111000)
263.
264.  def LCOH(I,LCOE,f_p,eff,stack_lifetime=90000,percent_remp=0.4):
265.      P_inst=100 #Installed power of the electrolyser [MW]
266.      i=0.07
267.      h=8760 #Hours in a year
268.      N_rep=stack_lifetime/(f_p*h)
269.      I=I+I*percent_remp*(1-i)**N_rep
270.      n=30
271.      FRC=(i*((1+i)**n))/(((1+i)**n)-1)  #Capital Recovery Factor
272.      M=0.05 #Maintenance cost function as a percentage of investment, dependent on plant
    factor
273.      Q_h2=20.3 #Hydrogen production capacity [kg/h]
274.      Q_H2O=0.017  #Amount of water consumed [m3/kg of hydrogen]
275.      P_H2O=1.4 #Water price [USD/m3]
276.      Q_e=33.3/eff  #Amount of electricity consumed [kWh/kg of hydrogen]
277.      P_e=LCOE
278.      Q_O2=7.8 #Sale of oxygen taking into account the quantity produced [kgO2/kg of
    hydrogen] (optional term)
279.      P_O2=0.03 #Selling price of oxygen [USD/kgO2] (optional term)
280.      LCOH = I*(FRC+M)*33.3/(h*f_p*eff)+Q_H2O*P_H2O+Q_e*P_e
281.
282.      Water=Q_H2O*P_H2O
```

```
283.      Electricity=Q_e*P_e
284.      Electrolysis=I*(FRC+M)*33.3/(h*f_p*eff)
285.      return(LCOH,Water,Electricity,Electrolysis)
286.
287.  # **LCOH - HYBRID - ALK - 2021**
288.
289.  LCOH_hybrid_alk_2021=LCOH(500,LCOE_hybrid_2021/1000,CF_elect_hybrid_alk,0.63,100000)[0]
290.  LCOH_hybrid_alk_2021
291.  get_ipython().run_line_magic('store', 'LCOH_hybrid_alk_2021')
292.
293.  # **LCOH - HYBRID - PEM - 2021**
294.
295.  LCOH_hybrid_PEM_2021=LCOH(1100,LCOE_hybrid_2021/1000,CF_hybrid,0.56)[0]
296.  LCOH_hybrid_PEM_2021
297.  get_ipython().run_line_magic('store', 'LCOH_hybrid_PEM_2021')
298.
299.  # **LCOH - HYBRID - ALK - 2030**
300.
301.  LCOH_hybrid_alk_2030=LCOH(400,LCOE_hybrid_2030/1000,CF_elect_hybrid_alk,0.65,100000,0.15)[
    0]
302.  LCOH_hybrid_alk_2030
303.
304.  # **LCOH - HYBRID - PEM - 2030**
305.
306.  LCOH_hybrid_PEM_2030=LCOH(650,LCOE_hybrid_2030/1000,CF_hybrid,0.63,percent_remp=0.15)[0]
307.  LCOH_hybrid_PEM_2030
308.
309.  W1 =
    [LCOH(500,LCOE_hybrid_2021/1000,CF_elect_hybrid_alk,0.63,100000)[1],LCOH(1100,LCOE_hybrid_20
    21/1000,CF_hybrid,0.56)[1]]
310.  Electri1 =
    [LCOH(500,LCOE_hybrid_2021/1000,CF_elect_hybrid_alk,0.63,100000)[2],LCOH(1100,LCOE_hybrid_20
    21/1000,CF_hybrid,0.56)[2]]
311.  Electro1 =
    [LCOH(500,LCOE_hybrid_2021/1000,CF_elect_hybrid_alk,0.63,100000)[3],LCOH(1100,LCOE_hybrid_20
    21/1000,CF_hybrid,0.56)[3]]
312.
313.  get_ipython().run_line_magic('store', 'W1')
314.  get_ipython().run_line_magic('store', 'Electri1')
315.  get_ipython().run_line_magic('store', 'Electro1')
316.
317.  labels = ['HYBRID-ALK-2021',"HYBRID-PEM-2021","HYBRID-ALK-2030","HYBRID-PEM-2030"]
318.  W =
    [LCOH(500,LCOE_hybrid_2021/1000,CF_elect_hybrid_alk,0.63,100000)[1],LCOH(1100,LCOE_hybrid_20
    21/1000,CF_hybrid,0.56)[1],LCOH(400,LCOE_hybrid_2030/1000,CF_elect_hybrid_alk,0.65,100000,0.
    15)[1],LCOH(650,LCOE_hybrid_2030/1000,CF_hybrid,0.63,percent_remp=0.15)[1]]
319.  Electri =
    [LCOH(500,LCOE_hybrid_2021/1000,CF_elect_hybrid_alk,0.63,100000)[2],LCOH(1100,LCOE_hybrid_20
    21/1000,CF_hybrid,0.56)[2],LCOH(400,LCOE_hybrid_2030/1000,CF_elect_hybrid_alk,0.65,100000,0.
    15)[2],LCOH(650,LCOE_hybrid_2030/1000,CF_hybrid,0.63,percent_remp=0.15)[2]]
320.  Electro =
    [LCOH(500,LCOE_hybrid_2021/1000,CF_elect_hybrid_alk,0.63,100000)[3],LCOH(1100,LCOE_hybrid_20
    21/1000,CF_hybrid,0.56)[3],LCOH(400,LCOE_hybrid_2030/1000,CF_elect_hybrid_alk,0.65,100000,0.
    15)[3],LCOH(650,LCOE_hybrid_2030/1000,CF_hybrid,0.63,percent_remp=0.15)[3]]
321.  width = 0.5       # the width of the bars: can also be len(x) sequence
322.
323.  fig, ax = plt.subplots()
324.
325.  bars = np.add(Electri, Electro).tolist()
326.
327.  ax.bar(labels, Electri, width, label='Electricity')
328.  ax.bar(labels, Electro, width, bottom=Electri,label='Electrolysis')
329.  ax.bar(labels, W, width, bottom=bars,label='Water')
330.  ax.legend()
331.
332.  ax.set_ylabel("USD/kg")
333.  ax.set_title('Levelised Cost of Hydrogen - CSP + PV hybrid')
```

```
334.
335.  #ax.bar(labels, women_means, width, bottom=men_means,label='Women')
336.
337.  fig, ax = plt.subplots(figsize=(8, 4), tight_layout=True, facecolor='w')
338.  ax.plot(pd.date_range(start='1/1/2021',
    end='01/01/2022',periods=8760),gen_comb,label='CSP',c="tab:orange")
339.  ax.plot(pd.date_range(start='1/1/2021',
    end='01/01/2022',periods=8760),gen_pv,label='PV',c="tab:blue")
340.  ax.plot(pd.date_range(start='1/1/2021',
    end='01/01/2022',periods=8760),gen_with_curtailment,label='Hybrid',  c="tab:green")
341.
342.  ax.set_ylabel('kW')
343.  ax.set_xlabel('Days of the year')
344.  #ax.set_title('Hourly energy generated by the system')
345.  ax.legend(loc=1, ncol=3, bbox_to_anchor=(0.7, 0.2))
346.  plt.savefig("Ejemplo2.png")
347.  fig.autofmt_xdate()
348.
349.  gen_csp=gen_comb
350.  Sum_Enero=sum(gen_csp[0:744])
351.  Sum_Febrero=sum(gen_csp[744:1416])
352.  Sum_Marzo=sum(gen_csp[1416:2160])
353.  Sum_Abril=sum(gen_csp[2160:2880])
354.  Sum_Mayo=sum(gen_csp[2880:3624])
355.  Sum_Junio=sum(gen_csp[3624:4344])
356.  Sum_Julio=sum(gen_csp[4344:5088])
357.  Sum_Agosto=sum(gen_csp[5088:5832])
358.  Sum_Septiembre=sum(gen_csp[5832:6552])
359.  Sum_Octubre=sum(gen_csp[6552:7296])
360.  Sum_Noviembre=sum(gen_csp[7296:8016])
361.  Sum_Diciembre=sum(gen_csp[8016:8760])
362.
363.  Month =[Sum_Enero, Sum_Febrero, Sum_Marzo, Sum_Abril, Sum_Mayo, Sum_Junio, Sum_Julio,
    Sum_Agosto, Sum_Septiembre, Sum_Octubre, Sum_Noviembre,Sum_Diciembre]
364.
365.  Months=["Jan","Feb","Mar","Apr","May","Jun","Jul","Aug","Sept","Oct","Nov","Dec"]
366.  fig, ax = plt.subplots(figsize=(8, 4), tight_layout=True, facecolor='w')
367.
368.  ax.bar(range(12),
369.         height=Month,
370.         label='CSP',
371.         width=0.8, bottom=0, align='center',
372.         color="tab:orange", edgecolor=None, linewidth=None);
373.  ax.bar(range(12),
374.         height=month_pv,
375.         bottom=Month,
376.         label='PV',
377.         #width=0.8, bottom=0, align='center',
378.         color="tab:blue", edgecolor=None, linewidth=None);
379.  ax.set_ylabel('kWh')
380.  ax.set_xlabel('Months')
381.  ax.set_title('Monthly system power generated')
382.  ax.legend(loc=1, ncol=3, bbox_to_anchor=(0.6, 1))
383.  ax.set_xticklabels(Months)
384.  ax.set_xticks(range(12))
385.
386.  LHV=33.3 #(kWh/KgH2)
387.  eff_PEM=0.56
388.  eff_ALK=0.63
389.  df1=pd.DataFrame(np.array(Month)*0.96+np.array(month_pv))
390.  df1["PEM"]=(df1[0]/(LHV/eff_PEM + 6.4))*(LHV/eff_PEM)
391.  df1["Liq"]=(df1[0]/(LHV/eff_PEM + 6.4))*6.4
392.  df1["Alk"]=(df1[0]/(LHV/eff_ALK + 6.4))*(LHV/eff_ALK)
393.  df1["Liq1"]=(df1[0]/(LHV/eff_ALK + 6.4))*6.4
394.  df1["PEM1"]=(df1[0]/(LHV/eff_PEM + 1.05))*(LHV/eff_PEM)
395.  df1["Comp"]=(df1[0]/(LHV/eff_PEM + 1.05))*1.05
396.  df1["Alk1"]=(df1[0]/(LHV/eff_ALK + 1.05))*(LHV/eff_ALK)
```

```
df1["Comp1"]=(df1[0]/(LHV/eff_ALK + 1.05))*1.05

Months=["Jan","Feb","Mar","Apr","May","Jun","Jul","Aug","Sept","Oct","Nov","Dec"]
df1.index=Months
df1.columns=["Energy", "PEM","Liq","Alk","Liq1","PEM1","Comp","Alk1","Comp1"]

x=range(12)
fig, ax = plt.subplots(2, 2)
fig.set_size_inches(15, 10)

ax[0, 0].bar(x=range(12),
       height=df1["PEM"],
       label='PEM',
       width=0.8, bottom=0, align='center',
       color=None, edgecolor=None, linewidth=None);
ax[0, 0].bar(x=range(12),
       height=df1["Liq"],
       bottom=df1["PEM"],
       label='Liq',
       #width=0.8, bottom=0, align='center',
       color=None, edgecolor=None, linewidth=None);
ax[0, 0].set_ylabel('kWh')
#ax[0, 0].set_xlabel('Months')
#ax[0, 0].set_title('Monthly system power generated')
ax[0, 0].legend(loc=1, ncol=3, bbox_to_anchor=(0.75, 1))
ax[0, 0].set_xticklabels(Months)
ax[0, 0].set_xticks(range(12))
ax[0, 0].grid(alpha=0.5,axis='y')

ax[0, 1].bar(x=range(12),
       height=df1["Alk"],
       label='Alk',
       width=0.8, bottom=0, align='center',
       color=None, edgecolor=None, linewidth=None);
ax[0, 1].bar(x=range(12),
       height=df1["Liq1"],
       bottom=df1["Alk"],
       label='Liq',
       #width=0.8, bottom=0, align='center',
       color=None, edgecolor=None, linewidth=None);
ax[0, 1].set_ylabel('kWh')
#ax[0, 1].set_xlabel('Months')
#ax[0, 1].set_title('Monthly system power generated')
ax[0, 1].legend(loc=1, ncol=3, bbox_to_anchor=(0.75, 1))
ax[0, 1].set_xticklabels(Months)
ax[0, 1].set_xticks(x)
ax[0, 1].grid(alpha=0.5,axis='y')

ax[1, 0].bar(x=range(12),
       height=df1["PEM1"],
       label='PEM',
       width=0.8, bottom=0, align='center',
       color=None, edgecolor=None, linewidth=None);
ax[1, 0].bar(x=range(12),
       height=df1["Comp"],
       bottom=df1["PEM1"],
       label='Comp',
       #width=0.8, bottom=0, align='center',
       color=None, edgecolor=None, linewidth=None);
ax[1, 0].set_ylabel('kWh')
#ax[1, 0].set_xlabel('Months')
#ax[1, 0].set_title('Monthly system power generated')
ax[1, 0].legend(loc=1, ncol=3, bbox_to_anchor=(0.75, 1))
ax[1, 0].set_xticklabels(Months)
ax[1, 0].set_xticks(x)
ax[1, 0].grid(alpha=0.5,axis='y')

```

```
ax[1, 1].bar(x=range(12),
       height=df1["Alk1"],
       label='Alk',
       width=0.8, bottom=0, align='center',
       color=None, edgecolor=None, linewidth=None);
ax[1, 1].bar(x=range(12),
       height=df1["Comp1"],
       bottom=df1["Alk1"],
       label='Comp',
       #width=0.8, bottom=0, align='center',
       color=None, edgecolor=None, linewidth=None);
ax[1, 1].set_ylabel('kWh')
#ax[1, 1].set_xlabel('Months')
#ax[1, 1].set_title('Monthly system power generated')
ax[1, 1].legend(loc=1, ncol=3, bbox_to_anchor=(0.75, 1))
ax[1, 1].set_xticklabels(Months)
ax[1, 1].set_xticks(x)
ax[1, 1].grid(alpha=0.5,axis='y')

gen_csp=gen_with_curtailment
Sum_Enero=sum(gen_csp[0:744])
Sum_Febrero=sum(gen_csp[744:1416])
Sum_Marzo=sum(gen_csp[1416:2160])
Sum_Abril=sum(gen_csp[2160:2880])
Sum_Mayo=sum(gen_csp[2880:3624])
Sum_Junio=sum(gen_csp[3624:4344])
Sum_Julio=sum(gen_csp[4344:5088])
Sum_Agosto=sum(gen_csp[5088:5832])
Sum_Septiembre=sum(gen_csp[5832:6552])
Sum_Octubre=sum(gen_csp[6552:7296])
Sum_Noviembre=sum(gen_csp[7296:8016])
Sum_Diciembre=sum(gen_csp[8016:8760])

comb1 =np.array([Sum_Enero, Sum_Febrero, Sum_Marzo, Sum_Abril, Sum_Mayo, Sum_Junio,
    Sum_Julio, Sum_Agosto, Sum_Septiembre, Sum_Octubre, Sum_Noviembre,Sum_Diciembre])

#2021

LHV=33.3 #(kWh/KgH2)
eff_PEM=0.56
eff_ALK=0.63
H2_PEM_Liq=(comb1/(LHV/eff_PEM+6.4))*(1/1000)
H2_PEM_Comp=(comb1/(LHV/eff_PEM+1.05))*(1/1000)
H2_Alk_Liq=(comb1/(LHV/eff_ALK+6.4))*(1/1000)
H2_Alk_Comp=(comb1/(LHV/eff_ALK+1.05))*(1/1000)

fig, ax = plt.subplots(figsize=(8, 4), tight_layout=True, facecolor='w')
y=np.arange(12)
width1 = 0.2
ax.bar(y - 1.5*width1,
       height=H2_PEM_Liq,
       label="PEM - Liq",
       width=0.2, color="#4059AD");

ax.bar(y +1.5*width1,
       height=H2_PEM_Comp,
       label='PEM - Comp',
       width=0.2,color="#6B9AC4");

ax.bar(y-0.5*width1,
       height=H2_Alk_Liq,
       label='Alk - Liq',
       width=0.2,color="#97D8C4");

ax.bar(y + 0.5*width1,
       height=H2_Alk_Comp,
       label='Alk - Comp',
```

```
        width=0.2, color="#F4B942");

ax.set_ylabel('Tons of hydrogen')
ax.set_xlabel('Months')
#ax.set_title('Monthly Hydrogen Production 2021')
ax.legend(loc=1, ncol=4, bbox_to_anchor=(1, 0.1))
ax.set_xticklabels(Months)
ax.set_xticks(y)
ax.grid(alpha=0.5,axis='y')

# In[125]:

#2030
LHV=33.3 #(kWh/KgH2)
eff_PEM=0.63
eff_ALK=0.65
H2_PEM_Liq=(comb1/(LHV/eff_PEM+6.4))*(1/1000)
H2_PEM_Comp=(comb1/(LHV/eff_PEM+1.05))*(1/1000)
H2_Alk_Liq=(comb1/(LHV/eff_ALK+6.4))*(1/1000)
H2_Alk_Comp=(comb1/(LHV/eff_ALK+1.05))*(1/1000)

fig, ax = plt.subplots(figsize=(8, 4), tight_layout=True, facecolor='w')
y=np.arange(12)
width1 = 0.2
ax.bar(y - 1.5*width1,
       height=H2_PEM_Liq,
       label="PEM - Liq",
       width=0.2, color="#4059AD");

ax.bar(y +1.5*width1,
       height=H2_PEM_Comp,
       label='PEM - Comp',
       width=0.2,color="#6B9AC4");

ax.bar(y-0.5*width1,
       height=H2_Alk_Liq,
       label='Alk - Liq',
       width=0.2,color="#97D8C4");

ax.bar(y + 0.5*width1,
       height=H2_Alk_Comp,
       label='Alk - Comp',
       width=0.2, color="#F4B942");

ax.set_ylabel("Tons of hydrogen")
ax.set_xlabel('Months')
#ax.set_title('Monthly Hydrogen Production 2021')
ax.legend(loc=1, ncol=4, bbox_to_anchor=(1, 0.1))
ax.set_xticklabels(Months)
ax.set_xticks(y)
ax.grid(alpha=0.5,axis='y')

day_prod=(sum(gen_with_curtailment)/365)*0.63/33.3
flow_max=np.array(gen_with_curtailment).max()*0.63/33.3

#Compressed hydrogen gas storage system

i=0.07
n_conversion=15
n_storage=20

FRC_conversion=(i*((1+i)**n_conversion))/(((1+i)**n_conversion)-1)
FRC_storage=(i*((1+i)**n_storage))/(((1+i)**n_storage)-1)

M_storage=2/100
M_conversion=4/100

```

```
597.  storage_module=500*day_prod*((FRC_storage+M_storage)/(sum(gen_with_curtailment)*0.63/33.3)
    )  #USD
598.  conversion_module=3900*flow_max*1.05*((FRC_conversion+M_conversion)/(sum(gen_with_curtailm
    ent)*0.63/33.3))
599.
600.  GH2=storage_module+conversion_module
601.
602.  #Liquid hydrogen
603.
604.  i=0.07
605.  n_conversion=20
606.  n_storage=20
607.
608.  FRC_conversion=(i*((1+i)**n_conversion))/(((1+i)**n_conversion)-1)
609.  FRC_storage=(i*((1+i)**n_storage))/(((1+i)**n_storage)-1)
610.
611.  M_storage=2/100
612.  M_conversion=8/100
613.
614.  storage_module=90*day_prod*((FRC_storage+M_storage)/(sum(gen_with_curtailment)*0.63/33.3))
     #USD
615.  conversion_module=50000*flow_max*((FRC_conversion+M_conversion)/(sum(gen_with_curtailment)
    *0.63/33.3))
616.  LH2=storage_module+conversion_module
```

It is also possible to download the source code from the following GitHub repository:

https://github.com/fcomoraga/Master-s_thesis_Francisco_Moraga